

Temperature Activation Mechanism of TRP Ion Channels

by

Jason Omar Sosa Pagán

Department of Neurobiology
Duke University

Date: _____

Approved:

Jörg Grandl, Supervisor

Rebecca Yang, Chair

Hiroaki Matsunami

Seok-Yong Lee

Dissertation submitted in partial fulfillment of
the requirements for the degree of Doctor
of Philosophy in the Department of
Neurobiology in the Graduate School
of Duke University

2017

ABSTRACT

Temperature Activation Mechanism of TRP Ion Channels

by

Jason Omar Sosa Pagán

Department of Neurobiology
Duke University

Date: _____

Approved:

Jörg Grandl, Supervisor

Rebecca Yang, Chair

Hiroaki Matsunami

Seok-Yong Lee

An abstract of a dissertation submitted in partial
fulfillment of the requirements for the degree
of Doctor of Philosophy in the Department of
Neurobiology in the Graduate School of
Duke University

2017

Copyright by
Jason Omar Sosa Pagán
2017

Abstract

Organisms need to sense temperature to avoid detrimental damage to cells and tissues. In mammals, this is thought to be mediated, at least in part, by several members of the transient receptor potential (TRP) superfamily of ion channels. Most TRP channels are outwardly rectifying channels with 6 transmembrane segments that assemble as a tetramer. Some TRP channels are activated by cold or heat, chemicals, and depolarizing voltages. Temperature sensitive TRP channels are expressed in a variety of cell types including keratinocytes and medium- to small-diameter nociceptors where they are involved in the detection of noxious chemicals, inflammatory mediators, and temperature. In response to noxious stimuli, TRP channels mediate the depolarization of nociceptors ultimately leading to the perception of pain. Due to their critical role in nociception they are excellent candidates for the development of analgesic drugs that can be used as treatments for different pain modalities. However, drugs that target these ion channels have many unwanted side effects that include hypo or hyperthermia. Clearly, a thorough understanding of the structures and mechanisms that mediate temperature activation of TRP channels is needed for the development of novel drugs that do not evoke these side effects.

Although countless studies have tried to identify the structures and mechanisms that confer temperature sensitivity to TRP channels, no consensus has yet been attained.

One recent proposed mechanism argues that temperature activation is driven by the exposure of hydrophobic residues to solvent. This mechanism further predicts that residues are exposed to solvent in a coordinated fashion, while not necessarily being near each other. However, there is little experimental evidence supporting this mechanism in TRP channels. Here I tackle these questions using a variety of approaches: First, I tested the sufficiency of the pore domain of TRPV1 towards temperature sensitivity using minimal 'pore-only' channels, but found that my minimalistic approach did not yield functional channels. I then tested the sufficiency of the entire ankyrin repeat 6, as well as single-point mutations on the same repeat of *drosophila* TRPA1 for inverting the temperature directionality of the channel, but found that the structure was not sufficient to make heat-activated *drosophila* TRPA1 cold sensitive. Lastly, I took a combinatorial approach and used random mutagenesis, coupled to high-throughput screening and massive parallel sequencing to identify and characterize mutations from ~7,300 randomly mutated TRPV1 clones. I found that residues important for temperature activation are randomly spread throughout the entire sequence of the channel indicating that temperature does not activate the channel by acting on any single domain, but rather on the entire protein. This implies that it will be very complicated to develop analgesic drugs that do not affect the temperature activation mechanism because residues throughout the protein are involved in temperature sensitivity. Additionally, I found that large decreases in hydrophobicity of amino acids

are better tolerated for activation by capsaicin than for activation by heat, suggesting that strong hydrophobicity might be specifically required for temperature activation. This provides initial support for a previously hypothesized temperature activation mechanism involving amino acid hydrophobicity in TRP ion channels.

Dedication

To my mother and father, who silently inspired me to complete this work. To my wife Joan, who has always supported me on my life's adventures.

Contents

Abstract	iv
List of Tables.....	xii
List of Figures	xiii
Acknowledgements	xviii
1. Introduction	1
1.1 Temperature detection circuitry.....	1
1.2 Transient receptor potential (TRP) channels	4
1.3 Potential mechanisms of temperature activation of TRP ion channels	12
1.3.1. TRP channels as downstream temperature sensitive molecules.....	12
1.3.2. Is temperature sensitivity of TRP channels linked to voltage activation?	13
1.3.3. Temperature activation may be mediated through allosterically integrated conformational changes.....	14
1.3.4. The role of heat capacity on temperature activation of TRP channels	16
1.4 Summary.....	20
2. Determination of the minimal structures for temperature activation of TRP channels	21
2.1 Introduction.....	21
2.2 Materials and Methods	26
2.2.1 Engineering of chimeric constructs.....	26
2.2.2 Cell culture	26
2.2.3 Electrophysiology.....	27
2.2.4 Data analysis	28

2.3 Results	28
2.3.1 Identification of aligning residues in the pore domain of TRPV1 and inwardly rectifying K ⁺ (K _{ir}) ion channels	28
2.3.2 Chimeric channels are insensitive to voltage, temperature, and chemicals	34
2.4 Discussion.....	38
3. The role of ankyrin repeat 6 on modulating temperature activation directionality of drosophila TRPA1.....	41
3.1 Introduction.....	41
3.2 Materials and Methods	45
3.2.1 Cell culture	45
3.2.2 Sequence alignments.....	45
3.2.3 Site-directed mutagenesis and generation of chimeras	45
3.2.4 High-resolution structure illustrations.....	45
3.2.5 Electrophysiology.....	45
3.2.6 Data analysis	46
3.3 Results	46
3.3.1 Mouse ankyrin repeat 6 is not interchangeable	46
3.3.2 Mouse ankyrin repeat 6 is not interchangeable	49
3.4 Discussion.....	51
4. Temperature activation of TRPV1 is specifically sensitive to large decreases in amino acid hydrophobicity.....	54
4.1 Introduction.....	54
4.2 Materials and Methods.....	56

4.2.1 Library generation and functional screening	56
4.2.2 Categorization of mutant library	56
4.2.3 Sample preparation and sequencing	57
4.2.4 Aligning and mapping of variants.....	58
4.2.5 Determination of variant call accuracy and mutational frequency.....	58
4.2.6 Alignment of TRPV1 ankyrin repeats and TRPV1 S4	59
4.2.7 High-resolution structure illustrations.....	59
4.2.8 Site-directed mutagenesis	59
4.2.9 Cell culture	59
4.2.10 Electrophysiology.....	60
4.2.11 Data analysis and statistical tests	61
4.3 Results	62
4.3.1 Ultra-deep sequencing identifies 535 functionally characterized mutations....	62
4.3.2 Most structural domains of TRPV1 are tolerant to mutations	66
4.3.3 Decrease in amino acid hydrophobicity is less frequently tolerated for activation by temperature than for activation by capsaicin	70
4.3.4 Hydrophobicity of Three Pore Residues Contributes to overall Temperature Sensitivity	73
4.4 Discussion.....	79
5. Concluding remarks	85
Appendix A.....	88
Appendix B	95
References	115

Biography 124

List of Tables

Table 1: List of temperature- and capsaicin-characterized 'functional' mutations with their corresponding change in hydrophathy. 88

Table 2: List of temperature- and capsaicin-characterized 'less functional' mutations with their corresponding change in hydrophathy 95

List of Figures

- Figure 1: Circuitry for temperature sensation at the spinal cord. The inset shows the layers of the gray matter in which nociceptors synapse. 2
- Figure 2: Sensory neurons are activated by a variety of stimuli. Illustration of axon terminals from sensory fibers activated by several physical and chemical entities. 3
- Figure 3: TRP channels are architecturally similar to K_v channels. (A-C) Monomeric (A) or tetrameric (B-C) high-resolution structure of TRPV1 (3J5P) as observed from the side (A-B) or the outside (C) of the cell. For clarity, only S1-S6 is displayed on C. (D-F) High-resolution structure of TRPA1 (3J9P) showed as a monomer (D) or tetramer (E-F). Structure on D and E is observed from the side and on F is observed from the inside of the cell. (G-I) Monomeric (G) or tetrameric (H-I) high-resolution structure of a K_v channel (2A79) as observed from the side (G-H) or the outside (I) of the cell. 8
- Figure 4: Temperature sensitive TRP channels. Topology models for several temperature sensitive TRP channels activated at different temperature ranges. The heat map at the bottom illustrates the temperature ranges for activation from noxious cold (deep blue) to noxious heat (red). At the top are chemical structures of some of the chemical activators of TRP channels. Circles at the N-terminal indicate the number of ankyrin repeats. 11
- Figure 5: Temperature dependence of ΔG for an arbitrary process. Plotted is $\Delta G = \Delta H(T_0) + \Delta C_p \cdot (T - T_0) - T \cdot \Delta S - T \cdot \Delta C_p \cdot \ln(T/T_0)$, where T_0 is an arbitrarily chosen temperature. 17
- Figure 6: Temperature dependence of ΔG for two arbitrary processes with different ΔC_p . Plotted is two iterations of $\Delta G = \Delta H(T_0) + \Delta C_p \cdot (T - T_0) - T \cdot \Delta S - T \cdot \Delta C_p \cdot \ln(T/T_0)$, where T_0 is an arbitrarily chosen temperature. 18
- Figure 7: Temperature sensitivity of two arbitrary cold or heat sensitive ion channels. Plotted is two iterations of $\Delta G = \Delta H(T_0) + \Delta C_p \cdot (T - T_0) - T \cdot \Delta S - T \cdot \Delta C_p \cdot \ln(T/T_0)$, where T_0 is an arbitrarily chosen temperature. 19
- Figure 8: Structural domains involved in the temperature activation of TRP channels. Orange, cyan, and blue indicates domains involved in the modulation of temperature sensitivity of TRPV1, TRPV2, and TRPA1. Magenta and red highlight structures required for temperature activation of TRPA1, TRPV1, and TRPV3. 23

Figure 9: Structural domains not required for temperature activation of TRP channels. In purple are domains not required for temperature activation of TRPV1, whereas in blue is a domain that is unnecessary for temperature activation of TRPA1. 24

Figure 10: Structure of a K_{ir} ion channel. Structure of a bacterial K_{ir} channel from *Burkholderia pseudomallei*. For clarity, only two subunits are displayed. Structure illustration was made on Chimera (UCSF) using the PDB (1P7B) coordinates. 25

Figure 11: Illustration of ‘pore-only’ TRPV1 chimeric channels. Representation of the approach used to make TRPV1 ‘pore-only’ chimeric channels. 29

Figure 12: Illustration of TRPV1 chimeric channels with the pore swapped by the K_{ir} pore. Representation of the approach used to build chimeric constructs where the TRPV1 pore was replaced by the mouse K_{ir} pore. 30

Figure 13: Sequence alignment of S5 and S6 of several TRP channels and S1 and S2 of several $K_{ir}2.x$ channels. Top: Sequence alignment between S5 of rat TRPV1, mouse TRPV3, human TRPA1, and S1 of mouse $K_{ir} 2.1 - 2.4$. Bottom: Sequence alignment between S6 of rat TRPV1, mouse TRPV3, human TRPA1, and S2 of mouse $K_{ir} 2.1 - 2.4$. Boxes on top indicate the topology of TRPV1 according to the high-resolution structure. Boxes at the bottom indicate the topology of $K_{ir}2.2$ according to the high-resolution structure of chicken $K_{ir}2.2$. Letters (a', b', c') and numbers (1', 2', 3', 4', 5') on top of the alignment indicates aligning residues that can potentially be used as intercrossing positions for making chimeric constructs. Sequence alignments were made by hand. ... 31

Figure 14: Schematic representation of chimeric constructs. List of chimeric constructs made for measuring temperature sensitivity in or outside the pore of TRPV1. Bars are not at scale. m is mouse, red is TRPV1, gray is mouse $K_{ir}2.1$ 33

Figure 15: Temperature activation of TRPV1 chimeric channels. (A) Representative current-voltage (I-V) plots for pcDNA, TRPV1, TRPV1 a'c', and mouse K_{ir} in TRPV1 a'c' before (25°C), during (40°C), and after (25°C - 2) a heating. (B) Average current at 25°C and +100 mV for chimeric channels. (C) Average current fold changes at +100 mV for chimeric channels tested with a heating ramp from 25°C to 40°C. Data represent average \pm SEM. Numbers on top of bars indicate the total number of individual patches. Dashed line indicates pcDNA levels. 36

Figure 16: Capsaicin sensitivity of TRPV1 chimeric channels. (A) Representative I-V plots for TRPV1 and mouse K_{ir} in TRPV1 a'c' before (pre-capsaicin), during (capsaicin), and after (post-capsaicin) application of 1 μ M capsaicin. (B) Average current at =100 mV

during application of capsaicin for chimeric channels. (C) Average current fold change at +100 mV for chimeric channels tested with a capsaicin pulse. Data represent average \pm SEM. Numbers on top of bars indicate the total number of individual patches. 37

Figure 17: Residues of ankyrin repeat 6 found to invert the temperature sensitivity of mouse TRPA1 from cold to warm temperatures. Top: Sequence alignment between ankyrin repeat 6 of mouse TRPA1 and ankyrin repeat 13 of human TRPA1. In red are the residues mutated in ankyrin repeat 6 of mouse TRPA1 found to invert temperature directionality. Bottom: High-resolution structure of ankyrin repeat 12-14 of human TRPA1 (3J9P). In red are the corresponding residues to the ones identified in ankyrin repeat 6 of mouse TRPA1. In pink is ankyrin repeat 12, in cyan is ankyrin repeat 13, and in gold is ankyrin repeat 14. 42

Figure 18: Topology and sequence of ankyrin repeat 13 of human TRPA1. Position of residues (Top), the level of amino acid conservation (Mosavi et al., 2002), and the topology of an ankyrin repeat (bottom) are showed. 43

Figure 19: Temperature activation of mouse and drosophila TRPA1 chimeric channels. (A) Sequence alignment of ankyrin repeat 6 of mouse and drosophila TRPA1. (B-C) Representative current traces from pcDNA, wild type dTRPA1, mTRPA1-dAR6, and dTRPA1-mAR6 transfected cells recorded with a \pm 100 mV ramp upon application of a heat (B) or cold (C) stimuli. (D-E) Average of maximal current changes at +100 mV upon application of a heat (D) or cold (E) stimuli to constructs on B and C. Data represent average \pm SEM. Numbers on top of the bars indicate the number of individual patches. m is mouse, d is drosophila. 48

Figure 20: Temperature activation of drosophila TRPA1 single point mutants. (A) Sequence alignment of ankyrin repeat 6 of mouse and drosophila TRPA1. (B-C) Representative current traces from pcDNA, wild type dTRPA1, and dTRPA1 K287G transfected cells recorded with a \pm 100 mV upon application of a heat (B) or cold (C) stimuli. (D-E) Average of maximal current changes at +100 mV for pcDNA, wild type dTRPA1, dTRPA1 G276N, and dTRPA1 K287G upon stimulation with hot (D) or cold (E) temperature. Data represents average \pm SEM. Numbers on top of the bars represent the number of individual patches. m is mouse, d is drosophila. 50

Figure 21: Schematic representation of experimental approach. Illustration of random mutagenesis, calcium-based functional screening, pooling of clones with identical functionality, and deep sequencing of pooled clones. Fluorescence responses of 94 mutant clones (4 responses per clone) upon heat (top panel) or capsaicin (bottom panel) stimulation. Wild type TRPV1 (black), pcDNA (green), 'functional' clones (blue), and

'less functional' clones (gray). Wild type TRPV1 and pcDNA are average responses of $n = 4$ wells. Error bars represent s.d..... 63

Figure 22: Numbers of base pairs mutations of TRPV1 identified by sequencing clones stimulated with temperature and capsaicin. (A) Normalized mutation frequency for wild type bases for the temperature and capsaicin screened libraries. (B) Numbers and identity of base pair mutations in correlation to the wild type base. (C) Number of times wild type amino acids were mutated. (D) Frequency of mutant amino acid..... 65

Figure 23: (A) Illustration of the location of identified mutations screened with temperature (top panel) or capsaicin (bottom panel) for 'functional' clones (blue and yellow), 'less functional' clones (gray) or all identified mutations pooled together (purple). In yellow are 'functional' mutations that conserved wild type amino acid hydrophathy. In blue are 'functional' mutations that did not conserved amino acid hydrophathy. Mutations were considered hydrophathy-conserving if the Δ hydrophathy ($\text{hydrophathy}_{\text{mutant}} - \text{hydrophathy}_{\text{WT}} = \pm 0.6$). Mutations outside of that range are considered non-conserving. Each bar indicates one single mutation and boxes on top illustrate the structural domains of TRPV1. (B) Histogram of frequencies of gap lengths between mutations of temperature (top) or capsaicin (bottom) 'functional' category and gap lengths within ten random distributions of 287 (temperature, top) or 248 (capsaicin, bottom) mutations in 838 positions. Error bars are SEM. 68

Figure 24: 'Temperature functional' (top panel) and 'capsaicin functional' (bottom panel) mutations localized onto the apo high-resolution structure of TRPV1. Temperature mutations are in red. Capsaicin mutations are in blue..... 70

Figure 25: Hydrophathy changes induced by mutations. (A) Histograms showing the change in hydrophathy ($\text{hydrophathy}_{\text{mutant}} - \text{hydrophathy}_{\text{WT}}$) for mutations in 'functional' clones screened with temperature or capsaicin. Data is normalized so that the sum of a bin from the 'functional' group and the respective bin from the 'less functional' group is equal to 100%. (B) Change in hydrophathy for all 1,110 temperature- and 1,145 capsaicin-characterized mutations..... 71

Figure 26: Heat sensitivity of TRPV1 single-point mutants with mutations that neutralized amino acid hydrophobicity. (A) Structural location of all the residues mutated in the ankyrin repeats and the beginning of the S4-S5 linker. In cyan are residues that when mutated to Thr, lead to non-functional channels. In purple are residues that, when mutated to Thr, do not affect temperature activation. (B) Average conductance at +160 mV as a function of temperature for mutants. Data represent mean \pm SEM. N on top of the bars represent number of individual patches. (C) Conductance-

voltage (G-V) relationship of plateau current for wild type TRPV1, V292T, L337T, I352T, and F559T at different temperatures. (D) Voltage of half maximal activation (V_{half}) for wild type TRPV1, V292T, L337T, I352T, and F559T as a function of temperature. V_{half} was obtained from the fitting parameters of a Boltzmann distribution to the G-V. Data represent mean \pm SEM. Lines are linear fits to the data. Wild type TRPV1 n = 7, V292T n = 9, L337T n = 11, I352T n = 5, and F559T n = 7. Each V_{half} value was tested for statistical significance using an unpaired Student's t-test. n.s. indicates not significant ($p > 0.05$). .75

Figure 27: Temperature sensitivity of TRPV1 triple mutants with mutations that conserved or neutralized amino acid hydrophobicity. (A) Location of the three residues mutated to amino acids that conserve or neutralize amino acid hydrophobicity. (B-D) Representative current traces (top) and conductance-voltage (G-V) curves (bottom) of plateau currents at different temperatures for wild type TRPV1 (B), V658L, I661L, L664I (C), and V658T, I661T, L664T (D) triple mutants upon voltage step protocols (-120 mV to +160 mV at 20 mV increments). Lines are fits of a Boltzmann distribution to the data. Dashed lines indicate zero current. (E) Average conductance at +160 mV and different temperatures for wild type TRPV1 and triple mutants with mutations that conserved (V658L, I661L, L664I) or neutralized (V658T, I661T, L664T) amino acid hydrophobicity. Data represent mean \pm SEM. N on top of the bars indicate numbers of individual patches. (F) Voltage of half maximal activation (V_{half}) for wild type TRPV1 and triple mutants at different temperatures. V_{half} values were obtained from the Boltzmann fitting parameters to the G-V curves. Data represent mean \pm SEM. Lines are linear fits to the data. TRPV1 n = 5, V658L, I661L, L664I n = 6, and V658T, I661T, L664T n = 7. Stars indicate statistical significance as compared to wild type TRPV1 at the specified temperature (** $p < 0.01$). n.s. indicates not significant ($p > 0.05$). (G) Representative current traces at 16°C (purple) and 25°C (cyan) from pcDNA (negative control, left), wild type TRPM8 (positive control, middle), and TRPV1 V659T, I661T, L664T triple mutant (right) transfected cells stimulated with a ± 100 mV ramp protocol. (H) Average of current change at -100 mV and +100 mV upon application of cold temperature for transfected cells on (G). Data represent mean \pm SEM. Numbers above bars indicate individual number of patches. Stars denote statistical significance as compared to pcDNA using an unpaired Student's t-test (* $p < 0.05$, *** $p < 0.005$). n.s. indicate not significant ($p > 0.05$).78

Acknowledgements

I want to thank my advisor, Jörg Grandl for experimental advice and financial support, as well as the rest of the members of the laboratory for invigorating and enlightening conversations. I also want to thank my committee for guidance over the last few years.

In addition, I want to give a special acknowledgement to Edwin S. Iversen for unconditional help on conducting extensive statistical testing for part of the work presented here.

1. Introduction

1.1 *Temperature detection circuitry*

Organisms have the capacity to accurately sense temperature. Indeed, they have developed elaborate mechanisms that allow them to react noxious temperatures to avoid detrimental effects such as protein damage, cell apoptosis, tissue damage, or even death (Brown et al., 2012; Leon and Bouchama, 2015; Tattersall et al., 2012). In mammals, a set of specialized sensory neurons mediates the conversion of thermal, as well as mechanical and chemical stimuli into action potentials that make it possible for organisms to react to environmental cues. These neurons have a pseudounipolar shape with one axon extending to the skin, mucosa, and visceral organs, while the other delivers the gathered information to second order neurons in the sensory nucleus of the brain or the dorsal horn (Vriens et al., 2014). The cell bodies of the neurons that innervate the head and face cluster their cell bodies in the trigeminal ganglia (TG), while the sensory neurons that innervate the rest of the body cluster their cell bodies in the dorsal root ganglia (DRG) (Figure 1).

of temperature, pressure, and chemical stimuli. Afferents that respond to all these stimuli are polymodal nociceptors, and are involved in the perception of pain (Figure 2).

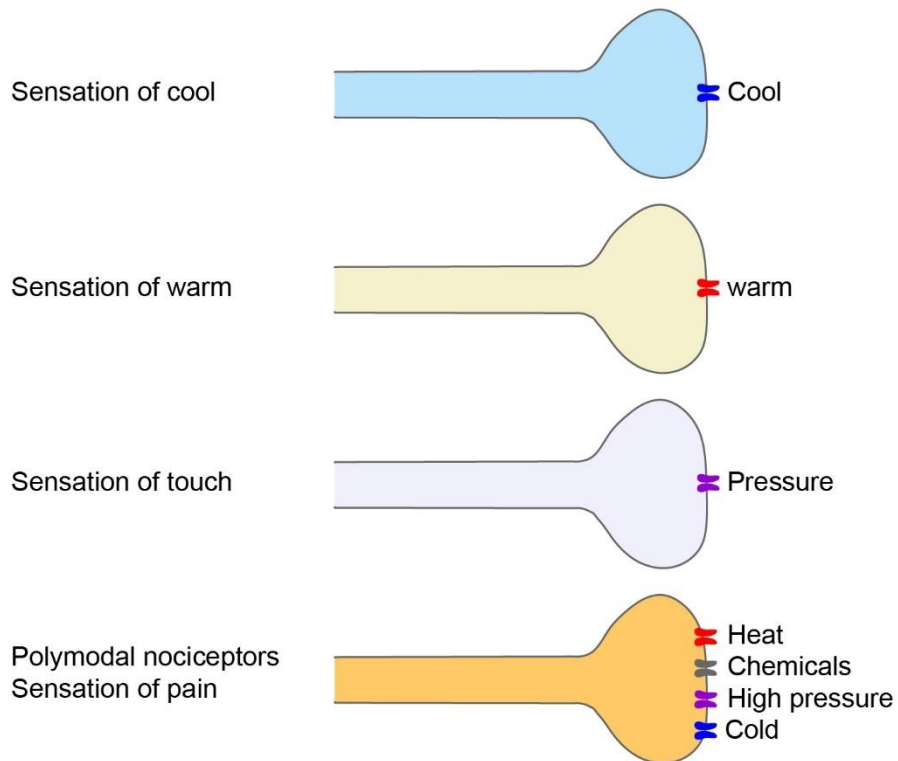


Figure 2: Sensory neurons are activated by a variety of stimuli. Illustration of axon terminals from sensory fibers activated by several physical and chemical entities.

Nociceptors are excitatory neurons that primarily communicate through the release of glutamate and other peptides including Substance P, somatostatin, and the calcitonin gene-related peptide (CGRP) (Dubin and Patapoutian, 2010). Nociceptor fibers enter the spinal cord through the intervertebral foramina and synapse in the dorsal or posterior horn of the spinal cord mostly in laminae I, II, and V (Figure 1).

There, afferents form synapses with interneurons that in turn synapse to motor neurons

to mediate an immediate response to the environmental insults such as noxious temperatures. Additionally, temperature-mediated electrical signals from the skin and visceral organs are transmitted to the preoptic area (POA) of the hypothalamus where the information is processed to mediate autonomic adaptations, such as vasodilation and shivering, that mediate thermal homeostasis (Song et al., 2016; Vriens et al., 2014).

Temperature sensitive cells are critical for the fast and acute perception of temperature. This is due to the presence of a specialized set of proteins that include transient receptor potential (TRP) ion channels and the calcium-activated chloride (TMEM16A) channel (Cho et al., 2012; Wetsel, 2011). As it will be discussed in the next section, these ion channels can be activated by hot or cold temperatures with a sub-millisecond latency making them excellent candidates for the acute sensitivity of temperature sensitive cells.

1.2 Transient receptor potential (TRP) channels

Transient receptor potential (TRP) channels were originally identified in a *drosophila* phototransduction mutant that exhibits a transient response to light (Montell and Rubin, 1989). It was described as a 1,275 amino acid membrane protein with eight putative transmembrane domains that is involved in the transduction of light by depolarizing photoreceptors in response to the photoactivation of rhodopsin (Montell, 1998; Montell and Rubin, 1989). Almost a decade later, the first TRP mammalian

homolog was identified as a receptor of capsaicin, the active ingredient in hot peppers (Caterina et al., 1997). Moreover, this channel also responded to other vanilloid-like compounds, so it was named the transient receptor potential vanilloid 1 (TRPV1) ion channel. Interestingly, TRPV1 responded to noxious heat temperatures with a threshold for activation of 42°C and a coefficient of thermal activation (Q_{10}), defined as the ratio of current increase due to a change of 10°C, of about 20 (Caterina et al., 1997; Liu et al., 2003; Tominaga et al., 1998). This makes TRPV1 about 10 to 20 times more sensitive to temperature than voltage-gated K^+ (K_v) and Ca^{2+} (Ca_v) channels (van Lunteren et al., 1993; Tiwari and Sikdar, 1999). Immunohistochemical staining of DRGs shows that TRPV1 is present in about 25% of unmyelinated (C fibers) and lightly myelinated ($A\delta$ -fibers) nociceptors that expressed proinflammatory peptides such as Substance P, as well as in non-peptidergic DRG neurons that expressed isolectin B4 (IB4) (Caterina et al., 2000). TRPV1 knock-out (TRPV1 KO) mice are virtually insensitive to capsaicin and have deficiencies in sensing noxious hot temperatures (Caterina et al., 2000). Particularly interesting is the fact that TRPV1 KO mice exhibit reduced thermal hyperalgesia, indicating that this channel may be critically involved in nociception and thermal perception.

Transient receptor potential ankyrin-repeat 1 (TRPA1) is a distantly related TRP ion channel found in unmyelinated C- and lightly-myelinated $A\delta$ -fibers that express the

calcitonin gene-related peptide (CGRP), Substance P, and most interestingly TRPV1 (Story et al., 2003). Although the role of TRPA1 on temperature sensation is rather disputed, this channel has been found to be a target for exogenous and endogenous inflammatory mediators and many noxious chemicals (Bautista et al., 2013; Caspani and Heppenstall, 2009; Macpherson et al., 2007). Additionally, TRPA1 plays a critical role on the release of neuropeptides by nociceptors. Altogether, this suggests that TRPA1 may be critically involved in the inflammatory response pathway.

Another TRP channel, TRP melastatin 8 (TRPM8), is activated by innocuous to noxious cold (<25°C) temperatures (McKemy et al., 2002). It is expressed in a small population of C-fiber nociceptors that do not overlap with TRPV1-expressing fibers (Peier et al., 2002a). Like TRPV1, TRPM8 has a Q_{10} of about 20, stressing its high temperature sensitivity (McKemy et al., 2002). TRPM8 KO mice are essentially insensitive to icillin, show an attenuated response to acetone, and have deficiencies in avoiding innocuous cold temperature, indicating that TRPM8 may be critical for sensing cold temperatures and cooling-mediating chemicals (Bautista et al., 2007; Colburn et al., 2007; Dhaka et al., 2007).

Notably, the expression of temperature sensitive channels is not restricted to DRG neurons. TRPV3 is a warm-activated TRP channel predominantly expressed in keratinocytes, the cells that form most of the epidermis (Peier et al., 2002b; Smith et al.,

2002; Xu et al., 2002). Additionally, these ion channels are sensitive to the topical anesthetic camphor (Moqrich et al., 2005; Xu et al., 2005). TRPV3 KO mice showed deficiencies sensing innocuous and noxious heat, indicating that this keratinocyte-expressed channel may also be important for sensing hot temperatures (Moqrich et al., 2005).

Structurally, temperature sensitive TRP channels have an architecture that resembles that of K_v and Na_v channels (Liao et al., 2013; Long et al., 2005; Paulsen et al., 2015; Zubcevic et al., 2016). For instance, TRP channels form tetrameric structures that have 6 transmembrane segments (S1-S6) and a central ion permeation pathway, formed by S5-S6, that is surrounded by S1-S4 (Figure 3).

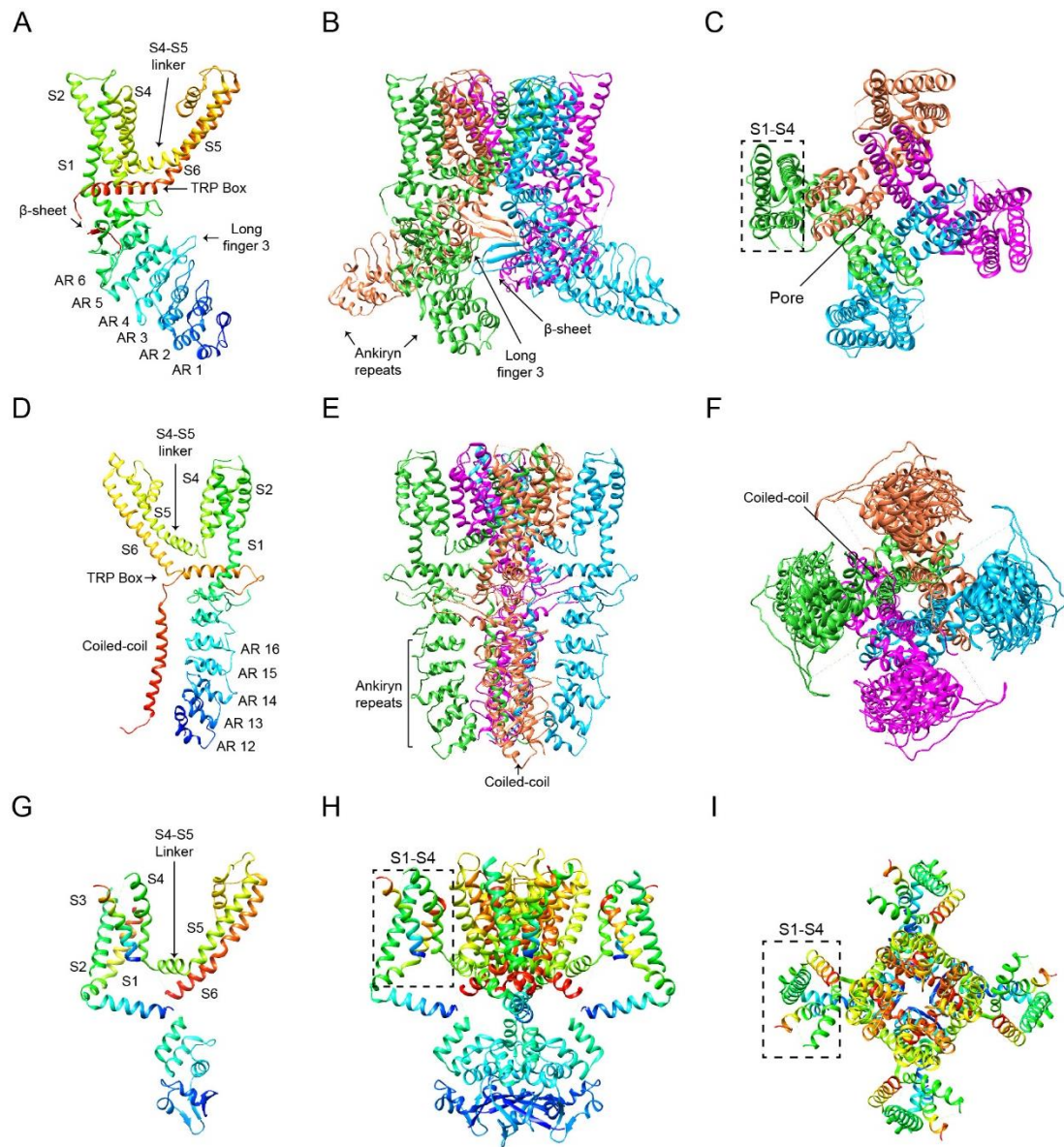


Figure 3: TRP channels are architecturally similar to K_v channels. (A-C) Monomeric (A) or tetrameric (B-C) high-resolution structure of TRPV1 (3J5P) as observed from the side (A-B) or the outside (C) of the cell. For clarity, only S1-S6 is displayed on C. (D-F) High-resolution structure of TRPA1 (3J9P) showed as a monomer (D) or tetramer (E-F). Structure on D and E is observed from the side and on F is observed from the inside of

the cell. (G-I) Monomeric (G) or tetrameric (H-I) high-resolution structure of a K_v channel (2A79) as observed from the side (G-H) or the outside (I) of the cell.

In contrast to other voltage-gated channels, TRP channels do not have amino acids with large positive charges in the S4, and thus they are about 15 times less sensitive to voltage than a K_v channel (Aggarwal and MacKinnon, 1996; Schoppa et al., 1992; Voets et al., 2007). More so, TRP channels have a longer and highly flexible N-terminus that in some channels, form multiple ankyrin repeats. Ankyrin repeats are 33 amino acid motif that are involved in cell-cell signaling, cytoskeleton integrity, inflammatory response, and transcription and cell cycle regulation (Mosavi et al., 2004; Sedgwick and Smerdon, 1999). Even though the architectures of the N-terminal of TRPV1 and TRPA1 are very different, they both bind channel activators and regulatory modulators (Figure 3). For example, many TRPA1 activators form covalent bonds with cysteines on some of the repeats, whereas ATP and calmodulin bind to residues in the repeats of TRPV1, indicating that these domains are critical for activation of TRP channels by a wide variety of substances (Julius, 2013; Lishko et al., 2007; Macpherson et al., 2007). The C-terminal of TRP channels has a peculiar and highly conserved 25 amino acid motif, called the TRP box which sits parallel to the membrane. In the homologous TRPV4, the TRP box was found to be critical for channel trafficking and tetramerization (Garcia-Elias et al., 2015).

The high-resolution structure of TRPV1 and TRPA1 show some other unique features of these channels. The structure of TRPV1 shows an interaction between residues in the S4-S5 linker and the TRP box that may be critical for the proper assembly of the channels (Garcia-Elias et al., 2015; Liao et al., 2013). Additionally, it shows that the pore has an upper and a lower gate that change conformations in response to the chemicals agonists resiniferatoxin (RTX), capsaicin, and the tarantula double-knot toxin (DkTx) (Cao et al., 2013a). On the other hand, the TRPA1 structure exhibits a central coiled-coil structure at the C-terminus that is surrounded by the N-terminal-containing ankyrin repeats arranged perpendicular to the membrane (Figure 3). The coiled-coil domain shows extensive interaction with each other and is involved in the binding of inositol hexakisphosphate (InsP₆) (Paulsen et al., 2015). Interestingly, polyphosphates are required for maintaining channel activation in excised patches, indicating that the coiled-coil domain may be involved in conserving the structural integrity of TRPA1 (Paulsen et al., 2015)

Arguably, the most fascinating property of TRP channels is their exquisite sensitivity for temperature. Currently, more than a handful of temperature sensitive TRP channels have been characterized. Notably, each of these channels is activated by either cold, warm, or hot temperatures (Figure 4).

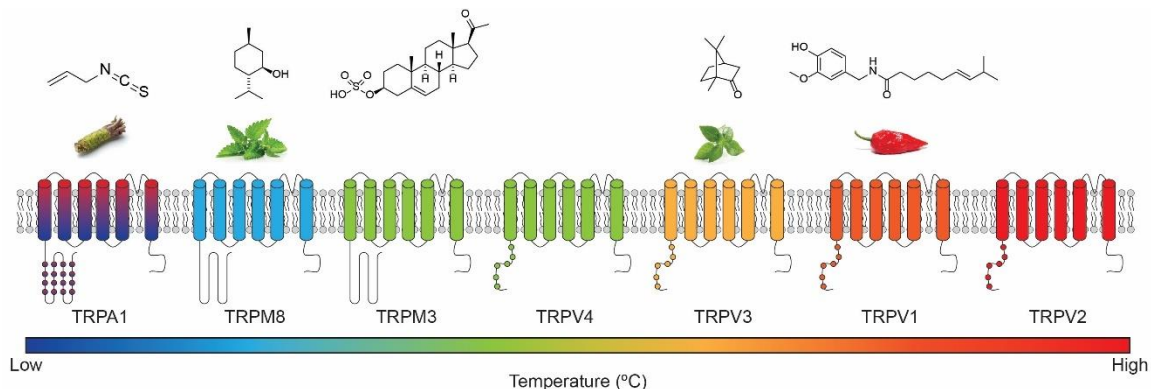


Figure 4: Temperature sensitive TRP channels. Topology models for several temperature sensitive TRP channels activated at different temperature ranges. The heat map at the bottom illustrates the temperature ranges for activation from noxious cold (deep blue) to noxious heat (red). At the top are chemical structures of some of the chemical activators of TRP channels. Circles at the N-terminal indicate the number of ankyrin repeats.

However, the molecular structures that govern temperature activation are still poorly understood. The high-resolution structures of TRPV1, TRPV2, and TRPA1 were elucidated in the presence or absence of chemical agonists and not at different temperatures and thus unfortunately do not provide any conclusive information about the molecular structures involved in temperature activation.

Although a substantial amount of work has been put into understanding how temperature activates these ion channels, the mechanism that mediates their temperature sensitivity is not known. Yet, several ideas for how temperature may lead to channel opening have been proposed and will be covered in the next section.

1.3 Potential mechanisms of temperature activation of TRP ion channels

1.3.1. TRP channels as downstream temperature sensitive molecules

It was previously proposed that temperature, instead of opening the ion channel itself, may mediate the secretion and binding of second messengers to TRP channels. Indeed, phosphatidylinositol 4,5-bisphosphate (PIP₂) was found to regulate the temperature activation of TRPV1 and TRPM8 (Fujita et al., 2013; Prescott and Julius, 2003). However, multiple studies have found that several TRP channels can be activated by temperature in inside-out patches and on artificial bilayers of several lipid compositions, indicating that second messengers are not required for temperature activation (Cao et al., 2013b; Tominaga et al., 1998; Voets et al., 2004; Zakharian et al., 2010).

An alternative mechanism suggests that TRP channels may sense temperature-induced changes in lipid membrane tension. In fact, lipid dislocation has been identified as a possible allosteric regulator of TRPV1 activation, however fundamental thermodynamic properties, such as temperature activation directionality (heat vs. cold), threshold, and sensitivity (Q₁₀ value) are determined by the protein and not the bilayer composition (Cordero-Morales et al., 2011; Gao et al., 2016; Jabba et al., 2014; Yao et al., 2011). Together, these results argue against the necessity of second messengers and

lipids for temperature activation of TRP channels, and support the idea that temperature acts directly on the channel to activate it.

1.3.2. Is temperature sensitivity of TRP channels linked to voltage activation?

Temperature sensitive TRP channels are weakly sensitive to voltage. In fact, the gating charge of TRPM8 is about 15 times lower than the Shaker channel (Aggarwal and MacKinnon, 1996; Schoppa et al., 1992; Voets et al., 2007). Voets and colleagues beautifully demonstrated that heat or cold temperatures shifts the voltage activation curve of TRPV1 and TRPM8, respectively (Voets et al., 2004). Specifically, they found that cooling of TRPM8 from 37°C to 15°C decreases the voltage of half maximal activation (V_{half}) by 150 mV, while heating of TRPV1 from 17°C to 40°C mediated a 200 mV decrease in V_{half} . Interestingly, current simulations using a simple two-state model, where the channels are either open or closed, recapitulated all experimental observations including the V_{half} shift induced by cooling of TRPM8 or heating of TRPV1. Furthermore, they found a 10-fold difference in the activation energies (E_a) associated with the opening and closing of these channels, a feature that seems to be unique to temperature activated channels, as the E_a associated with the opening and closing of temperature insensitive channels is about the same (van Lunteren et al., 1993; Tiwari and Sikdar, 1999). This led them to hypothesize that temperature activation works by merely modifying the voltage sensitivity of the channel, suggesting that temperature activation

is tightly linked to voltage activation. However, multiple studies have found that temperature, chemical, and voltage activation mechanisms can be molecularly and individually separated without affecting other activation modalities (Bandell et al., 2006; Chen et al., 2013; Grandl et al., 2008, 2010; Hu et al., 2009; Jordt et al., 2002, 2000). More substantial evidence against this mechanism came from Matta and Ahern who demonstrated that voltage is a partial agonist of TRPV1 and TRPM8 and that different activation modalities work to synergistically activate the channels (Matta and Ahern, 2007).

1.3.3. Temperature activation may be mediated through allosterically integrated conformational changes

Heat and cold can mediate the denaturation or unfolding of proteins (Bischof and He, 2005; Privalov, 1989). Denaturation is a process in which the structure of a protein in its ordered (folded) state is transformed into a less ordered state due to the elimination of noncovalent interactions such as hydrogen bonds (Alberts et al., 2008). As expected, this induces an increase in the disorder of the protein which is reflected as an increase in the entropy (S) of the system and measured by the change in entropy (ΔS) (Bischof and He, 2005; Privalov, 1989). This is also accompanied by a release or adsorption of energy, a quantity typically measured by the change in enthalpy of the system (ΔH).

Interestingly, temperature activation of TRP channels is accompanied by large changes in ΔH and ΔS . For example, cold activation of TRPM8 is accompanied by a $\Delta H = -122$ kcal/mol and a $\Delta S = -384$ cal/mol·K, while heat activation of TRPV1 is accompanied by a $\Delta H = 101$ kcal/mol and a $\Delta S = 315$ cal/mol·K (Brauchi et al., 2004; Yao et al., 2010a). Considering these data, with the fact that temperature, voltage, and chemicals can only partially activate TRP channels, investigators hypothesized that temperature activation of TRP channels can be mediated through temperature-induced conformational changes that are integrated and transmitted to the activation gate through a dual-allosteric mechanism (Brauchi et al., 2004; Matta and Ahern, 2007; Yao et al., 2010a). The dual-allosteric mechanism was initially developed to explain the gating of large conductance Ca^{2+} -activated K^+ (BK) channels and indicates that each activation modality (voltage, temperature, chemicals) must have a separate and independent sensor that is allosterically coupled to the channel's activation gate (Horrigan and Aldrich, 2002). Thus, an interesting implication of this model is that each activation modality must have a distinct structural domain or 'sensor' on which the agonists act upon. In the case of temperature activation, this concept makes sense as protein secondary structures differ largely in thermodynamic stability. This can lead to highly localized effects of temperature on protein conformation. Simulations of TRP channel currents using a dual-allosteric model were capable of faithfully recreating experimental observations

including temperature and chemical mediated shifts in V_{half} , stressing the possibility that these agonists activate the channel through independent mechanisms that can be allosterically integrated (Brauchi et al., 2004; Matta and Ahern, 2007; Yao et al., 2010a).

Although it is possible that this model accurately explains how temperature mediates the gating of TRP ion channels, several aspects of this model should be examined more carefully. For a protein to be allosterically modulated there needs to be a structural domain in where an agonist binds (sensor) and another distinct domain that enhances (enhancer) or influences agonist binding (Goulding et al., 1994; Tibbs et al., 1997). The molecular identities of the enhancers and certain sensors have not yet been identified. More importantly, this model assumes that ΔH and ΔS are independent of temperature, ignoring well-established knowledge that the ΔH and ΔS corresponding to changes in a protein's conformation must be temperature-dependent (Baldwin, 1986; Kautzman, 1959). This led to the consideration of other thermodynamic quantities that may help explain how temperature mediates the gating of TRP channels (Chowdhury et al., 2014; Clapham and Miller, 2011).

1.3.4. The role of heat capacity on temperature activation of TRP channels

Heat capacity is defined as the increase in energy or heat of a system with temperature, providing temperature dependence to ΔH and ΔS (Prabhu and Sharp, 2005). Cooling or heating of proteins cause changes in heat capacity (ΔC_p) that originate

from the hydration of structures (single residues, α -helices, etc.) and the formation/breaking of protein-protein interactions (Prabhu and Sharp, 2005). Hydration of structures is the most substantial contributor of cooling- and heating-mediated ΔC_p . Calorimetric studies have shown that the solvation of hydrophobic residues is associated with a $+\Delta C_p$, while solvation of hydrophilic residues is associated with a $-\Delta C_p$ (Prabhu and Sharp, 2005). ΔG as a function of temperature for a given process involving a ΔC_p can be described by a parabolic function. (Figure 5).

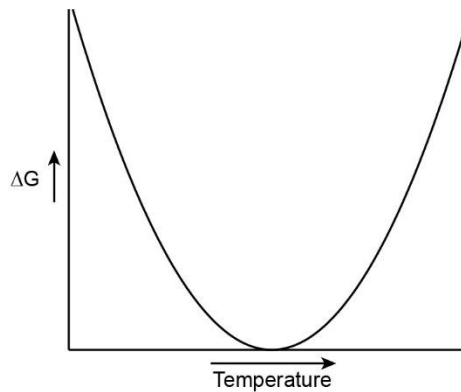


Figure 5: Temperature dependence of ΔG for an arbitrary process. Plotted is $\Delta G = \Delta H(T_0) + \Delta C_p \cdot (T - T_0) - T \cdot \Delta S - T \cdot \Delta C_p \cdot \ln(T/T_0)$, where T_0 is an arbitrarily chosen temperature.

According to the ΔG equation, the arms of the graph represent the ΔH and ΔS involved in the process, and their steepness depend on the ΔC_p (Figure 6) (Clapham and Miller, 2011).

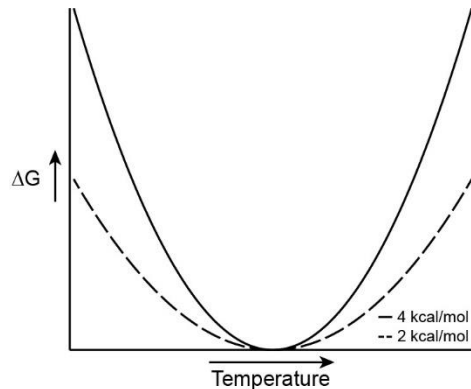


Figure 6: Temperature dependence of ΔG for two arbitrary processes with different ΔC_p . Plotted is two iterations of $\Delta G = \Delta H(T_0) + \Delta C_p \cdot (T - T_0) - T \cdot \Delta S - T \cdot \Delta C_p \cdot \ln(T/T_0)$, where T_0 is an arbitrarily chosen temperature.

Finally, the vertex of the parabola represents the temperature of the lowest change in free energy of the system.

As stated above, cooling or heating of TRP channels mediate conformational changes of the protein. Clapham and Miller reasoned that such changes will cause a large and positive ΔC_p (2-5 kcal/mol·K), originating from the exposure and hydration of a scattered population of hydrophobic residues (Clapham and Miller, 2011). A graphical representation of the $\Delta G(T)$ of a temperature sensitive channel should show a similar graph to Figure 6 with the vertex representing the temperature of minimal channel activation or T_0 . Interestingly, the steepness of the arms will indicate the temperature sensitivity of the channel, that is, the steeper the arms the higher the temperature sensitivity and the larger the Q_{10} . This indicates that the same mechanism could explain why some ion channels are more sensitive to temperature than others. This mechanism

has some interesting implications: First, it suggests that cold and heat sensitivity of TRP channels arises from the same type of conformational changes. Second, it implies that every temperature-sensitive channel must be activated by both cold and heat. Third, it indicates that there is not a coherent and distinct temperature sensor, but rather that temperature sensitivity originates from the coordinated exposure of several hydrophobic residues to solvent during temperature-mediated gating. Nevertheless, no channel with dual-temperature activation has ever been identified. Possibly, the reason for this is that the T_0 of different channels is positioned at temperatures that shift the activation curve so that only one arm of the graph can be measured (Figure 7).

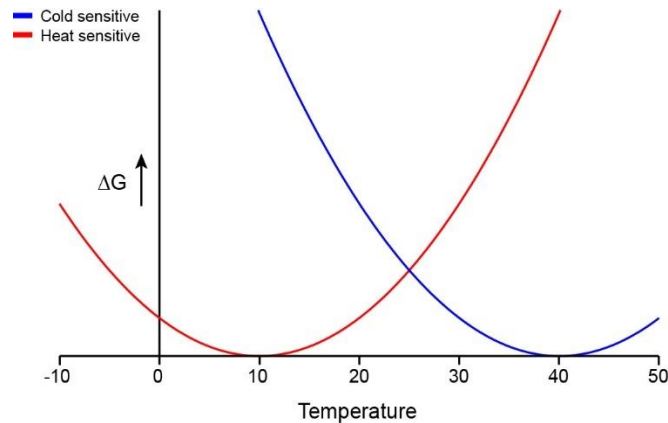


Figure 7: Temperature sensitivity of two arbitrary cold or heat sensitive ion channels. Plotted is two iterations of $\Delta G = \Delta H(T_0) + \Delta C_p \cdot (T - T_0) - T \cdot \Delta S - T \cdot \Delta C_p \cdot \ln(T/T_0)$, where T_0 is an arbitrarily chosen temperature.

Interestingly, Chowdhury and colleagues engineered a temperature insensitive K_v channel to become sensitive to cold or heat by introducing hydrophobic mutations into residues that may interact with water during gating (Chowdhury et al., 2014). Although

this is a strong conceptual demonstration, evidence supporting this mechanism in TRP channels is still lacking.

1.4 Summary

Temperature sensitive TRP channels are extraordinary molecular machines activated by a variety of chemicals, voltage, and temperature. These channels are expressed in DRG nociceptors where they play pivotal roles in the perception of noxious chemicals and temperature. One of their most fascinating features is their exquisite sensitivity for temperature. Yet, the structures and mechanisms that mediate their temperature activation are still not well understood. The work presented here approaches these questions using a variety of approaches that include: chimeric channels, random mutagenesis, high-throughput screening, massive parallel (next generation) sequencing, and single-point mutation analysis. My work suggests that there are no independent temperature sensors and demonstrate that temperature activation of TRP channels is strongly dependent on the amino acid hydrophobicity of amino acids present in the channels.

2. Determination of the minimal structures for temperature activation of TRP channels

2.1 Introduction

Generally, ion channels have a modular architecture, with distinct structures for specific channel functions, such as voltage sensors, ligand binding pockets, or pore domains, suggesting the existence of a distinct temperature sensor domain (Aggarwal and MacKinnon, 1996; Bandell et al., 2006; Doyle et al., 2013; Seoh et al., 1996). TRP channels were assumed to follow this paradigm because they have high structural similarity to voltage-gated potassium (K_v) and sodium (Na_v) channels (Latorre et al., 2007; Liao et al., 2013). This concept is also supported by the fact that protein secondary structures differ substantially in thermodynamic stability, which can lead to highly localized effects of temperature on protein conformation (Haltia and Freire, 1995; White and Wimley, 1999). Following this concept numerous researchers have tried to elucidate the identity of the 'temperature sensor' using mutagenesis and chimeric approaches. High-throughput mutagenesis identified three residues in the outer pore domain of TRPV1 (N628, N652, and Y653), TRPV3 (I644, N647, and Y661), and TRPA1 (G878) that are specifically required for temperature activation (Figure 8) (Chen et al., 2013; Grandl et al., 2008, 2010). Stressing the importance of the outer pore domain towards temperature sensitivity of TRP channels, Kim and colleagues found that temperature mediates conformational changes of single amino acids in the outer pore domain of TRPV1 (A657 and Y653) and TRPV3 (I652 and L655) (Kim et al., 2013). Interestingly, the

high-resolution structure of TRPV1 in the presence of chemical agonists show that channel activation involves rearrangements in the outer pore domain and dilation of structures in the lower gate, while transmembrane segments 1-4 (S1-S4) remain stationary suggesting that the S1-S4 segment may not be required for channel activation (Cao et al., 2013a). Altogether, this suggests that structures for temperature sensing may be localized to the pore domain of TRP channels and that structures outside the pore may not be required for channel activation. However, the N-terminal domain has also been associated with temperature activation of TRP channels. Analysis of *drosophila* TRPA1 isoforms and chimeric constructs between TRPA1 orthologues and between TRPV1 and TRPV2 implicate different portions of the N-terminal domain in the modulation of temperature activation threshold and the thermal sensitivity coefficient (Q_{10}) (Figure 8) (Cordero-Morales et al., 2011; Kang et al., 2012; Yao et al., 2011; Zhong et al., 2012). In addition, work from our laboratory identified single point mutations that invert the temperature activation of mouse TRPA1 from cold to heat (Jabba et al., 2014).

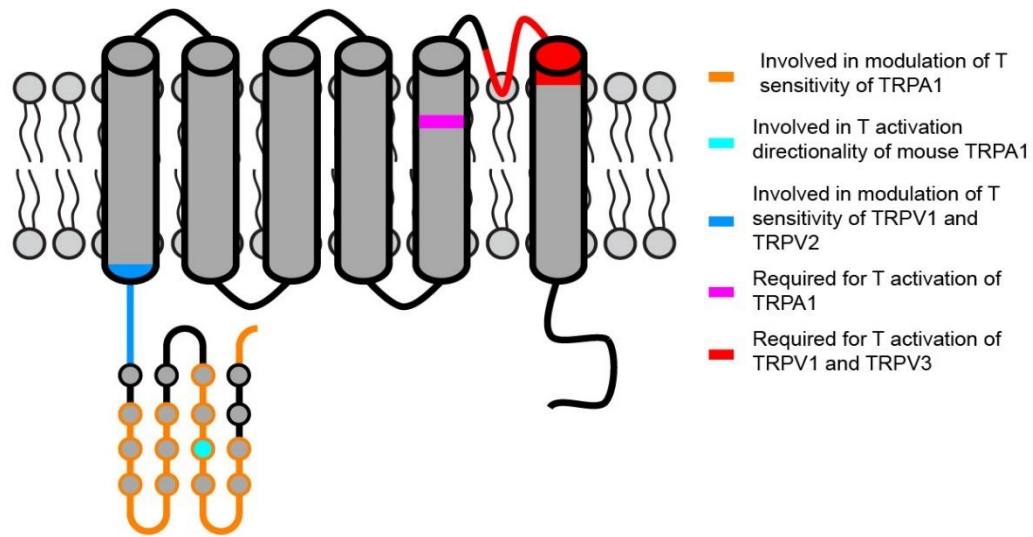


Figure 8: Structural domains involved in the temperature activation of TRP channels. Orange, cyan, and blue indicates domains involved in the modulation of temperature sensitivity of TRPV1, TRPV2, and TRPA1. Magenta and red highlight structures required for temperature activation of TRPA1, TRPV1, and TRPV3.

Together, these studies suggest that the N-terminal of TRP channels may be involved in the temperature activation machinery and that some temperature sensitivity could reside outside the pore. Though all the above studies determine structures or residues required for temperature sensitivity, none of them determined residues that are sufficient for thermal activation.

To study the sufficiency of protein structures for functionalities, truncated or ‘minimal’ proteins are commonly used. For example, a minimal ‘pore-only’ sodium channel made by deleting TM1 to TM4 of each of its four domain was found to permeate ions, albeit with different ionic permeation properties when compared to the full-length channel, and to be sensitive to veratridine, a chemical activator of Na⁺ channels (Chen et

al., 2002). Similar deletion approaches were also used on TRP channels. For example, deletion of the N-terminus (M1-P109), 15 residues between S5 and the pore helix loop, and the C-terminus (N765-K838) of TRPV1, or the complete N-terminus of human TRPA1 did not affect temperature activation, demonstrating that truncated constructs of TRP channels can retain the temperature activation properties of the full-length ion channel (Figure 9) (Liao et al., 2013; Moparathi et al., 2014; Yao et al., 2010b).

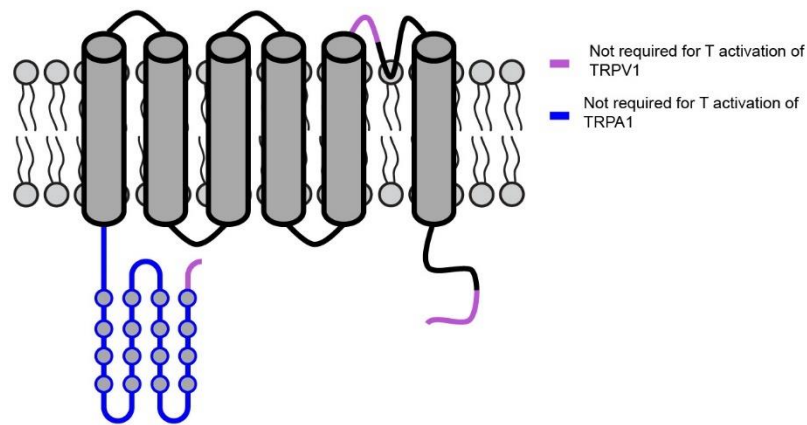


Figure 9: Structural domains not required for temperature activation of TRP channels. In purple are domains not required for temperature activation of TRPV1, whereas in blue is a domain that is unnecessary for temperature activation of TRPA1.

Together, these demonstrate that minimal constructs can be used to study the structure-function relationship of different families of ion channels, including TRP ion channels.

Inwardly-rectifying K^+ channels play a critical role in maintaining the resting membrane potential of many excitable and non-excitable cells (Hibino et al., 2010). This superfamily of ion channels is formed by 7 subfamilies that are characterized by their rectification strengths and ability to be regulated by second messengers (Bichet et al.,

2003; Hibino et al., 2010). Structurally, these ion channels are tetramers that have only two transmembrane segments that flank the ion permeation pathway forming an inverted tepee (Figure 10).

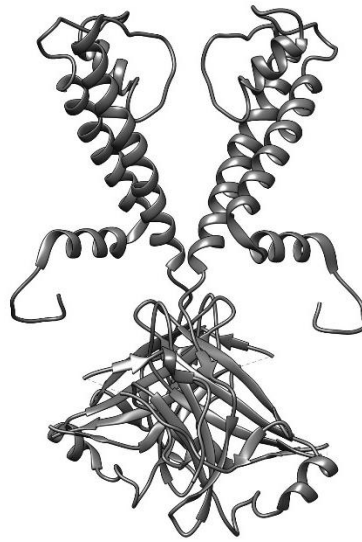


Figure 10: Structure of a K_{ir} ion channel. Structure of a bacterial K_{ir} channel from *Burkholderia pseudomallei*. For clarity, only two subunits are displayed. Structure illustration was made on Chimera (UCSF) using the PDB (1P7B) coordinates.

The $K_{ir2.x}$ subfamily is formed by constitutively active, strong rectifier ion channels which activity is not regulated by any signaling molecules or temperature (Hibino et al., 2010). Notably, the inward rectification comes from the intracellular block by Mg^{2+} and polyamines that bind to negatively charged residues on the second transmembrane segment (D172) and the C-terminal (E224 and E299 (Kubo and Murata, 2001; Yang et al., 1995)). The structural simplicity of $K_{ir2.x}$ channels, coupled with the lack of regulation by signaling molecules or temperature make these channels prime candidates for forming chimeric channels where only the pore is present.

Here, we made minimalistic ‘pore-only’ chimeric channels of TRPV1 to measure the sufficiency of the pore of TRPV1 for temperature activation. Also, we took a similar approach to test the contribution of structures outside the pore towards temperature activation. We found that none of the 16 constructs we made were functional indicating that more structurally inclusive approaches should be used to test the sufficiency of structures for temperature activation of TRP channels.

2.2 Materials and Methods

2.2.1 Engineering of chimeric constructs

‘Pore-only’ chimeric constructs were made between mouse Kir2.1 and rat TRPV1. To identify aligning residues between the pore of mouse Kir2.1 and rat TRPV1 we made sequence alignments between the pore domains of both channels and used the aligning residues as transition points to ligate the N- and C-terminus of mouse Kir2.1 to the pore domain of TRPV1. cDNA coding for the pore domains was synthesized (Genewiz, Inc.) and subcloned into a pcDNA 3.1 vector using XhoI and Bsp119I restriction enzymes. To engineer chimeric constructs of TRPV1 ion channels bearing the pore domain of mouse Kir2.1 we took an identical approach to the one detailed here for ‘pore-only’ chimeras. After ligation, all constructs were verified by full-length sequencing.

2.2.2 Cell culture

Chinese hamster ovary (CHO) cells were cultured in Ham’s F-12K Media (Life Technologies) supplemented with 10% heat-inactivated fetal bovine serum (Life

Technologies), 50 units/mL penicillin (Sigma), and 50 mg/mL streptomycin (Sigma).

Twenty-four to forty-eight hours before recording, cells were seeded onto 10 mm glass coverslip (Warner Instruments) and transiently transfected with wild type TRPV1, a chimeric channel, or pcDNA 3.1 (empty vector) using Fugene 6.0 (Promega) following the manufacturer's protocol in the presence of 10 μ m ruthenium red (a pore blocker).

Cells were co-transfected with GFP as a fluorescent reporter.

2.2.3 Electrophysiology

Patch-clamp recordings were performed using an EPC10 amplifier and Patchmaster software (HEKA Elektronik) in the whole cell configuration. Data was sampled at 5 kHz and filtered at 2.9 kHz. Borosilicate glass pipettes (Sutter Instruments) had a resistance of 2-5 M Ω when filled with pipette buffer containing (in mM): 140 KCl, 1 EGTA, 10 HEPES, pH = 7.4 with KOH. The bath buffer was composed of (in mM): 140 NaCl, 1 EGTA, 1 MgCl₂, 10 HEPES, pH=7.4 with NaOH. The bath buffer was applied through a gravity-driven perfusion system and temperature-controlled using a CL-100 temperature controller (Warner Instruments) and a SC-20 dual in-line heater (Harvard Apparatus). Temperature near the cell of interest was monitored using a TA-29 thermistor placed near the patched cell. Cells were recorded with a 200 ms voltage ramp protocol from -100 mV to +100 mV while increasing the temperature from 25°C to 40°C and then back to 25°C. Plateau currents at +100 mV were analyzed before (25°C), during (40°C), and after (25°C-2) the temperature ramp.

For measuring capsaicin activation of chimeric constructs transfected cells were recorded before, during, and after application of 1 μ M capsaicin with a 200 ms, \pm 100 mV ramp. Capsaicin activation experiments were conducted at room temperature (\sim 21°C).

2.2.4 Data analysis

Electrophysiological data were analyzed using Igor Pro (WaveMetrics). Graph plots were made with Igor Pro (WaveMetrics) and Prism (GraphPad). Illustrations were made on Illustrator (Adobe Systems).

2.3 Results

2.3.1 Identification of aligning residues in the pore domain of TRPV1 and inwardly rectifying K⁺ (K_{ir}) ion channels

Previous work identified residues in the pore of TRPV1, TRPV3, and TRPA1 that are required for temperature activation of these channels, suggesting that temperature sensing structures may be localized to the pore domain. However, it is not known if the pore is sufficient to confer temperature activation to these channels. To test the sufficiency of the pore we made a set of chimeric channels where the pore of TRPV1 was ligated to the N- and C-terminal of a temperature insensitive K_{ir} ion channel (Figure 11).

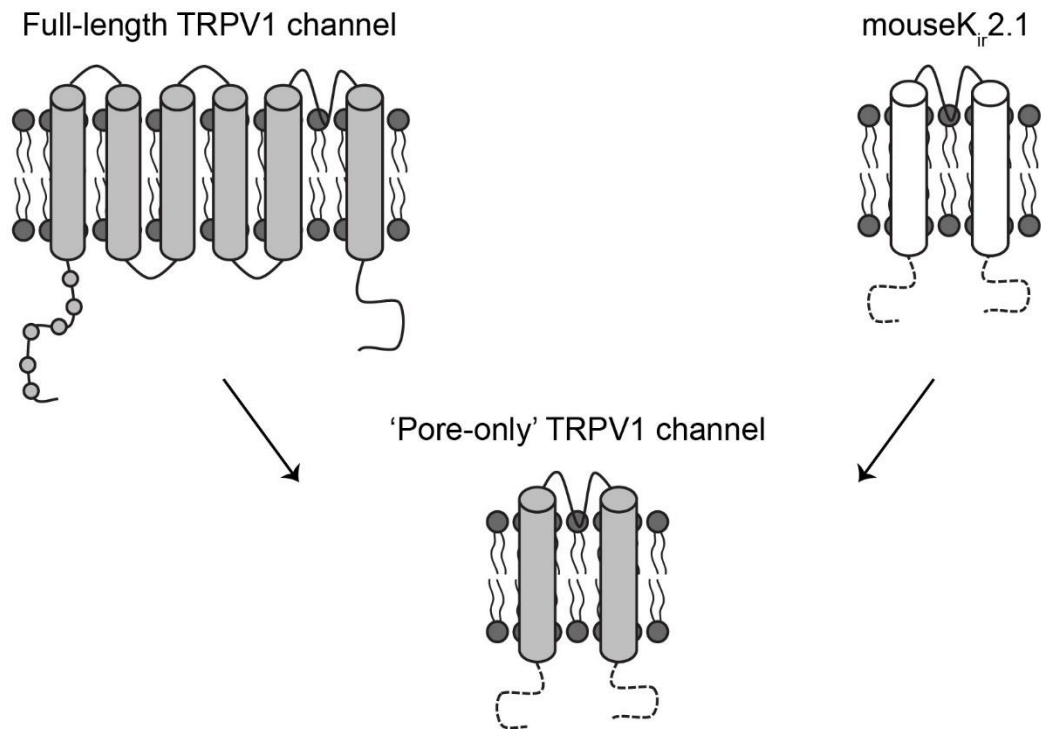


Figure 11: Illustration of 'pore-only' TRPV1 chimeric channels. Representation of the approach used to make TRPV1 'pore-only' chimeric channels.

Although previous work points towards the pore as the domain where temperature sensing structures are located, we also wanted to measure the contribution of all the structures outside the pore to overall temperature sensitivity. Specifically, we made a group of chimeric constructs where different portions of the pore domain of TRPV1 were swapped by the corresponding portion of the pore of a temperature insensitive K_{ir} ion channel (Figure 12).

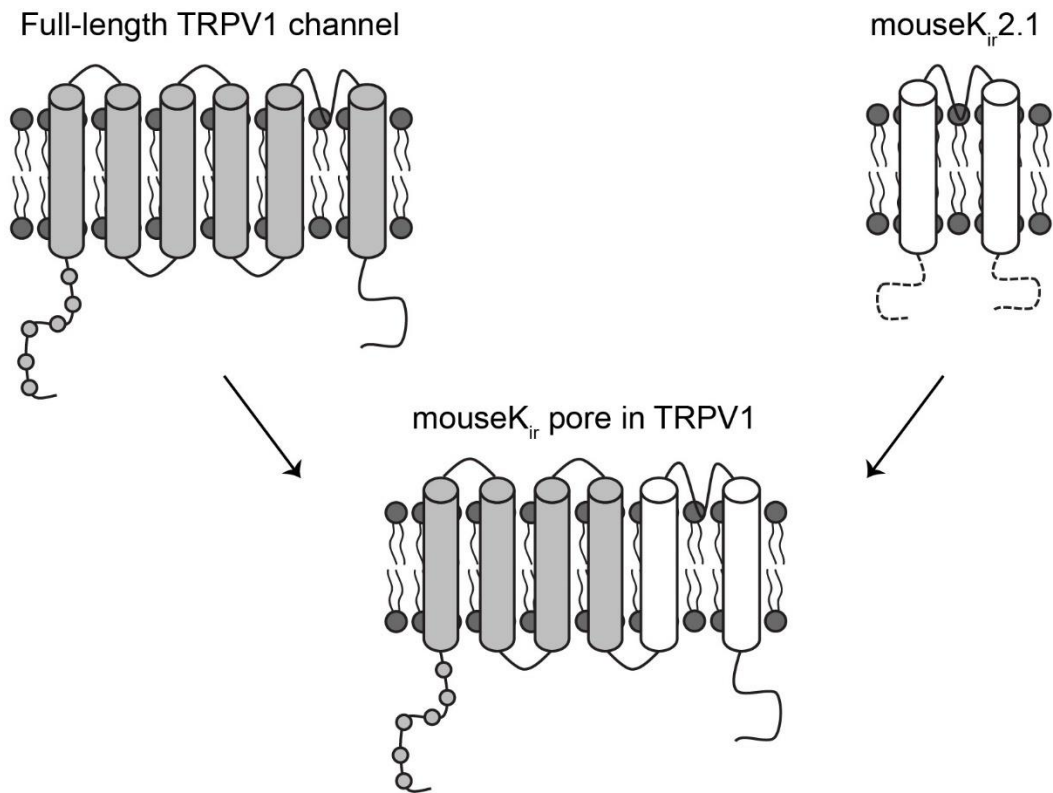


Figure 12: Illustration of TRPV1 chimeric channels with the pore swapped by the K_{ir} pore. Representation of the approach used to build chimeric constructs where the TRPV1 pore was replaced by the mouse K_{ir} pore.

Inwardly rectifying potassium 2.1 channels are particularly convenient for our experiment because of their very low temperature sensitivity and overall architecture. In addition, the N- and C-terminal of K^+ channels have been found to be important for heteromerization and transport of the channel to the membrane (Li et al., 1992; Schulteis et al., 1996; Vivienne Shen et al., 1993). Thus, addition of these domains in our constructs should ensure proper folding, expression, and incorporation of chimeric ‘pore-only’ channels into the membrane. While sequence alignment between the pore of rat TRPV1 and mouse $K_{ir}2.1$ channels show that at the sequence level these domains are not

homologous (23% homology), high-resolution structures of TRPV1 and Kir2.2 show that these channels share a similar architecture, suggesting that their structures may be complementary (Liao et al., 2013; Tao et al., 2009). Careful examination of sequence alignments shows that several residues before and throughout the pore are homologous (Figure 13). Interestingly, these residues are also conserved between different members of the TRP and the Kir family of ion channels indicating that they may be important for ion channel function. To keep the structure of the pores as intact as possible we used aligning residues before (S5) and after (S6) the pore as transition positions between TRPV1 and Kir2.1.

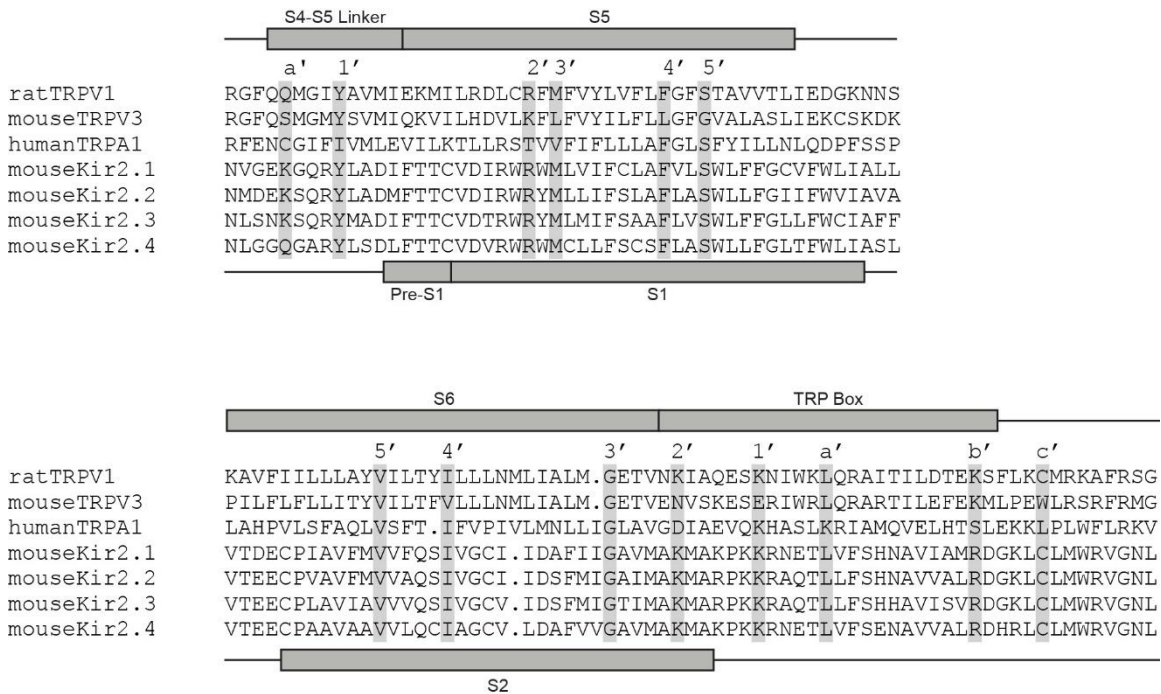


Figure 13: Sequence alignment of S5 and S6 of several TRP channels and S1 and S2 of several Kir2.x channels. Top: Sequence alignment between S5 of rat TRPV1, mouse TRPV3, human TRPA1, and S1 of mouse Kir 2.1 – 2.4. Bottom: Sequence alignment between S6 of rat TRPV1, mouse TRPV3, human TRPA1, and S2 of mouse Kir 2.1 – 2.4.

Boxes on top indicate the topology of TRPV1 according to the high-resolution structure. Boxes at the bottom indicate the topology of Kir2.2 according to the high-resolution structure of chicken Kir2.2. Letters (a', b', c') and numbers (1', 2', 3', 4', 5') on top of the alignment indicates aligning residues that can potentially be used as intercrossing positions for making chimeric constructs. Sequence alignments were made by hand.

These led to a total of 16 chimeric constructs between rat TRPV1 and mouse Kir2.1

(Figure 14). To eliminate inward rectification of the Kir portion of the constructs we introduced mutations E224G and E299S found to abolish ion channel rectification (Kubo and Murata, 2001; Yang et al., 1995).

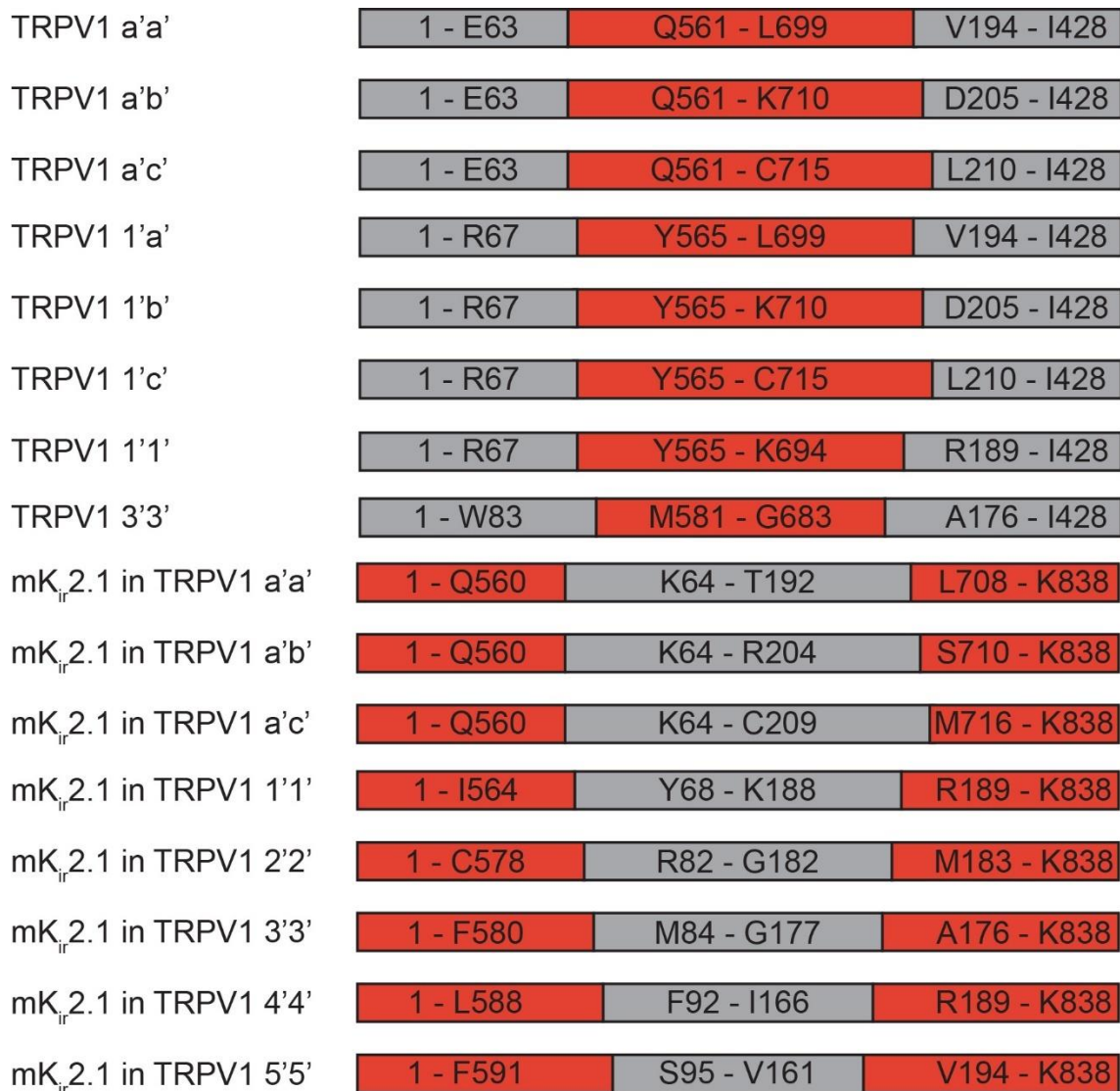


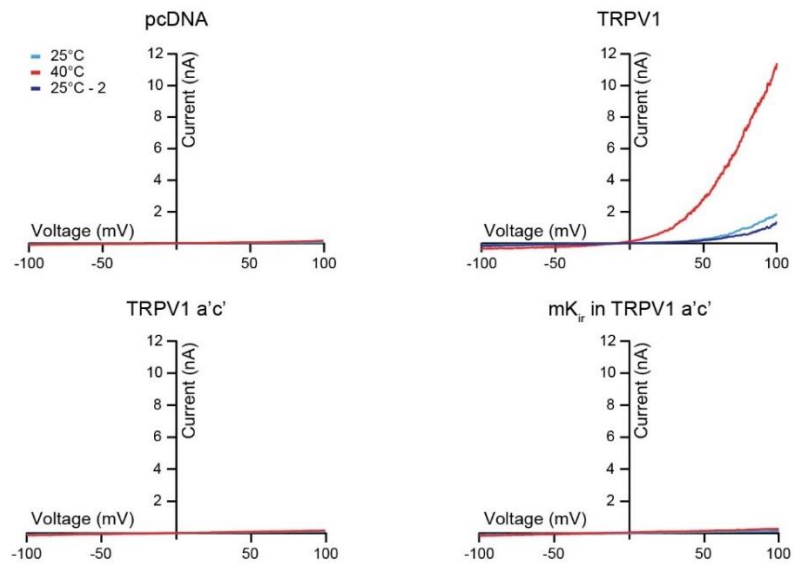
Figure 14: Schematic representation of chimeric constructs. List of chimeric constructs made for measuring temperature sensitivity in or outside the pore of TRPV1. Bars are not at scale. m is mouse, red is TRPV1, gray is mouse K_v2.1.

Altogether, this approach will allow us to test the contribution of the pore or structure outside of it towards temperature sensitivity without the influence of other temperature sensitive structures.

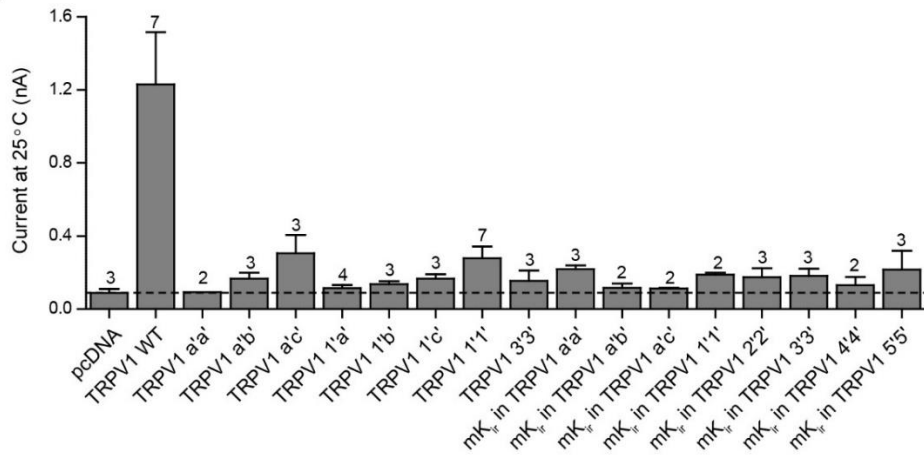
2.3.2 Chimeric channels are insensitive to voltage, temperature, and chemicals

To characterize the activation properties of chimeric channels Chinese hamster ovary (CHO) cells were transfected with each of the 'pore-only' chimeric constructs. To measure their temperature sensitivity, cells were challenged with a heating ramp from 25°C to 40°C while current was monitored with a ± 100 mV ramp. As expected, at 25°C TRPV1-transfected cells show large outwardly-rectifying currents that were not present in pcDNA- (vector) transfected cells (Figure 15A-B). Moreover, raising the temperature of the bath from 25°C to 40°C caused massive activation of TRPV1 as measured by a large increase in outward current and an average current fold change of about 8x (Figure 15A and C). However, cells transfected with any of the 16 chimeric constructs showed currents at 25°C that were similar to pcDNA levels (Figure 15A-B). Moreover, increasing the temperature of the bath to 40°C did not induced any increase in channel activation (Figure 15A and C). Indeed, average current fold changes for all chimeric-transfected cells were similar to pcDNA-transfected cells (Figure 15C).

A



B



C

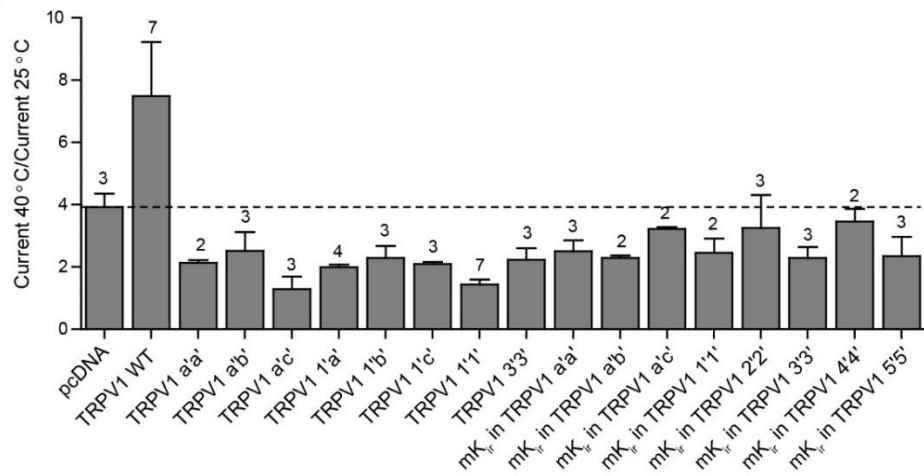


Figure 15: Temperature activation of TRPV1 chimeric channels. (A) Representative current-voltage (I-V) plots for pcDNA, TRPV1, TRPV1 a'c', and mouse Kir in TRPV1 a'c' before (25°C), during (40°C), and after (25°C - 2) a heating. (B) Average current at 25°C and +100 mV for chimeric channels. (C) Average current fold changes at +100 mV for chimeric channels tested with a heating ramp from 25°C to 40°C. Data represent average \pm SEM. Numbers on top of bars indicate the total number of individual patches. Dashed line indicates pcDNA levels.

To test if chimeric channels retain any sensitivity to TRPV1 agonists, patch-clamp experiments were conducted in chimeric-transfected cells in the presence or absence of capsaicin. Because the capsaicin binding site is located in S2 and S3 residues, only chimeric channels that retained those structures (mKir in TRPV1) were tested (Jordt et al., 2002). Whole-cell recordings show that application of capsaicin to TRPV1-transfected cells induced large increases in current with an average fold increase of about 12x (Figure 16). However, cells transfected with chimeric channels had virtually no increase in current upon application of capsaicin (Figure 16). Altogether, this suggested that all chimeric channels are not functional.

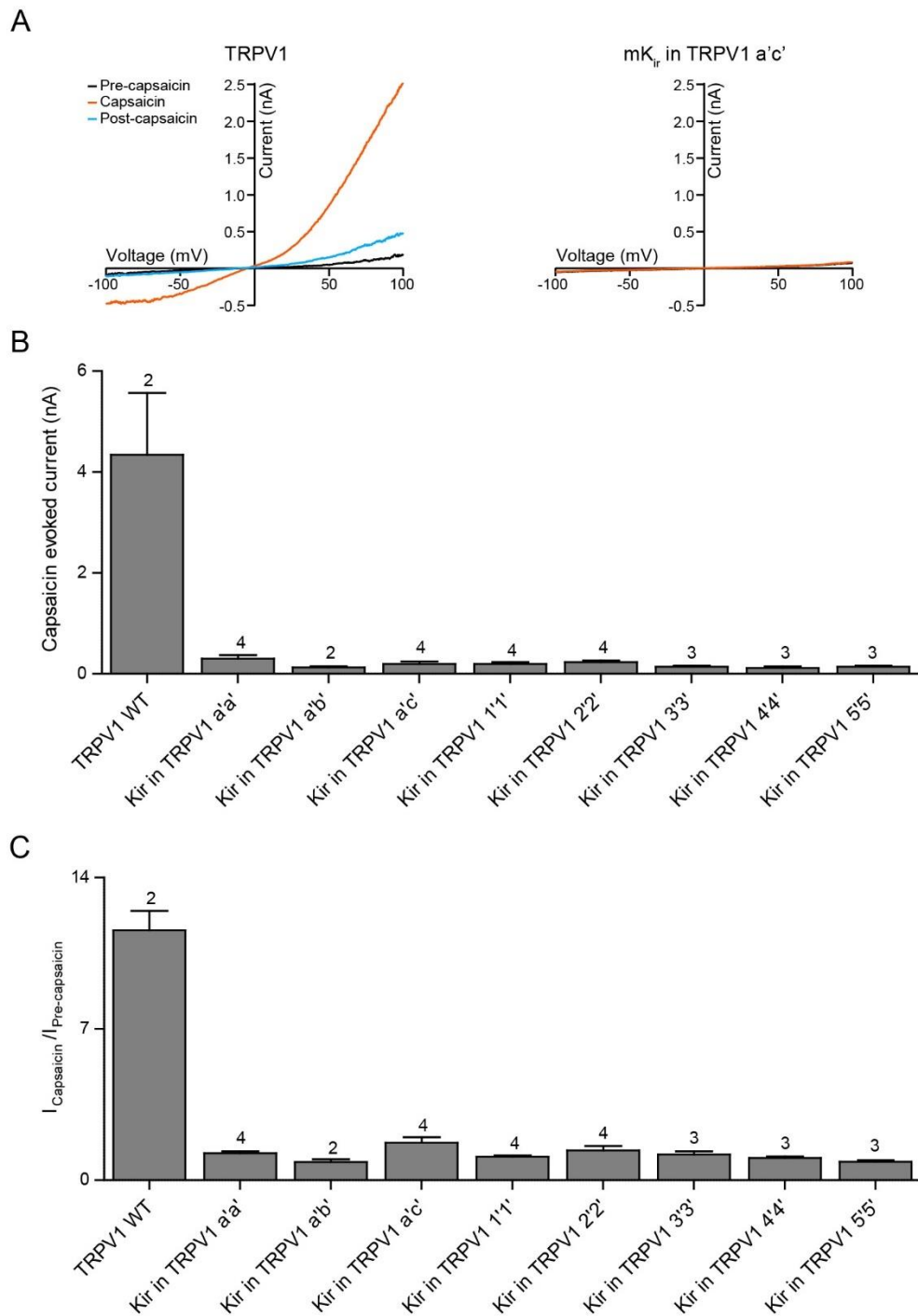


Figure 16: Capsaicin sensitivity of TRPV1 chimeric channels. (A) Representative I-V plots for TRPV1 and mouse Kir in TRPV1 a'c' before (pre-capsaicin), during (capsaicin), and after (post-capsaicin) application of 1 μ M capsaicin. (B) Average current at =100 mV during application of capsaicin for chimeric channels. (C) Average current fold change

at +100 mV for chimeric channels tested with a capsaicin pulse. Data represent average \pm SEM. Numbers on top of bars indicate the total number of individual patches.

2.4 Discussion

We sought to study the sufficiency of the pore of TRPV1 for conferring temperature activation to the channel. To study this, we made a set of 8 different chimeric channels in which the pore of TRPV1 was ligated to the N- and C- terminals of the temperature insensitive Kir2.1 channel. Furthermore, to measure the contribution of structures outside the pore towards temperature sensitivity, we made another 8 chimeric constructs by replacing different portions of the TRPV1 pore with the equivalent portion of a Kir2.1 ion channel. While chimeric approaches are commonly used to study the structure-function relationship of the domains of proteins, including TRP channels, none of the chimeric constructs reported here yielded ion channels that were activated by voltage, heat, or capsaicin indicating that all constructs were non-functional.

There are several reasons that could explain why this approach did not work. For instance, it is possible that elimination of TRPV1 structures affects the proper assembly of the chimeric channels. In fact, the high-resolution structure of TRPV1 exhibits extensive inter- and intra-subunit interactions between several domains, many of which are not present in our 'pore-only' chimeric channels. For example, the S1-S4 domains exhibit extensive hydrophobic interactions between residues of the same subunit (Liao et al., 2013). It is hypothesized that these interactions are critical for packing of the channel and may also help the S1-S4 domain to serve as an anchor to enable channel

gating through movement of the S4-S5 linker (Cao et al., 2013a; Liao et al., 2013). Moreover, several residues in the TRP box domain form electrostatic interactions with residues in the S4-S5 linker and pre-S1 helix. Most notably, an interaction between the long finger of the ankyrin repeat 3 and the inner helices of ankyrin repeat 3 and 4 with an antiparallel β -sheet formed by the linker domain of the same subunit and the C-terminal of an adjacent subunit is proposed to be critical for assembly and maintenance of the structural integrity of the cytoplasmic part of the channel (Figure 3A-B) (Liao et al., 2013). However, a key interaction between residue W697 on the TRP box and residue F559 at the S4-S5 linker was missing in several of the chimeric channels where the pore of TRPV1 was replaced with the pore of the Kir2.1 channel (Figure 14). Clearly, this indicates that the structure of TRPV1 is very complex and that the conservation of inter- and intra-subunit interactions must be achieved to obtain functional chimeric channels.

Another possibility for non-functionality of the chimeric channels may be desensitization. In fact, TRPV1 is known to desensitize at a relatively fast rate. While it is well known that this mechanism requires the presence of calcium ions, little is known about the molecular structures that mediates it. Thus, it is possible that chimeric constructs formed functional channels that desensitize very quickly, and therefore we were unable to capture channel activation with our experimental setup. Although we tried to diminish channel desensitization using calcium-free buffers, it is still possible that the channels are desensitizing through unknown mechanisms.

Evidently, temperature activation of ion channels is a very complicated phenomenon that requires the use of more structurally inclusive approaches. One potentially effective approach is the use of random mutagenesis paired to functional screening and next generation sequencing (NGS). This combinatorial approach has already been successfully used to study the structure-function relationship of regulatory RNA sequences, antibodies, enzymes, and receptors (Bill et al., 2014; Holmqvist et al., 2013; Starita et al., 2013; Traxlmayr et al., 2012).

3. The role of ankyrin repeat 6 on modulating temperature activation directionality of *drosophila* TRPA1

3.1 Introduction

Transient Receptor Potential Ankyrin 1 (TRPA1) is the sole member of the TRPA family of ion channels. Similar to other TRP channels, it has six transmembrane domains, a relatively short C-terminal domain, and a longer N-terminal domain (Story et al., 2003). However, in contrast to other TRP channels TRPA1 has a very characteristic N-terminal domain that, in humans, has 16 ankyrin repeats (Paulsen et al., 2015). TRPA1 can be activated by depolarizing membrane potential voltages and a wide variety of nucleophiles that form bonds with cysteines within the ankyrin repeats (Julius, 2013; Macpherson et al., 2007). Interestingly, some orthologues of TRPA1 can be activated by cold, while others are by heat. For example, mouse TRPA1 and *C. elegans* TRPA1 are both cold-activated in the presence of calcium, while green anole lizard TRPA1, western clawed frogs TRPA1, rattlesnake TRPA1, rat snake TRPA1, and *drosophila* TRPA1 are all heat-activated (Chatzigeorgiou, M., Yoo, S., Watson, J.D., Lee, W.H., Spencer, W.C. et al., 2010; Gracheva et al., 2010; Karashima et al., 2017; Kurganov et al., 2014; Saito et al., 2012; Story et al., 2003). On the other hand, human TRPA1 is arguably temperature insensitive (Knowlton et al., 2010).

Until recently, the structures responsible for temperature directionality, that is, cold versus heat activation, of TRPA1 remained a mystery. To elucidate the identity of

these structures, our laboratory took an unbiased approach that resulted in a library of 12,000 randomly mutated cold-activated mouse TRPA1 clones (Jabba et al., 2014). The library was screened with a heat stimulus that identified 7 heat sensitive clones. Patch-clamp experiments revealed that 3 mutations were individually sufficient to make cold-activated mouse TRPA1 warm sensitive. Interestingly, the mutations were localized in ankyrin repeat 6 suggesting that this repeat may serve as a modulator of temperature directionality in TRPA1 (Figure 17).

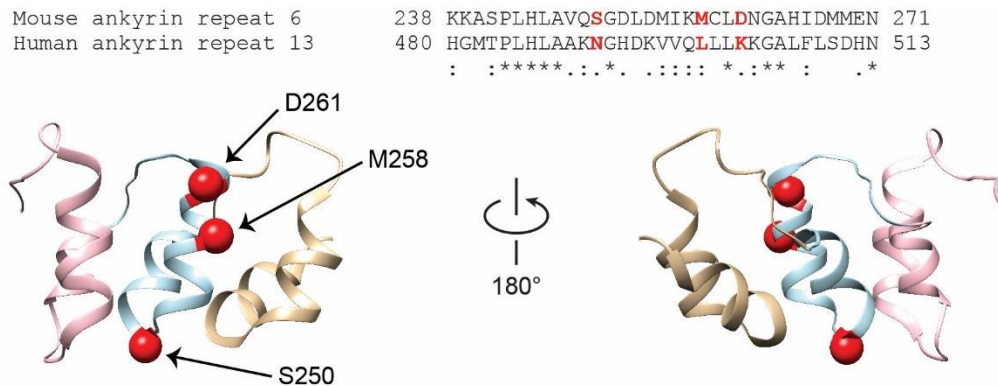


Figure 17: Residues of ankyrin repeat 6 found to invert the temperature sensitivity of mouse TRPA1 from cold to warm temperatures. Top: Sequence alignment between ankyrin repeat 6 of mouse TRPA1 and ankyrin repeat 13 of human TRPA1. In red are the residues mutated in ankyrin repeat 6 of mouse TRPA1 found to invert temperature directionality. Bottom: High-resolution structure of ankyrin repeat 12-14 of human TRPA1 (3J9P). In red are the corresponding residues to the ones identified in ankyrin repeat 6 of mouse TRPA1. In pink is ankyrin repeat 12, in cyan is ankyrin repeat 13, and in gold is ankyrin repeat 14.

Ankyrins are highly conserved 33 amino acid-long motif that fold into a short and a long antiparallel α -helices connected by a β -hairpin (Figure 17 and 18) (Mosavi et al., 2002; Sedgwick and Smerdon, 1999).

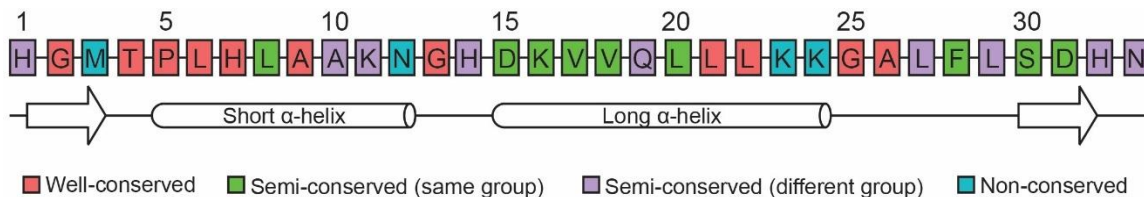


Figure 18: Topology and sequence of ankyrin repeat 13 of human TRPA1. Position of residues (Top), the level of amino acid conservation (Mosavi et al., 2002), and the topology of an ankyrin repeat (bottom) are showed.

Three or more of these motifs, connected thorough a longer hair pin loop, form an ankyrin repeat (Mosavi et al., 2002) (Figure 17). Structurally, these repeats are stabilized through extensive amino acid interactions. For example, the β -hairpin is stabilized through a hydrogen bond interaction with the semi-conserved residue in position 1 of the 33 amino acid motif (Figure 18) (Sedgwick and Smerdon, 1999). Moreover, the well-conserved TPLH motif of position 4 to 7 is stabilized by hydrogen bonding with well-conserved residues in position 6 and 9. Furthermore, stacking of the repeats is mostly achieved by hydrophobic interactions between repeats and hydrogen bonding between well-conserved and semi-conserved residues at positions 9, 16, and 31. In TRPA1, ankyrin repeat 15 and 16 formed a closely packed structure with a helix-turn-helix near the S1 that is thought to be involved in the transduction of information from the repeats to the pore (Paulsen et al., 2015). Additionally, ankyrin repeat 12 and 16 interact with the central coiled-coil domain enabling the stabilization of the intracellular portion of the channel.

Ankyrin repeats are found in many proteins. Currently, the SMART database identified more than 76,000 ankyrin repeat-containing proteins (Letunic et al., 2015; Schultz et al., 1998). They are involved in a variety of functions including cell-cell signaling, cytoskeleton integrity, inflammatory response, and transcription and cell cycle regulation (Mosavi et al., 2004). Additionally, they can serve as a place for protein-protein and protein-chemical interaction (Mosavi et al., 2004; Sedgwick and Smerdon, 1999). Indeed, in TRPA1 three ankyrin repeat cysteines were found to be required and nine others to be involved in activation of the channel by noxious nucleophiles such as mustard oil, icillin, and iodoacetamide (Macpherson et al., 2007). Additionally, chimeric constructs between TRPA1 orthologues as well as analysis of *drosophila* TRPA1 isoforms suggest that different portions of the N-terminal domain may be involved in the modulation of temperature activation threshold and Q₁₀ (Cordero-Morales et al., 2011; Kang et al., 2012; Zhong et al., 2012).

Here, we hypothesized that ankyrin repeat 6 works as a modulator of temperature activation directionality in TRPA1. To test our hypothesis, we used the heat-activated *drosophila* TRPA1 whose ankyrin repeat 6 is highly homologous to the corresponding ankyrin repeat in mouse TRPA1. Using a combination of chimeric constructs and single-point mutants we found that ankyrin repeat 6 is not able to invert the temperature directionality of *drosophila* TRPA1. Thus, our results indicate that the

mutations and mechanisms identified in mouse TRPA1 are not transferrable to the *drosophila* TRPA1 orthologue.

3.2 Materials and Methods

3.2.1 Cell culture

CHO cells were culture following the procedure detailed on chapter 2.2.2.

3.2.2 Sequence alignments

Alignment of ankyrin repeats were performed on Clustal Omega (Goujon et al., 2010; Sievers et al., 2011).

3.2.3 Site-directed mutagenesis and generation of chimeras

Single-point mutants were generated using a QuickChange Site-Directed Mutagenesis Kit (Agilent). Chimeras were engineered using overlapping PCR (Agilent). All mutants and chimeras were fully sequenced.

3.2.4 High-resolution structure illustrations

Illustration of point mutations on ankyrin repeats was made on the UCSF Chimera program using the high-resolution structure of TRPA1 (3J9P) (Paulsen et al., 2015; Pettersen et al., 2004).

3.2.5 Electrophysiology

Patch-clamp electrophysiology experiments were performed in the whole-cell configuration following the procedure detailed on chapter 2.2.3 with the following changes. Borosilicate pipettes (Sutter Instruments) had a resistance of 3 – 6 MΩ when

filled with the pipette buffer containing (in mM): 150 CsCl, 1 MgCl₂, 10 BAPTA (1, 2-bis [o-aminophenoxy] ethane-N, N, N', N'- tetraacetic acid), and 10 HEPES pH = 7.2 with CsOH. The bath solution was Ca²⁺-free and contained (in mM): 150 NaCl, 1 MgCl₂, 10 glucose, 1 EGTA, and 10 HEPES pH = 7.4 with NaOH. Cells were recorded using a ±100 mV 200 ms voltage ramp while changing the temperature from 25°C to 40°C and back to 25°C (heat experiments) or from 25°C to 13°C and back to 25°C (cold experiments). Cells were only analyzed if the initial resistance was >500 MΩ and the heat-evoked current was reduced by at least 50% upon reversal to 25°C.

3.2.6 Data analysis

Electrophysiological data were analyzed using Igor Pro (WaveMetrics). Graph plots were made with Igor Pro (WaveMetrics) and Prism (GraphPad). Statistical analysis was done using an unpaired Student's t-test on Excel (Microsoft).

3.3 Results

3.3.1 Mouse ankyrin repeat 6 is not interchangeable

We reasoned that TRPA1 orthologues with high sequence homology to the ankyrin repeat 6 of mouse TRPA1 will more likely tolerate swapping of the ankyrin repeat. We found that the ankyrin repeat 6 of cold-activated mouse TRPA1 has high sequence homology (>36%) with an ankyrin repeat of the heat-activated *drosophila* TRPA1 (Figure 19A). To test whether the ankyrin repeat 6 serves as a modulator of temperature directionality, we replaced ankyrin repeat 6 of cold-activated mouse TRPA1

with the corresponding repeat of heat-activated *drosophila* TRPA1 (mTRPA1-dmAR6). We also made another construct where ankyrin repeat 6 of heat-activated *drosophila* TRPA1 was replaced with the repeat of cold-activated mouse TRPA1 (dmTRPA1-mAR6). We hypothesized that swapping the ankyrin repeats will render cold-activated mouse TRPA1 warm sensitive and heat-activated *drosophila* TRPA1 cold sensitive.

Patch-clamp recordings of wild type *drosophila* TRPA1 expressing CHO cells showed that an increase in temperature from 25°C to 40°C mediates a robust increase in current that is not present in pcDNA-transfected cells (Figure 19B and D). Although some cells expressing mTRPA1-dmAR6 had a small outwardly rectifying current characteristic of TRPA1, cells expressing mTRPA1-dmAR6 or dmTRPA1-mAR6 show no increase in current upon application of a heat stimulus (Figure 19B and D). In fact, these cells had average current fold changes that were indistinguishable from pcDNA-transfected cells. To test if chimeric channels were sensitive to cold, transfected cells were challenged with a cold ramp from 25°C to 13°C. Similar to *drosophila* TRPA1-expressing cells, mTRPA1-dmAR6- or dmTRPA1-mAR6-transfected cells show average current fold changes that were nearly identical to cells expressing pcDNA (Figure 19C and E).

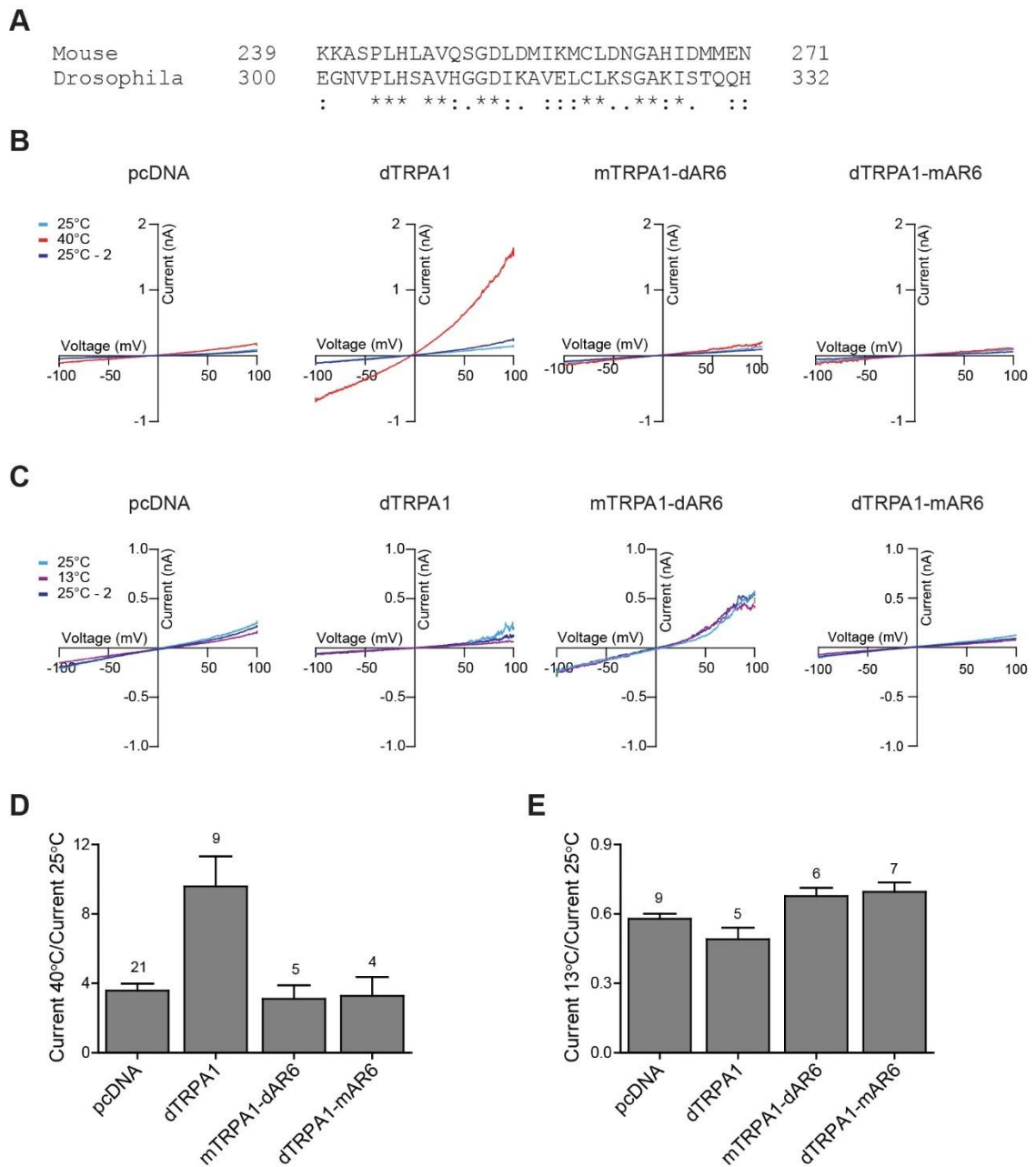


Figure 19: Temperature activation of mouse and *drosophila* TRPA1 chimeric channels. (A) Sequence alignment of ankyrin repeat 6 of mouse and *drosophila* TRPA1. (B-C) Representative current traces from pcDNA, wild type dTRPA1, mTRPA1-dAR6, and dTRPA1-mAR6 transfected cells recorded with a ± 100 mV ramp upon application of a heat (B) or cold (C) stimuli. (D-E) Average of maximal current changes at +100 mV upon application of a heat (D) or cold (E) stimuli to constructs on B and C. Data represent

average \pm SEM. Numbers on top of the bars indicate the number of individual patches. m is mouse, d is *drosophila*.

This indicates that ankyrin repeat 6 is not sufficient to invert the temperature sensitivity of the *drosophila* TRPA1 channel orthologue.

3.3.2 Mouse ankyrin repeat 6 is not interchangeable

We wondered how would the mutations found to invert temperature directionality in mouse TRPA1 affect temperature activation of *drosophila* TRPA1. Sequence alignment of ankyrin repeat 6 from mouse and *drosophila* TRPA1 shows that position S250 and L284 of mouse TRPA1 align with residues G276 and K287 of *drosophila* TRPA1, respectively (Figure 20A). We individually mutated the *drosophila* residues into the amino acids found the invert temperature directionality in mouse TRPA1 (G276N and K287G) and used patch-clamp electrophysiology to measure their effect on temperature activation. Patch-clamp recordings show that upon heat stimulation, cells transfected with *drosophila* TRPA1 channels carrying the G276N had current increases that were similar to pcDNA-transfected cells (Figure 20D). On the other hand, mutation K287G did not affect heat activation of the channel as compared to wild type *drosophila* TRPA1 (Figure 20B and D).

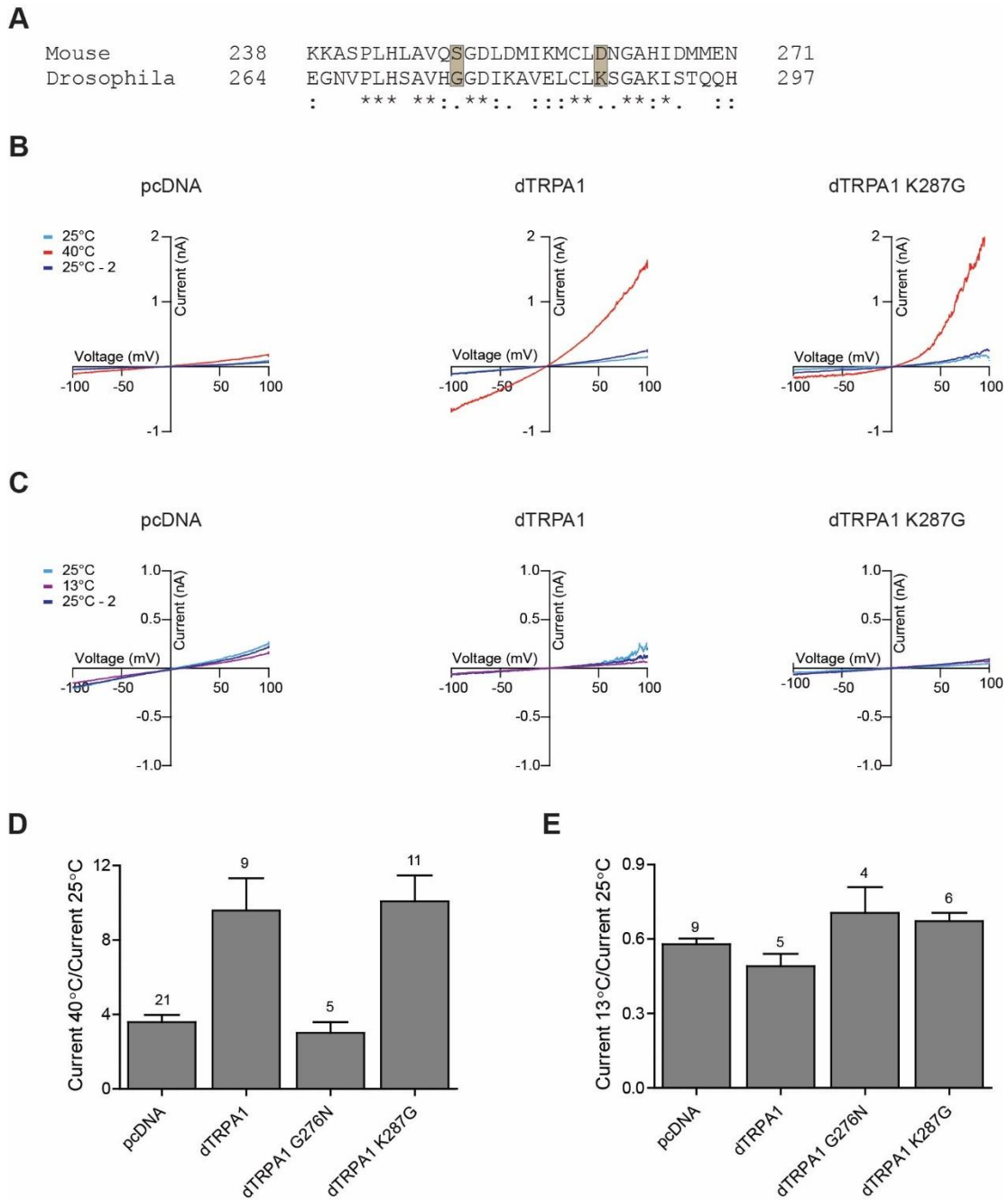


Figure 20: Temperature activation of drosophila TRPA1 single point mutants. (A) Sequence alignment of ankyrin repeat 6 of mouse and drosophila TRPA1. (B-C) Representative current traces from pcDNA, wild type dTRPA1, and dTRPA1 K287G transfected cells recorded with a ± 100 mV upon application of a heat (B) or cold (C) stimuli. (D-E) Average of maximal current changes at +100 mV for pcDNA, wild type dTRPA1, dTRPA1 G276N, and dTRPA1 K287G upon stimulation with hot (D) or cold

(E) temperature. Data represents average \pm SEM. Numbers on top of the bars represent the number of individual patches. m is mouse, d is *drosophila*.

This suggests that mutations identified in the mouse TRPA1 do not have the same effect in the *drosophila* TRPA1 orthologue.

To test whether the G276N and K287G mutations made *drosophila* TRPA1 cold sensitive, we recorded cells while decreasing the temperature from 25°C to 13°C. Patch-clamp experiments show that cells expressing *drosophila* TRPA1 G276N or *drosophila* TRPA1 K287G mutant channels had current increases that were virtually identical to pcDNA-transfected cells (Figure 20C and E). Together, this indicates that the mutations found to invert temperature directionality in mouse TRPA1 are not universally capable of inverting temperature directionality on other highly homologous channels like *drosophila* TRPA1 and that the mechanism identified in mouse TRPA1 may be unique to that channel.

3.4 Discussion

We sought to investigate the role of ankyrin repeat 6 of the cold-sensitive mouse TRPA1 in modulating temperature directionality. Previous studies in mouse TRPA1 identified mutations in the ankyrin repeat 6 that can invert the temperature sensitivity from cold to warm temperatures, suggesting that ankyrin repeat 6 may serve as a modulator of temperature activation directionality.

Due to the high homology of the ankyrin repeat 6 of *drosophila* TRPA1 with the ankyrin repeat of mouse TRPA1, we made chimeric channels in which we swapped the

repeats between these two channels. However, chimeric channels show no sensitivity to heat nor to cold temperatures, indicating that these channels are temperature insensitive. There are a few potential reasons that may explain this outcome. First, swapping of the ankyrin repeats may cause conformational changes that block the intracellular side of the pore. Although ankyrin repeat 6 is not resolved in the high-resolution structure of TRPA1, some of the resolved repeats show extensive interactions between repeats (ankyrin repeats 15 and 16) and between repeats and the central coiled-coil domain (ankyrin repeats 12, 13, and 16) (Paulsen et al., 2015). Thus, it may be possible that the mouse ankyrin repeat 6 undergoes similar interactions that the *drosophila* repeat cannot emulate. This may cause a destabilization of the intracellular part of the channel that may obstruct the pore. Second, swapping of these domains may also shift the temperature activation threshold to temperatures that are experimentally inaccessible. Indeed, small differences in the sequence of TRP channels are known to modify the temperature activation properties (Chen et al., 2013; Grandl et al., 2008, 2010; Jabba et al., 2014).

To make subtler changes in the sequence of *drosophila* TRPA1 and to test the same mutations we identified in mouse TRPA1, we made two *drosophila* TRPA1 mutants each of them bearing a conserved single-point mutation. However, mutation S276N abolishes channel functionality, and mutation G287K did not affect heat sensitivity of the channel. Furthermore, this mutation was not capable of conferring cold sensitivity to

the channel. Clearly, the mutations found to invert temperature sensitivity of mouse TRPA1 do not have the same effect in the *drosophila* TRPA1 orthologue. We speculate that this may be due to a lack of plasticity of the temperature activation machinery on *drosophila* TRPA1. Alternatively, it is possible that in mouse TRPA1, these mutations caused structural changes that work in synergy to invert the temperature directionality, but that those structures are absent in *drosophila* TRPA1. Lastly, it is possible that the residues we chose to mutate were not perfectly aligned with those found to be important in mouse TRPA1.

Ultimately, our study was not targeted at extensively testing temperature directionality in *drosophila* TRPA1 and thus it does not indicate that such a feature is absent in the channel. It is still possible that the temperature activation directionality of *drosophila* TRPA1 can be inverted, but mediated by structures different from those we targeted. A more extensive and saturated mutagenesis study should be able to uncover the structures with the capacity to invert the temperature activation profile of the channel.

4. Temperature activation of TRPV1 is specifically sensitive to large decreases in amino acid hydrophobicity

4.1 Introduction

For almost two decades researchers have tried to find the identity of an elusive 'temperature sensor' domain. As discussed in chapter 2.1 many studies have identified several domains where residues are required for temperature activation or modulation of TRP channels. Briefly, the outer pore domain of TRPV1, TRPV3, and TRPA1 has been found to be specifically required for temperature activation, whereas the N-terminal domain of TRPV1, TRPV2, and TRPA1 was implicated on modulation of temperature activation sensitivity and directionality (Figure 8) (Chen et al., 2013; Cordero-Morales et al., 2011; Grandl et al., 2008, 2010; Jabba et al., 2014; Kang et al., 2012; Yao et al., 2011). Nonetheless, other TRP channel structures were also found to be unimportant for activation by temperature. For example, the entire N-terminal of TRPA1 was found to be unnecessary for temperature activation (Figure 9) (Moparthy et al., 2014). Moreover, parts of the N- and C-terminal, as well as 15 residues between S5 and the pore helix of TRPV1 were not required for temperature sensitivity (Figure 9) (Cao et al., 2013b; Liao et al., 2013; Yao et al., 2010b). Collectively, these studies implicate many domains in some aspect of temperature activation, which raises the possibility that a temperature sensing structure is not localized in a single coherent amino acid sequence, but instead formed by tertiary structure or in the interface between subunits of the tetramer. Unfortunately,

the available high-resolution structures of TRPV1, TRPV2, and TRPA1 were resolved in the presence or absence of chemical activators and not at different temperatures, thus not providing clear structural correlates of temperature activation (Cao et al., 2013a; Huynh et al., 2016; Liao et al., 2013; Paulsen et al., 2015; Zubcevic et al., 2016).

Alternatively, domains responsible for high temperature sensitivity in TRP channels might be distributed throughout the protein. This dispersed localization of structures is consistent with a mechanism assuming that large changes in heat capacity (ΔC_p), mediated by the coordinated exposure of hydrophobic residues to solvent, may drive activation by cold and heat (Clapham and Miller, 2011). Applying this thermodynamic principle, a temperature insensitive K_v channel was engineered to become cold or heat sensitive (Chowdhury et al., 2014). However, while this bottom-up approach is a strong conceptual demonstration, it remains unclear whether the same mechanism underlies temperature activation of TRP channels. While currently there is no experimental evidence for this mechanism, it makes the strong prediction that hydrophobicity of residues drives temperature activation.

Here, we used a combination of random mutagenesis, high-throughput screening, and deep sequencing to correlate the effects of 287 mutations to TRPV1 channel activation by temperature and 248 mutations to activation by capsaicin. We found that large decreases in hydrophobicity of TRPV1 amino acids are better tolerated for activation by capsaicin than for activation by hot temperature. This provides initial

correlative support for amino acid hydrophobicity being important for temperature activation of a TRP channel.

4.2 Materials and Methods

4.2.1 Library generation and functional screening

Generation and screening of the TRPV1 random mutant library was described previously in detail (Grandl et al., 2010). Briefly, error-prone PCR was performed with the full-length rat *Trpv1* gene (Diversify PCR random mutagenesis kit, Clontech) and yielded an average mutation frequency of 2 amino acid mutations per clone. Mutated DNA was mini-prepped, normalized to 40 ng/ μ l and plated in quadruplets in 384-well clear bottom assay plates (Greiner), transfection reagent (Fugene 6.0, Roche), and HEK293 cells were added. Each 384-well plate contained separate wells with wild type TRPV1 and pcDNA5 transfected cells as positive and negative controls, respectively. Two days after transfection cells were washed, loaded with the calcium sensitive fluorophore Fluo-3 and washed again. Plates were then transferred to a FLIPR-TETRA (Molecular Devices) plate reader to monitor the Fluo-3 fluorescence changes. The library was screened independently upon stimulation by heat (25°C to 45°C) and capsaicin (100 nM, final concentration).

4.2.2 Categorization of mutant library

Maximal fluorescence responses (x) were calculated for each well after baseline subtraction. For each plate mean maximal responses (\bar{x}) and standard deviations (σ)

were calculated for wild type TRPV1 (\bar{x}_{TRPV1} and σ_{TRPV1}) and pcDNA5 (\bar{x}_{pcDNA} and σ_{pcDNA}) transfected cells. Plates where \bar{x}_{TRPV1} and \bar{x}_{pcDNA} was not consistent for three of the four wells were discarded. Clones were selected as 'functional' if $x_{clone} > \bar{x}_{TRPV1} - 1\sigma_{TRPV1}$. Clones were classified as 'less functional' if $x_{clone} < \bar{x}_{TRPV1} - 1\sigma_{TRPV1}$. Clones that did not consistently fulfill these criteria for at least three of the four wells were not considered. In total ~7,300 out of ~8,500 clones were selected and their cDNA was picked for sequence analysis.

4.2.3 Sample preparation and sequencing

One μ l cDNA of each clone was collected by hand and subsequently cDNA was pooled for each of the categories. Next, clones were digested with HindIII and NotI restriction enzymes and the mutated TRPV1 insert was separated from pcDNA vector using gel electrophoresis. Mutated TRPV1 inserts were then gel-purified using a QIAquick[®] gel extraction kit (QIAGEN) and concentrated to 40 ng/ μ l using a DNA concentrator kit (Zymo Research). Mutated inserts were then fragmented by sonication (Covaris), multiplexed and sequenced with 150 paired-end reads using the illumina HiSeq 2500 sequencer in rapid mode (Duke University Genome Sequencing and Analysis Core). All clones were sequenced together in a single lane. Each clone was sequenced with a coverage of more than 700,000x. All sequences had a Phred score of at least 34 (99.96% accuracy).

4.2.4 Aligning and mapping of variants

Variants were aligned and mapped by the Duke University Genome Sequencing and Analysis Core. Adaptor sequences and low quality bases were removed using cutadapt (Martin, 2011). Forward and reverse paired reads were then repaired using a custom script (Duke University Genome Sequencing and Analysis Core). Sequences were aligned to wild type rat *Trpv1* using bwa for paired-end reads (Li and Durbin, 2009). Variant calls were made using SNVer (Wei et al., 2011).

4.2.5 Determination of variant call accuracy and mutational frequency

We postulated that sequences from clones categorized as ‘functional’ should not contain any stop codons before the pore domain (Q560) and applied a binomial distribution with 95% confidence level to empirically determine the variant probability to 0.0016. All mutations with a confidence level below 95% were discarded. The same p-value and 95% confidence interval was then applied to all mutations. The frequency of mutation for each base pair was calculated by dividing the total number of reads of a given residue by the number of times a non-silent substitution was read. The coverage at base pair level was calculated using the formula:

$$\left(\frac{\text{\# of identified base pair changes}}{\left(\text{\# of bases in WT TRPV1} \right) \left(\text{\# of possible base changes} \right)} \right) = \left(\frac{5546}{\left(2514 \right) \left(3 \right)} \right) = 73\%$$

The library coverage on an amino acid level was calculated using the formula:

$$\left(\frac{\text{\# of identified amino acid changes}}{\left(\text{\# of amino acids in WT TRPV1} \right) \left(\text{\# of possible amino acid changes} \right)} \right) =$$

$$\left(\frac{2255}{(838) (19)} \right) = 14\% .$$

4.2.6 Alignment of TRPV1 ankyrin repeats and TRPV1 S4

Alignments were performed on Clustal Omega (Goujon et al., 2010; Sievers et al., 2011). For aligning of ankyrin repeats of TRPV1 the start and end of each repeat was identified using the apo high-resolution structure (Liao et al., 2013).

4.2.7 High-resolution structure illustrations

Structure illustrations were made using the unliganded (apo) TRPV1 high-resolution structure (Liao et al., 2013; PDB ID: 3J5P) with the UCSF Chimera program (Pettersen et al., 2004).

4.2.8 Site-directed mutagenesis

All mutations were introduced into a wild type rat TRPV1 ligated to a pcDNA 3.1 expression vector. Mutants were generated using a QuickChange Site-Directed Mutagenesis Kit (Agilent). All mutants were fully sequenced using Sanger sequencing.

4.2.9 Cell culture

HEK293t cells were cultured in Dulbecco's Modified Eagle's Medium (DMEM) (Life Technologies) supplemented with 10% fetal bovine serum (Clontech Laboratories), 50 unit/mL penicillin (Life Technologies), and 50 mg/mL streptomycin (Life

Technologies). Cells were transiently transfected in 6-well plates in the presence of 10 μ M ruthenium red using Fugene 6.0 (Promega) ~48hr before recording. All cells were co-transfected with GFP or YFP as a fluorescent reporter. Transfected cells were re-plated at low density at least 16hr before recording in 10 mm glass coverslip (Warner Instruments) coated with Poly-L-lysine (Sigma) and laminin (Sigma).

4.2.10 Electrophysiology

Patch-clamp recordings were performed in the whole cell configuration as detailed in chapter 2.2.3 with the following modifications. Borosilicate glass pipettes (Sutter Instruments) had a resistance of 3-5 M Ω when filled with pipette buffer solution (in mM): 150 NaCl, 3 MgCl₂, 5 EGTA, 10 HEPES, pH = 7.2 with NaOH. The bath solution was (in mM): 150 NaCl, 6 CsCl, 1.5 CaCl₂, 1 MgCl₂, 10 glucose, 10 HEPES, pH = 7.4 with NaOH. Solutions were applied through a gravity-driven perfusion, and temperature was controlled using a CL-100 temperature controller (Warner Instruments) and a SC-20 dual in-line heater (Harvard Apparatus). Temperature was measured using a TA-29 thermistor (Warner Instruments) placed near the recorded cell. Heat activation experiments were done by increasing the temperature from 25°C to 40°C in 5°C intervals. At every temperature interval (25°C, 30°C, 35°C, and 40°C) we measured channel activation with a voltage step from -120 mV to +160 mV at 20 mV increases for 200 ms and used these data to calculate conductance-voltage (G-V) relationships. The currents for the G-V curves were obtained from plateau currents at the last 50 ms of the

voltage step. G-V curves were then fitted with Boltzmann functions on Igor Pro (WaveMetrics) and the V_{half} values were obtained from the fitting parameters.

Recordings were only analyzed for patches with an initial seal resistance of at least 1 G Ω , voltage-induced current at +160 mV and 25°C of at least 500 pA and series resistance (R_{series}) <10 M Ω at 25°C for wild type TRPV1 and mutant channels.

Experiments testing cold activation of V658T, I661T, L664T TRPV1 triple mutant were performed by decreasing the temperature of the bath buffer from 25°C to 16°C while measuring channel activation with a 200 ms \pm 100 mV ramp every two seconds. Currents at the voltage plateaus were obtained at 16°C and 25°C and analyzed for cells that have an initial seal resistance of at least 1 G Ω .

4.2.11 Data analysis and statistical tests

Mutation selection was performed on Excel (Microsoft). Graphs were made using Prism (GraphPad Software, Inc.) and Igor Pro (WaveMetrics). Illustrations were made in Illustrator (Adobe Systems). Histograms of gap lengths between mutations were generated by counting gap lengths (for 'temperature functional' or 'capsaicin functional' mutations), or by generating 10 random distributions of 287 (temperature) or 248 (capsaicin) mutations over 838 positions with Excel (Microsoft) and then counting gap lengths. Electrophysiological data were analyzed with Igor Pro (WaveMetrics).

Statistical analysis of hydropathy histograms was performed on R using a custom-made script. We used a likelihood ratio (LRT) to test whether the frequency of

temperature-characterized mutations with Δ hydropathy > -2 is the same between each of the two functional categories. V_{half} statistical analysis was done using an unpaired Student's t-test by comparing wild type TRPV1 to each mutant. Statistical testing for cold activation was performed with an unpaired Student's t-test by comparing TRPM8 (positive control) or triple TRPV1 mutant to pcDNA (negative control).

4.3 Results

4.3.1 Ultra-deep sequencing identifies 535 functionally characterized mutations

We made use of ~8,500 randomly mutated clones of rat TRPV1 that were previously functionally characterized for temperature and capsaicin activation with a fluorescence based calcium influx assay (Grandl et al., 2010). We compared heat-evoked (25°C to 45°C) responses of each clone to wild type TRPV1 and pcDNA. We then selected all clones that showed normal activation by temperature or capsaicin as compared to wild type controls on the same assay plate (see Materials and Methods) (Figure 21).

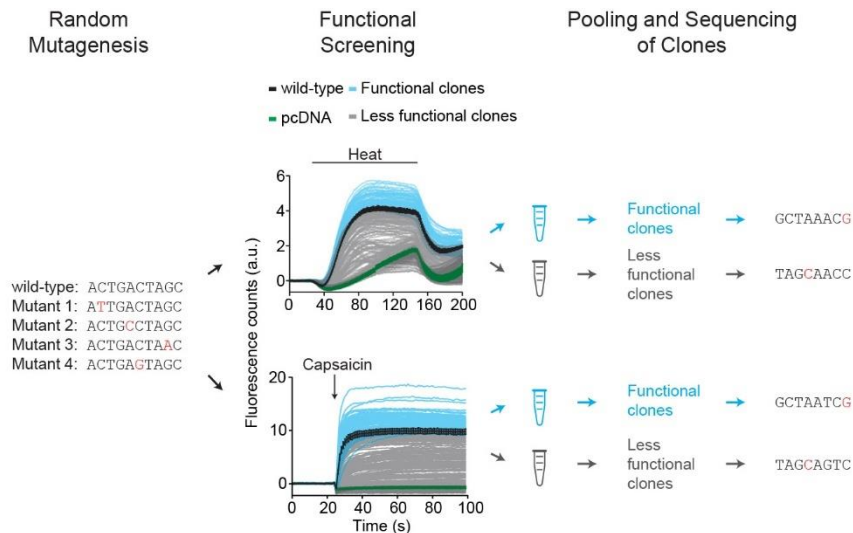


Figure 21: Schematic representation of experimental approach. Illustration of random mutagenesis, calcium-based functional screening, pooling of clones with identical functionality, and deep sequencing of pooled clones. Fluorescence responses of 94 mutant clones (4 responses per clone) upon heat (top panel) or capsaicin (bottom panel) stimulation. Wild type TRPV1 (black), pcDNA (green), ‘functional’ clones (blue), and ‘less functional’ clones (gray). Wild type TRPV1 and pcDNA are average responses of $n = 4$ wells. Error bars represent s.d.

We further refer to these clones as ‘temperature functional’ and ‘capsaicin functional’, respectively. Clones were tested in quadruplets, and each of them was only considered for further analysis if at least three of the four quadruplets were identically assigned. This resulted in a total of ~1,795 categorized ‘temperature functional’ and ~1,479 ‘capsaicin functional’ clones.

To identify mutations that do not affect temperature or capsaicin responses, ‘temperature functional’ and ‘capsaicin functional’ clones were pooled and sequenced in a single lane with 150 paired-end read length in an illumina HiSeq 2500 sequencer. In order to explore the sequence diversity of the mutant library we sequenced the clones

that were classified as temperature 'less functional' (~5,505) and capsaicin 'less functional' (~5,821) in the same lane as 'functional' clones (see Materials and Methods). We obtained an average coverage of more than 700,000x, which allowed us to detect low frequency (~1 in 600 bp) mutations. We determined the variant call threshold by adjusting the error rate of a binomial distribution, postulating that no stop codons should be present before the pore domain (Q560) of the ion channel in the 'capsaicin functional' category with a confidence level of 95%. The determined error rate (0.0016) was then applied to all sequenced mutations (see Materials and Methods). Analysis of all base pair mutations showed that wild type bases were mutated at nearly equal frequencies (A and G = 1.2, C = 1.0, and T = 1.1) with a minor bias of transversions T_v (purine to pyrimidine and pyrimidine to purine) compared to transitions T_s (purine to purine and pyrimidine to pyrimidine), with a ratio $T_s/T_v = 0.7$, which is consistent with the error-prone PCR method we used (Figure 22A and B).

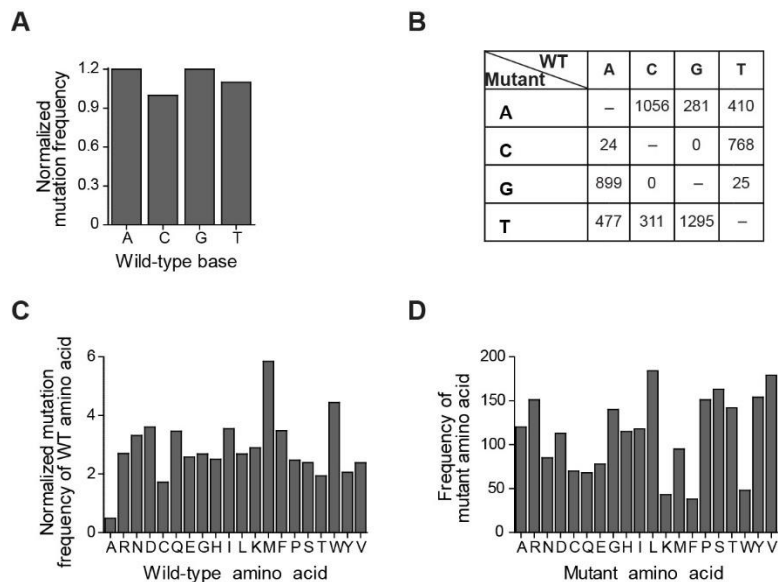


Figure 22: Numbers of base pairs mutations of TRPV1 identified by sequencing clones stimulated with temperature and capsaicin. (A) Normalized mutation frequency for wild type bases for the temperature and capsaicin screened libraries. (B) Numbers and identity of base pair mutations in correlation to the wild type base. (C) Number of times wild type amino acids were mutated. (D) Frequency of mutant amino acid.

Moreover, on a base pair level the library explored a large fraction (73%) of the attainable sequence space (see Materials and Methods). At the amino acid level, most wild type residues were mutated at similar frequencies (~ 2-4x), with the exception of less frequently mutated alanines (~0.5x) and more frequently mutated methionines (~6x) and tryptophans (~5x) (Figure 22C). Due to the varying occurrence of wild type amino acids and the degeneration of the genetic code, the number of introduced mutant residues differed more widely (~30-180 per amino acid) (Figure 22D). Altogether, the library covered ~14% of the total amino acid sequence space.

We identified 287 ‘temperature functional’ and 248 ‘capsaicin functional’ amino acid mutations and 1,720 additional ‘less functional’ amino acid mutations for a total of

2,255 amino acid mutations in the whole library covering 80.1% (671 of 838) of all amino acids of TRPV1 (Figure 22C and Appendix A and B). Since various processes that are unrelated to the mechanisms of temperature and capsaicin activation, such as protein misfolding, inefficient channel trafficking, or altered ion permeation, can all compromise channel function, we focused exclusively on 'temperature functional' and 'capsaicin functional' mutations and analyzed the remaining 1,720 amino acid mutations only to characterize the diversity of the library. We reasoned that although 'functional' clones may carry more than one mutation, it is unlikely that any of these is compromising function by itself and only leading to a wild type like phenotype because it is rescued by a second mutation, thus making a misclassification of mutations from 'functional' clones highly unlikely.

Altogether ~39% of the mutated residues were mutated once, ~30% mutated twice, and ~10% mutated more than two times. Furthermore, we found that 49.1% of 'temperature functional' mutations were also 'capsaicin functional'. Taken together, our approach of combining random mutagenesis and high-throughput functional screening with next generation sequencing thus identified an unprecedented number of mutations that did not affect temperature or capsaicin activation of TRPV1.

4.3.2 Most structural domains of TRPV1 are tolerant to mutations

Due to the low throughput of site-directed mutagenesis and high costs of Sanger sequencing, knowledge about the effects point mutations have on temperature and

capsaicin activation is limited to only a small number of amino acids (Winter et al., 2013). Our data from 287 'temperature functional' and 248 'capsaicin functional' mutations might thus point towards large structures, domains, or motifs for temperature and capsaicin activation. Specifically, we hypothesized that residues/domains important for temperature or capsaicin activation should be sensitive to mutations, whereas residues/domains not important should be more tolerant. By mapping all 'functional' mutations onto the primary amino acid sequence, we found that for both stimuli, mutations were distributed throughout the entire protein sequence (Figure 23A).

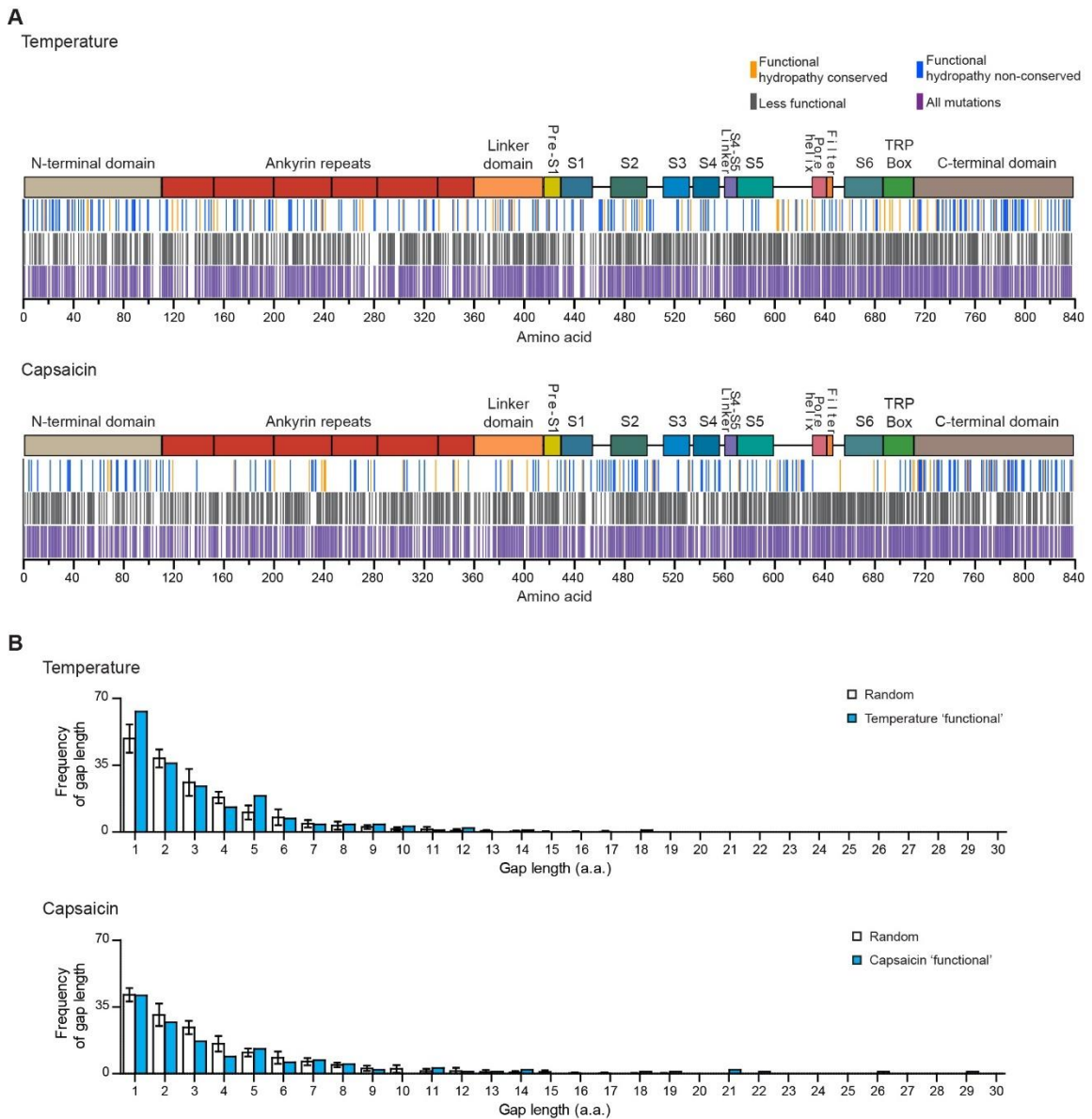


Figure 23: (A) Illustration of the location of identified mutations screened with temperature (top panel) or capsaicin (bottom panel) for ‘functional’ clones (blue and yellow), ‘less functional’ clones (gray) or all identified mutations pooled together (purple). In yellow are ‘functional’ mutations that conserved wild type amino acid hydropathy. In blue are ‘functional’ mutations that did not conserved amino acid hydropathy. Mutations were considered hydropathy-conserving if the Δ hydropathy ($\text{hydropathy}_{\text{mutant}} - \text{hydropathy}_{\text{WT}} = \pm 0.6$). Mutations outside of that range are considered non-conserving. Each bar indicates one single mutation and boxes on top illustrate the structural domains of TRPV1. (B) Histogram of frequencies of gap lengths between

mutations of temperature (top) or capsaicin (bottom) 'functional' category and gap lengths within ten random distributions of 287 (temperature, top) or 248 (capsaicin, bottom) mutations in 838 positions. Error bars are SEM.

Particularly, the fact that these mutations are distributed throughout the primary sequence contrasts with the idea that within the TRPV1 ion channel coherent domains or sequence motifs mediate channel activation by temperature or capsaicin. To analyze if the introduced mutations were similar to wild type amino acids we quantified the change in amino acid hydrophathy ($\text{hydrophathy}_{\text{mutant}} - \text{hydrophathy}_{\text{wild type}}$) using the Kyte-Doolittle scale and found that out of 287 temperature-characterized mutations 80 were hydrophathy-conserving and 207 were non-conserving mutations (Figure 23A) (Kyte and Doolittle, 1982). For capsaicin 59 of the 248 mutations were hydrophathy-conserving, whereas 189 were non-conserving. To test quantitatively if the temperature 'functional' mutations are distributed randomly or instead reveal domains that are sensitive to mutations, we generated a histogram of the frequencies of gap lengths between 'temperature functional' mutations and found that it was nearly identical to a distribution of ten randomly mutated sequences (Figure 23B). We also mapped all temperature 'functional' mutations onto the high-resolution structure of TRPV1, but did not find obvious regions that are enriched or devoid of mutations (Figure 24).

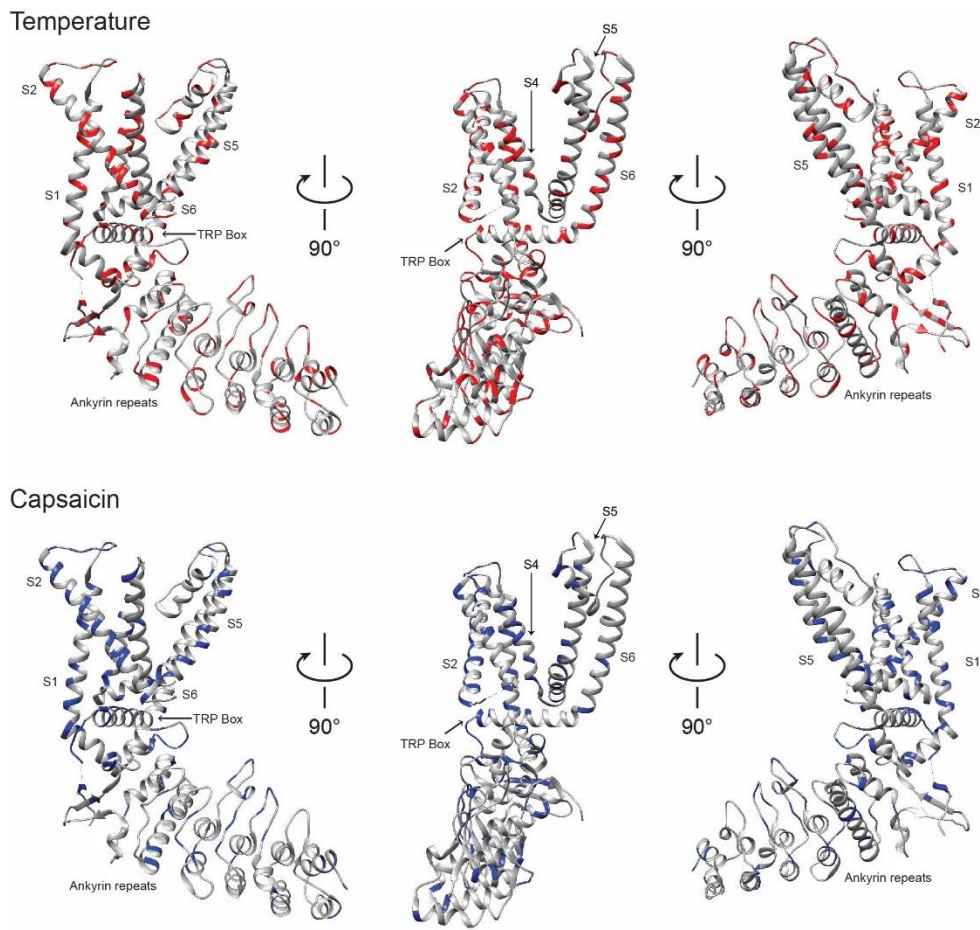


Figure 24: ‘Temperature functional’ (top panel) and ‘capsaicin functional’ (bottom panel) mutations localized onto the apo high-resolution structure of TRPV1. Temperature mutations are in red. Capsaicin mutations are in blue.

Altogether, our data do not point towards large and coherent structural domains that are intolerant to mutations.

4.3.3 Decrease in amino acid hydrophobicity is less frequently tolerated for activation by temperature than for activation by capsaicin

As introduced before, a proposed mechanism suggests that heat capacity mediated by exposure of hydrophobic residues to solvent may provide high temperature sensitivity of TRP channels (Clapham and Miller, 2011). We hypothesized

that mutations that decrease the hydrophobicity of amino acids will reduce overall temperature sensitivity, whereas mutations that maintain or increase hydrophobicity will less likely affect it. To test our hypothesis, we analyzed how hydrophobicity was changed in our identified mutations. Specifically, we used a Kyte-Doolittle hydrophathy scale to calculate the change in hydrophathy ($\text{hydrophathy}_{\text{mutant}} - \text{hydrophathy}_{\text{WT}}$) (Kyte and Doolittle, 1982). We then generated histograms of the number of mutations as a function of the changes in hydrophobicity (Figure 25A).

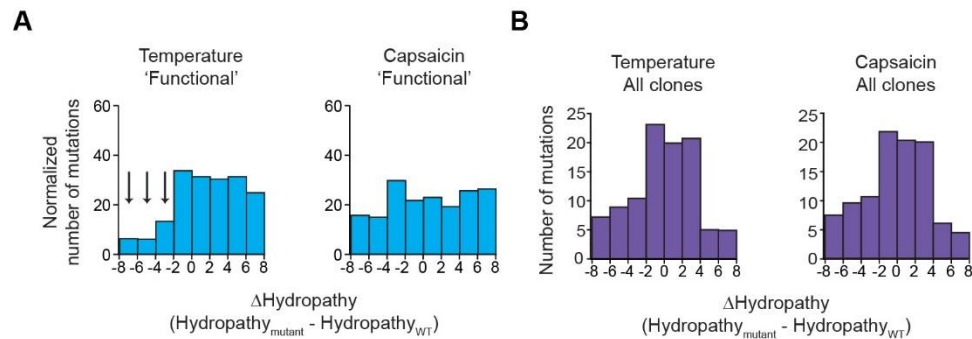


Figure 25: Hydrophathy changes induced by mutations. (A) Histograms showing the change in hydrophathy ($\text{hydrophathy}_{\text{mutant}} - \text{hydrophathy}_{\text{WT}}$) for mutations in ‘functional’ clones screened with temperature or capsaicin. Data is normalized so that the sum of a bin from the ‘functional’ group and the respective bin from the ‘less functional’ group is equal to 100%. (B) Change in hydrophathy for all 1,110 temperature- and 1,145 capsaicin-characterized mutations.

As we expected from our prediction, the analysis showed that mutations that cause a large decrease in hydrophathy ($\Delta\text{hydrophathy} < -2$) are not frequently found (9.1% or 26 out of 287 mutations) within the ‘temperature functional’ mutations, whereas mutations without changes or with moderate and strong increases in hydrophathy ($\Delta\text{hydrophathy} > -2$) occur frequently (90.9% or 261 out of 287 mutations). On the contrary, in the ‘capsaicin

functional' library mutations with large decrease in hydrophathy (Δ hydrophathy < -2) are more frequent (25.8% or 64 out of 248 mutations) and mutations without changes or with moderate and strong increases in hydrophathy (Δ hydrophathy > -2) are less frequent (74.2% or 184 out of 248 mutations). To statistically test this observation for both temperature- and capsaicin-characterized mutations, we performed a likelihood ratio test and found that the number of temperature- and capsaicin-characterized mutations with Δ hydrophathy < -2 is significantly different (p value = 4.6×10^{-129}) from the number of mutations with a Δ hydrophathy > -2 (see Materials and Methods). This indicates that mutations in TRPV1 that strongly reduce hydrophobicity may cause a decrease in overall temperature response possibly by affecting specific parts of the activation process, such as temperature sensing or gating. This result shows that the temperature activation mechanism may be more sensitive to mutations that decrease hydrophobicity as compared to the capsaicin activation mechanism. Importantly, this pronounced statistical difference in stimulus specificity is not caused by a bias of the mutant library and clone selection, as histograms representing hydrophobicity changes of all 2,255 mutations are nearly identical for both temperature and capsaicin (Figure 25B). Taken together, these results correlate strong decreases in hydrophobicity of certain amino acids as being underrepresented in clones normal for temperature activation, but not in clones normal for capsaicin activation and provide a potential mechanistic link between temperature activation of TRPV1 to changes in hydrophobicity.

4.3.4 Hydrophobicity of Three Pore Residues Contributes to overall Temperature Sensitivity

Our results show on the ensemble level that hydrophobicity of amino acids is correlated with normal temperature activation of TRPV1. To test this mechanism further, we engineered single-point mutations to threonine that neutralized amino acid hydrophobicity for eight positions within the ankyrin repeats that are highly conserved between individual repeats of rat TRPV1, and one aligning position in the S4 that had been found to confer temperature sensitivity to Kv1.2 (see Materials and Methods) (Figure 26A) (Chowdhury et al., 2014; Liao et al., 2013). In addition, we engineered triple mutant TRPV1 ion channels by introducing three mutations that conserved (V658L, I661L, L664I) (Δ hydrophathy = -0.4), decreased (V658A, I661A, L664A) (Δ hydrophathy = -7.1), or neutralized (V658T, I661T, L664T) (Δ hydrophathy = -14.6) the hydrophobicity of three residues in S6 (Figure 27A). We focused on these three specific hydrophobic residues, because the pore had previously been implicated in temperature sensitivity and the selected residues are strongly hydrophobic and at the same time highly conserved between different temperature activated TRP ion channels (Chen et al., 2013; Grandl et al., 2008, 2010; Yang et al., 2015). We transiently expressed all constructs in HEK293 cells and measured currents upon voltage step protocols (-120 to +160 mV) at different temperatures (25°C, 30°C, 35°C, and 40°C) using patch-clamp electrophysiology (Figure 26 and 27). Because the determination of temperature thresholds and Q_{10} values has technical and conceptual shortcomings, we probed

temperature sensitivity by measuring the voltage of half maximal activation (V_{half}) as a function of temperature and tested how titrating amino acid hydrophobicity of residues affects overall temperature sensitivity of TRPV1 (Voets, 2012; Voets et al., 2004). While mutations at five positions within the ankyrin repeats (L205T, I209T, L220T, L267T, and L288T) lead to non-functional channels, mutations V292T, L337T, I352T and, F559T resulted in channels that had conductance and V_{half} values indistinguishable from wild type TRPV1 (Figure 26B-D).

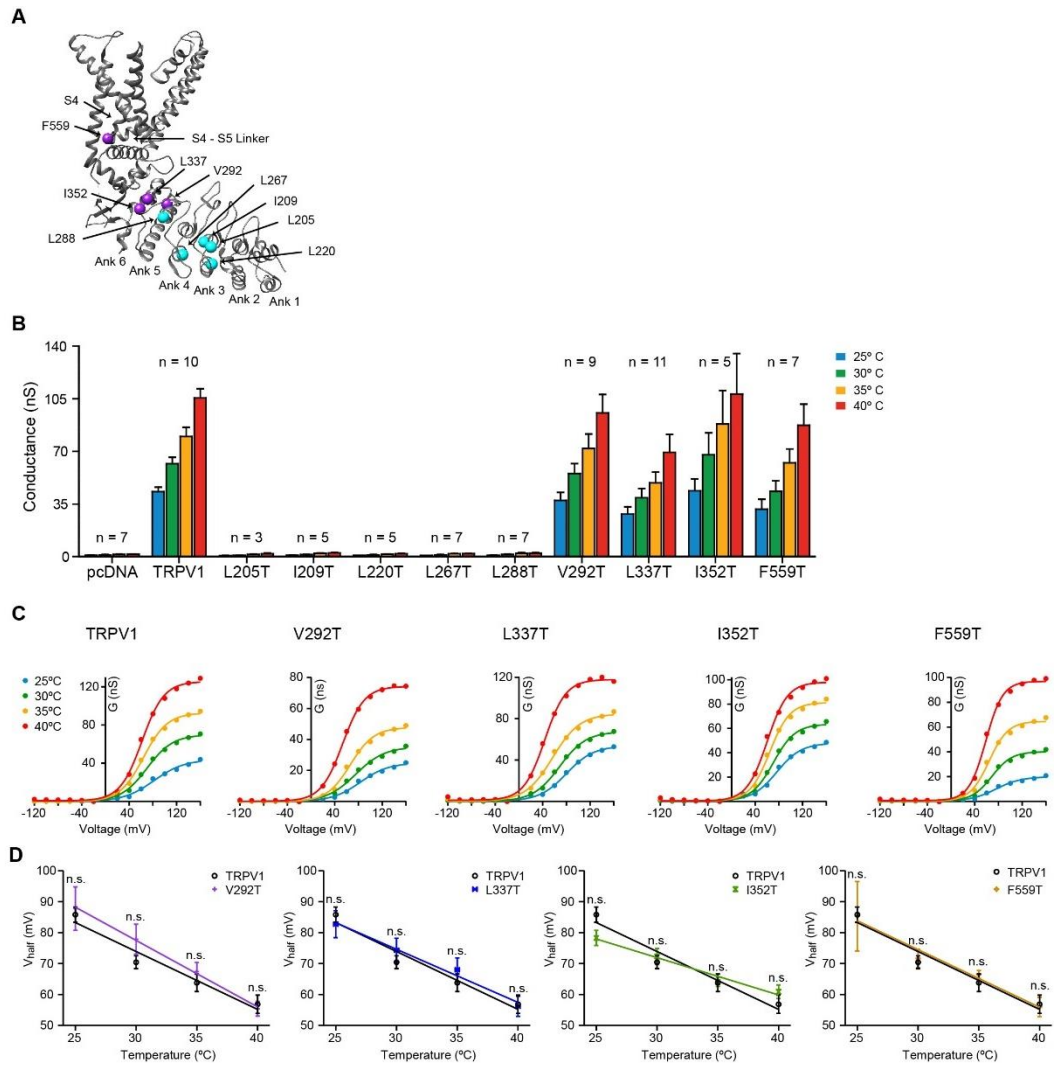


Figure 26: Heat sensitivity of TRPV1 single-point mutants with mutations that neutralized amino acid hydrophobicity. (A) Structural location of all the residues mutated in the ankyrin repeats and the beginning of the S4-S5 linker. In cyan are residues that when mutated to Thr, lead to non-functional channels. In purple are residues that, when mutated to Thr, do not affect temperature activation. (B) Average conductance at +160 mV as a function of temperature for mutants. Data represent mean \pm SEM. N on top of the bars represent number of individual patches. (C) Conductance-voltage (G-V) relationship of plateau current for wild type TRPV1, V292T, L337T, I352T, and F559T at different temperatures. (D) Voltage of half maximal activation (V_{half}) for wild type TRPV1, V292T, L337T, I352T, and F559T as a function of temperature. V_{half} was obtained from the fitting parameters of a Boltzmann distribution to the G-V. Data represent mean \pm SEM. Lines are linear fits to the data. Wild type TRPV1 n = 7, V292T n

= 9, L337T n = 11, I352T n = 5, and F559T n = 7. Each V_{half} value was tested for statistical significance using an unpaired Student's t-test. n.s. indicates not significant ($p > 0.05$).

Triple mutant channels bearing hydrophobicity-conserving mutations (V658L, I661L, L664I) had V_{half} values ($V_{\text{half}, 25^{\circ}\text{C}} = 93.5 \pm 3.1$ mV, $V_{\text{half}, 30^{\circ}\text{C}} = 87.4 \pm 1.9$ mV, $V_{\text{half}, 35^{\circ}\text{C}} = 75.7 \pm 2.6$ mV, $V_{\text{half}, 40^{\circ}\text{C}} = 58.8 \pm 2.2$ mV, $p > 0.05$, $n = 6$) that were indistinguishable from wild type TRPV1 ($V_{\text{half}, 25^{\circ}\text{C}} = 97.7 \pm 4.7$ mV, $V_{\text{half}, 30^{\circ}\text{C}} = 82.5 \pm 4.0$ mV, $V_{\text{half}, 35^{\circ}\text{C}} = 71.4 \pm 2.9$ mV, $V_{\text{half}, 40^{\circ}\text{C}} = 56.1 \pm 2.1$ mV, $n = 5$) at all temperatures (Figure 27B-C and F). While mutant channels that decreased hydrophobicity (V658A, I661A, L664A) did not yield any currents when stimulated by temperature or voltage, mutations that neutralized (V658T, I661T, L664T) hydrophobicity yielded channels with attenuated temperature dependence of V_{half} values ($V_{\text{half}, 25^{\circ}\text{C}} = 74.4 \pm 3.4$ mV, $V_{\text{half}, 30^{\circ}\text{C}} = 72.6 \pm 4.0$ mV, $V_{\text{half}, 35^{\circ}\text{C}} = 64.3 \pm 3.5$ mV, $V_{\text{half}, 40^{\circ}\text{C}} = 56.5 \pm 2.9$ mV, $p_{25^{\circ}\text{C}} < 0.01$, $p_{30^{\circ}\text{C}, 35^{\circ}\text{C}, 40^{\circ}\text{C}} > 0.05$, $n = 7$) (Figure 27D and F). In addition, mutant channels that conserved hydrophobicity (V658L, I661L, L664I) had lower average conductance values with only slightly increased values at higher temperatures, whereas mutant channels that neutralized (V658T, I661T, L664T) hydrophobicity had lower average conductance values that did virtually not depend on temperature, as compared to wild type TRPV1 channels (Figure 27E). These results demonstrate that hydrophobicity of three specific residues in S6 correlates with temperature sensitivity of TRPV1 and thus provide more direct evidence for a temperature mechanism that is driven by amino acid hydrophobicity.

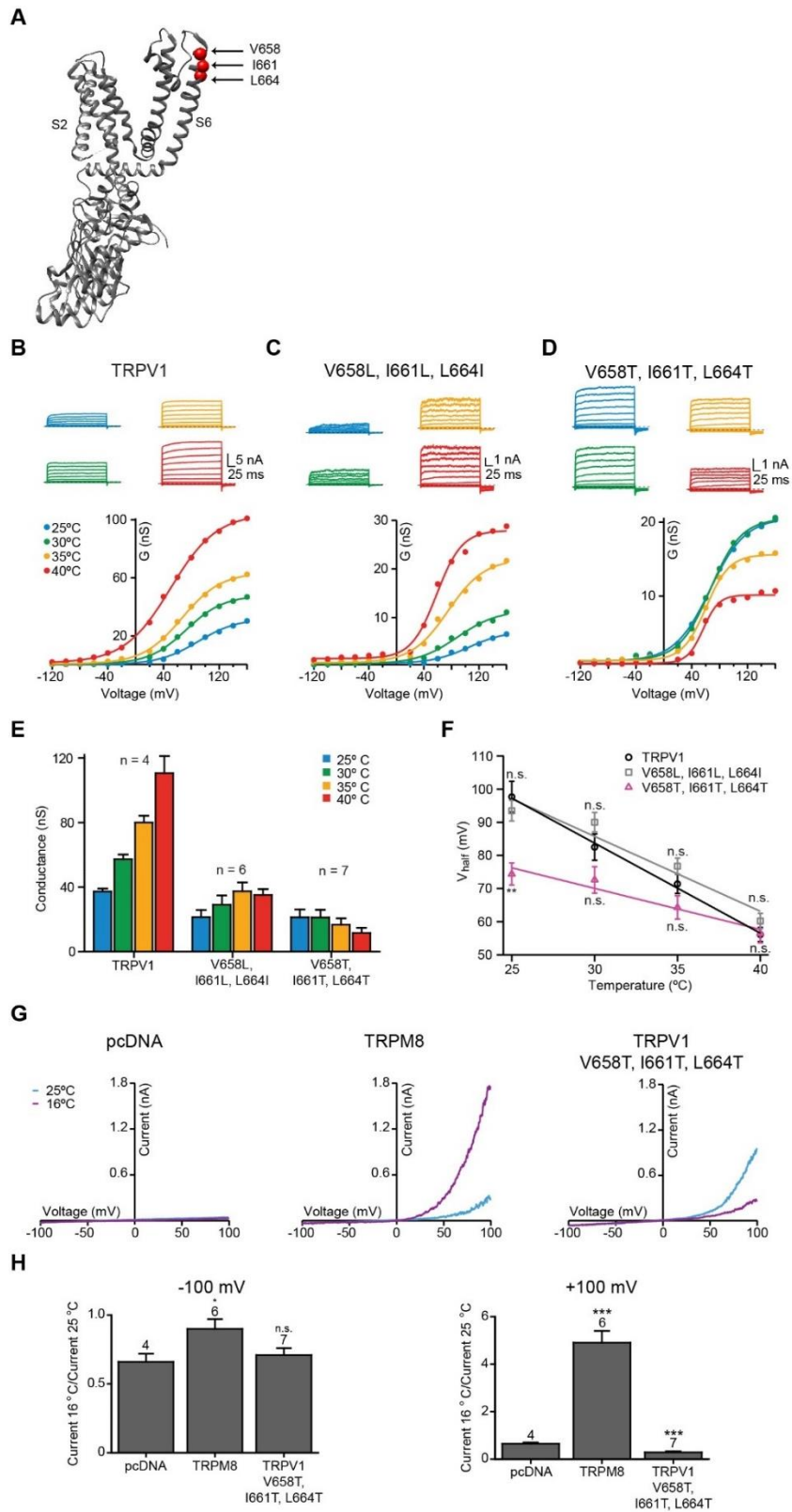


Figure 27: Temperature sensitivity of TRPV1 triple mutants with mutations that conserved or neutralized amino acid hydrophobicity. (A) Location of the three residues mutated to amino acids that conserve or neutralize amino acid hydrophobicity. (B-D) Representative current traces (top) and conductance-voltage (G-V) curves (bottom) of plateau currents at different temperatures for wild type TRPV1 (B), V658L, I661L, L664I (C), and V658T, I661T, L664T (D) triple mutants upon voltage step protocols (-120 mV to +160 mV at 20 mV increments). Lines are fits of a Boltzmann distribution to the data. Dashed lines indicate zero current. (E) Average conductance at +160 mV and different temperatures for wild type TRPV1 and triple mutants with mutations that conserved (V658L, I661L, L664I) or neutralized (V658T, I661T, L664T) amino acid hydrophobicity. Data represent mean \pm SEM. N on top of the bars indicate numbers of individual patches. (F) Voltage of half maximal activation (V_{half}) for wild type TRPV1 and triple mutants at different temperatures. V_{half} values were obtained from the Boltzmann fitting parameters to the G-V curves. Data represent mean \pm SEM. Lines are linear fits to the data. TRPV1 n = 5, V658L, I661L, L664I n = 6, and V658T, I661T, L664T n = 7. Stars indicate statistical significance as compared to wild type TRPV1 at the specified temperature (**p < 0.01). n.s. indicates not significant (p > 0.05). (G) Representative current traces at 16°C (purple) and 25°C (cyan) from pcDNA (negative control, left), wild type TRPM8 (positive control, middle), and TRPV1 V659T, I661T, L664T triple mutant (right) transfected cells stimulated with a \pm 100 mV ramp protocol. (H) Average of current change at -100 mV and +100 mV upon application of cold temperature for transfected cells on (G). Data represent mean \pm SEM. Numbers above bars indicate individual number of patches. Stars denote statistical significance as compared to pcDNA using an unpaired Student's t-test (*p < 0.05, ***p < 0.005). n.s. indicate not significant (p > 0.05).

Finally, we asked if mutations that neutralize hydrophobicity induce sensitivity to cold temperature by performing recordings of HEK293 cells transfected with triple mutant channels (V658T, I661T, L664T) and mouse TRPM8 and pcDNA as controls at 25°C and 16°C. We found that, while TRPM8-transfected cells responded robustly to cold, cells transfected with triple mutant channels that have hydrophobicity-neutralizing mutations (V658T, I661T, L664T) show currents that were nearly identical from those of pcDNA-transfected cells (Figure 27G and H). These results show that although

neutralization of hydrophobic residues at these positions reduces sensitivity to hot temperatures, it does not confer cold sensitivity.

4.4 Discussion

We set out to find the structures and mechanism by which temperature activates TRPV1 ion channels. We used a combination of random mutagenesis, high-throughput functional screening and deep sequencing to identify and correlate the effect of 535 mutations on channel activation by temperature or capsaicin. Deep mutational scanning is becoming a powerful method for the unbiased probing of protein function, largely due to rapid advances in sequencing technology. The unbiased and high-throughput nature of deep mutational scanning seems particularly suited for addressing the problem of temperature activation because it has thus far escaped approaches that are more targeted. While this approach had previously been used for the study of soluble proteins, to our knowledge this is the first case in which it has been used to study an ion channel (Adkar et al., 2012; Fowler et al., 2010; Holmqvist et al., 2013).

However, deep mutational scanning, and our approach, has two technical caveats which must be considered. First, for an ideal investigation of structure-function relationships, each amino acid would be mutated into every other of the 19 possible amino acids or even be replaced by unnatural amino acids. However, due to the degeneration of the genetic code, only a subset of coding mutations is attainable by error-prone PCR. Our library covered approximately 14% of this sequence space (see

Materials and Methods). Clearly, the library was not mutated to saturation and thus, many residues critical for temperature or capsaicin activation were likely missed. Nevertheless, we have identified 535 mutations, which is vastly surpassing the number of TRPV1 mutations characterized thus far (Winter et al., 2013). Second, we functionally screened clones using a calcium-based fluorescence assay that measures ion channel activity only indirectly. Ideally, ion channels should be functionally characterized with electrophysiological measurements to precisely determine channel open probability, but the method lacks the throughput required for screening thousands of mutants efficiently. Still, calcium based fluorescence assays have been used many times to reliably measure activation of TRP channels using a variety of agonists (Caterina et al., 1997; Jabba et al., 2014; McKemy et al., 2002). Moreover, since we focused only on functional clones, mutations that cause a loss of function perhaps due to a decrease in channel expression, protein misfolding, changes in ion permeation, overlap of multiple mutations in one clone, or through other unspecific mechanisms are not compromising the analysis we performed. For example, multiple different mutations would be classified as 'less functional' if they originated from the same clone containing only a single mutation that renders it non-functional. Additionally, by focusing on three residues in S6 we were able to test the relationship between amino acid hydrophobicity and temperature sensitivity more directly with electrophysiology.

Our analysis of the 'temperature functional' and 'capsaicin functional' mutations shows that a large decrease in amino acid hydrophobicity negatively correlates with the likelihood of ion channel activation by temperature. This result is specific for temperature activation, as capsaicin activation is not drastically affected by amino acid hydrophobicity. Importantly, this statistical observation matches a key prediction of the proposed heat capacity mechanism, and thus provides the first indication that this mechanism may underlie temperature activation in TRPV1. More evidence comes from our analysis of the location of mutations. Mapping of all 'temperature functional' mutations onto the primary structure shows that all structurally distinct domains, such as ankyrin repeats and transmembrane domains are, to a large extent, tolerant to mutations. This result argues for the absence of a distinct and coherent 'temperature sensor domain', in which all residues contribute to temperature sensitivity and might explain why previous studies identified multiple domains or several scattered residues within a single domain (Chen et al., 2013; Cordero-Morales et al., 2011; Grandl et al., 2008, 2010; Jabba et al., 2014; Kang et al., 2012; Liao et al., 2013; Moparthi et al., 2014; Yang et al., 2010; Yao et al., 2011, 2010b; Zhong et al., 2012). However, it is theoretically possible that the mutations we introduced and identified are not sufficiently disruptive for temperature activation and that an existing 'temperature sensor domain' has not emerged from our screen. The fact that the library is not sampling the majority of the sequence space is one possible explanation of why a putative temperature domain did

not emerge. It is also important to point out that mutations might affect temperature gating instead of sensing, both of which are still unknown mechanisms.

To further test our statistical observation, we introduced three single point mutations that conserved or neutralized the hydrophobicity of residues in the outer portion of S6. In agreement with a heat capacity mechanism of temperature activation triple mutant channels bearing mutation that neutralized hydrophobicity are less temperature sensitive than wild type channels, whereas mutations that conserved the hydrophobicity have no effect on temperature sensitivity. We thus propose that conformational changes of S6 could be an efficient mechanism to change solvent accessibility of multiple residues and thereby substantially contribute to overall temperature sensitivity. Specifically, a conformational change in the outer pore could expose hydrophobic residues in the upper part of S6 to the extracellular solvent and further propagate to the lower part of S6, which has been shown to function as a gate for chemical stimulation (Cao et al., 2013a; Liao et al., 2013). Indeed, an analysis of the ligand bound and unbound high-resolution structures of TRPV1 identified a high degree of flexibility on three residues of S6 (Romero-Romero et al., 2017). Moreover, substituted cysteine accessibility experiments already demonstrated temperature-mediated conformational changes in the outer pore of TRPV1 and TRPV3 (Kim et al., 2013; Salazar et al., 2009). Additionally, single-channel recordings demonstrate that mutations in S6 of TRPV1 destabilize temperature-induced pore opening, possibly by

inhibiting temperature induced exposure of hydrophobic residues to the solvent (Grandl et al., 2010). Alternatively, it is possible that the S6 mutations alter the temperature activation threshold, channel desensitization, or allosteric coupling by modulating the channel sensitivity to monovalent and divalent ions or through other mechanisms (Cao et al., 2014; Jara-Oseguera et al., 2016). In any case, our results do not suggest that the three mutated residues in S6 are solely responsible for temperature activation of the channel. In fact, Clapham and Miller estimated that ~20 side chains per subunit might be required to generate a substantial change in heat capacity (Clapham and Miller, 2011). Our experimental result that temperature sensitivity in the hydrophobicity-neutralizing mutant is not abolished, but only reduced agrees with this. However, the intuitive assumption that the effects of all hydrophobic residues are independent and thus additive might not be the case in the context of a protein structure. For example, temperature might drive a conformational change that simultaneously exposes several amino acids, which are structurally near the solvent. In fact, several hydrophobic amino acids are located around the residues we tested (V658, I661 and L664) and might contribute to a change in heat capacity upon solvent exposure. Conversely, mutating only one of these amino acids might inhibit this conformational change altogether, thus eliminating the contribution of all locally involved amino acids. Due to this complex interdependence, we do not expect all single amino acids contributing equally and therefore single-point mutations paired with functional analysis might only be able to

identify amino acids that contribute most prominently. Moreover, mutations reducing hydrophobicity might additionally affect other activation mechanisms so that effects cannot be assigned unambiguously to a temperature mechanism. For example, the S6 triple alanine mutant was not functional when stimulated by temperature and voltage and thus not informative.

Clearly, investigating the relationship between amino acid hydrophobicity and temperature sensitivity for all amino acids in TRPV1 is an enormous task. Deep mutational scanning with better library saturation and more accurate functional characterization seems specifically tailored to solve it. The correlative relationship demonstrated here is a first indication of the collective importance of hydrophobicity for temperature activation and the distributed nature of temperature sensitive structures. Additional evidence from protein calorimetry, cysteine accessibility, and high-resolution structures at different temperatures is needed to fully probe and perhaps establish a heat capacity mechanism of temperature activation.

5. Concluding remarks

The elucidation of the structures and mechanisms that mediate temperature activation of TRP channels is one of the most daunting tasks the ion channel community have dealt with in recent years. Here I shed some light on this pressing issue using a combination of approaches that included high-throughput mutagenesis and screening, massive parallel sequencing, and single-point mutation analysis. I found correlative evidence that suggests that temperature sensitive structures are scattered throughout the channel and that amino acid hydrophobicity is critical for temperature activation, supporting a mechanism in where ΔC_p drives temperature sensitivity. However, additional information from other experimental sources is needed to establish caloric capacity as the driver of temperature sensitivity on TRP channels. For instance, evidence from differential scanning calorimetry is needed to quantify ΔC_p throughout the temperature activation process. Moreover, information collected from high-resolution structures at different temperatures should provide definitive evidence about all the structures involved in temperature activation.

Nonetheless, my work has opened a whole new venue for the study of structure-function relationship of ion channels. For years, investigators have relied on using sequence homology analysis to pinpoint residues or structural domains that may be involved in a specific activation mechanism. This is typically followed by extensive cloning steps and eventual functional testing. However, this approach often results in

non-functional clones, leading to additional exhaustive trials of mutagenesis (see Chapter 2 and 3). Clearly, this is a very biased, unreliable, and inefficient way to study structure-function relationships of proteins. The work presented here (chapter 4) delineates an approach that eliminates most of the complications of traditional structure-function studies by introducing a minimal number of random mutations (1-2) in thousands of individual clones. When coupled with high-throughput screening, this allows the characterization of thousands of randomly mutated clones for a given functionality. Although some of these mutations may abolish channel functionality, many other clones should still be functional (see Chapter 4). Notably, this mutational approach also allows for the elimination of the inherent bias introduced by the experimenter in traditional approaches. Although this approach is still biased by the degeneration of the genetic code, this can be easily diminished using codon randomization approaches.

For years, researches have used similar random mutagenesis approaches. However, due to the high costs of Sanger sequencing only a handful of selected clones were typically sequenced. This, in turn, introduced additional bias by the experimenter. Several years ago, massive parallel sequencing was developed, and for a premium it could sequence thousands of clones in a mutant library. With the costs of this recent technology rapidly declining, this is no longer an issue. In fact, here I have demonstrated that massive parallel sequencing can successfully and efficiently sequence ~7,300

functionally characterized clones. Altogether, the approach presented here provides the experimenter with an excellent toolkit that can be applied to the study of structure-function of many ion channels without the intrinsic bias of commonly used approaches. In addition, this approach will be of great relevance for structure-function studies of newly discovered proteins or proteins with few or no other orthologues.

Appendix A

Table 1: List of temperature- and capsaicin-characterized ‘functional’ mutations with their corresponding change in hydrophathy.

Temperature-characterized mutations		Capsaicin-characterized mutations	
‘Functional clones’	Δ Hydrophathy (Hydrophathy _{mutant} - Hydrophathy _{WT})	‘Functional clones’	Δ Hydrophathy (Hydrophathy _{mutant} - Hydrophathy _{WT})
M1I	2.6	R4W	3.6
R4L	8.3	R4L	8.3
D8Y	2.2	S6N	-2.7
E11G	3.1	E11V	7.7
P15T	0.9	C21R	-7.0
P15Q	-1.9	P29H	-1.6
Q17K	-0.4	P35T	0.9
E18G	3.1	V36D	-7.7
E18D	0.0	K37E	0.4
C21Y	-3.8	K37M	5.8
D23Y	2.2	R46H	1.3
P24H	-1.6	R46C	7.0
D26V	7.7	S55L	4.6
D28Y	2.2	L61M	-1.9
P29H	-1.6	L61Q	-7.3
P35T	0.9	P64H	-1.6
V36D	-7.7	E67D	0.0
K37E	0.4	G69W	-0.5
H39N	-0.3	L70P	-5.4
H39L	7.0	P74H	-1.6
F41L	1.0	I75N	-8.0
R44M	6.4	V81A	-2.4
R46S	3.7	L82P	-5.4
R48W	3.6	G88W	-0.5
G51W	-0.5	G88V	4.6
K52E	0.4	D89V	7.7
K52N	0.4	S93R	-3.7
D54Y	2.2	S97L	4.6
S55P	-0.8	Q99K	-0.4
P60T	0.9	Q99R	-1.0
L61M	-1.9	S101T	0.1
P64H	-1.6	E106V	7.7
G69W	-0.5	P109Q	-1.9
P74H	-1.6	L111P	-5.4
I76N	-8.0	S116C	3.3
L82I	0.7	D119E	0.0

T83A	2.5	R138W	3.6
P87L	5.4	G168W	-0.5
G88W	-0.5	Q169R	-1.0
G88V	4.6	R181L	8.3
D89V	7.7	S185C	3.3
S93C	3.3	S193C	3.3
Q99K	-0.4	D196V	7.7
Q99R	-1.0	S197C	3.3
D100G	3.1	K200N	0.4
P109Q	-1.9	N213S	2.7
R114L	8.3	Q228H	0.3
R115G	4.1	A230V	2.4
R115S	3.7	A231T	-2.5
D119E	0.0	G233R	-4.1
Q123H	0.3	G233E	-3.1
Q127L	7.3	G233W	-0.5
E130G	3.1	G233V	4.6
R138S	3.7	K238E	0.4
K141E	0.4	K240N	0.4
D145Y	2.2	G241W	-0.5
F148L	1.0	L261Q	-7.3
D150Y	2.2	V264A	-2.4
E152D	0.0	K265M	5.8
K155N	0.4	A275T	-2.5
M162V	2.3	I277V	-0.3
G168W	-0.5	R280L	8.3
G168V	4.6	K303E	0.4
Q169R	-1.0	F304L	1.0
Q169H	0.3	T306I	5.2
D171Y	2.2	G316V	4.6
L175M	-1.9	H320P	1.6
R181L	8.3	T329S	-0.1
K182N	0.4	S343N	-2.7
D184Y	2.2	G344W	-0.5
S193C	3.3	G347W	-0.5
D196Y	2.2	R355M	6.4
D196V	7.7	V377M	-2.3
S197C	3.3	L381I	0.7
Y199N	-2.2	I387V	-0.3
Q202H	0.3	T389S	-0.1
R212L	8.3	C390R	-7.0
N213S	2.7	S402G	0.4
M214I	2.6	P407T	0.9
L219I	0.7	P407H	-1.6
G224V	4.6	R409S	3.7
A230V	2.4	D411N	0.0

G233W	-0.5	D411V	7.7
G233V	4.6	N419D	0.0
D234Y	2.2	W426L	4.7
K238E	0.4	F429L	1.0
T239A	2.5	R432H	1.3
T239S	-0.1	I433V	-0.3
G241W	-0.5	F436I	1.7
L252M	-1.9	F439L	1.0
L254M	-1.9	I446V	-0.3
V264A	-2.4	I447T	-5.2
F266L	1.0	Y453H	-1.9
Q269H	0.3	E458G	3.1
S271Y	-0.5	L460M	-1.9
R280L	8.3	P462T	0.9
D281Y	2.2	P462H	-1.6
L291M	-1.9	K464R	-0.6
D300Y	2.2	L465P	-5.4
K303E	0.4	N467S	2.7
F304L	1.0	V469A	-2.4
G316V	4.6	D471G	3.1
H320R	-1.3	Y472N	-2.2
P321H	-1.6	Y472C	3.8
T322S	-0.1	T476S	-0.1
E327G	3.1	I479T	-5.2
I328N	-8.0	S483L	4.6
K332R	-0.6	V486A	-2.4
S343N	-2.7	F488L	1.0
G344W	-0.5	F488S	-3.6
G347W	-0.5	F489S	-3.6
G347V	4.6	F490L	1.0
Q354K	-0.4	F490S	-3.6
R355M	6.4	F496S	-3.6
R363L	8.3	Q498R	-1.0
F369L	1.0	Q498L	7.3
G375W	-0.5	S502T	0.1
V377M	-2.3	L503I	0.7
S379Y	-0.5	K504M	5.8
L381I	0.7	S505G	0.4
D383Y	2.2	F507I	1.7
D388Y	2.2	F522L	1.0
T389S	-0.1	M523T	-2.6
C390R	-7.0	M523V	2.3
K392N	0.4	M523L	1.9
L396M	-1.9	F531L	1.0
P407T	0.9	S532G	0.4
P407H	-1.6	R534L	8.3

R409S	3.7	M541T	-2.6
H410N	-0.3	M541V	2.3
H410Q	-0.3	V542A	-2.4
D411Y	2.2	L545M	-1.9
L418F	-1.0	M547L	1.9
N419D	0.0	M552T	-2.6
R420L	8.3	M552V	2.3
W426L	4.7	Y555F	4.1
W426C	3.4	T556A	2.5
R432H	1.3	I564T	-5.2
F438L	1.0	K571R	-0.6
F439A	-1.0	M572T	-2.6
M445L	1.9	M572V	2.3
I446V	-0.3	C578Y	-3.8
I447T	-5.2	F582L	1.0
L460M	-1.9	F582S	-3.6
P461H	-1.6	L585I	0.7
P462T	0.9	T593A	2.5
P462H	-1.6	T593S	-0.1
K464R	-0.6	V596A	-2.4
N467S	2.7	G602W	-0.5
V469A	-2.4	N604S	2.7
G470W	-0.5	L607P	-5.4
G470V	4.6	M609K	-5.8
Y472C	3.8	M609V	2.3
I479T	-5.2	E610G	3.1
S481Y	-0.5	H614L	7.0
V486A	-2.4	R617W	3.6
F488L	1.0	R617L	8.3
F490L	1.0	S619T	0.1
G492W	-0.5	C621R	-7.0
Q494K	-0.4	K622R	-0.6
Q498R	-1.0	K622M	5.8
R500L	8.3	P623L	5.4
P501Q	-1.9	L630M	-1.9
L503I	0.7	N652D	0.0
F522L	1.0	I679V	-0.3
M523V	2.3	M682I	2.6
S526Y	-0.5	K688R	-0.6
F531L	1.0	Q700R	-1.0
Q533H	0.3	T704A	2.5
M541T	-2.6	T708A	2.5
M541V	2.3	T708I	5.2
F543L	1.0	K710R	-0.6
S544Y	-0.5	S711G	0.4
L545M	-1.9	K714R	-0.6

M547L	1.9	C715S	-3.3
M547I	2.6	C715R	-7.0
M552T	-2.6	M716K	-5.8
M562I	2.6	M716T	-2.6
R575G	4.1	M716R	-6.4
F582L	1.0	R717G	4.1
F582S	-3.6	R717M	6.4
L585I	0.7	K718E	0.4
F587L	1.0	K718R	-0.6
G602W	-0.5	A719V	2.4
K603R	-0.6	F720S	-3.6
S606Y	-0.5	K724E	0.4
L607M	-1.9	Q727R	-1.0
S611Y	-0.5	G729W	-0.5
R617W	3.6	F730Y	-4.1
R617L	8.3	F730L	1.0
G618W	-0.5	T731A	2.5
K622M	5.8	D733G	3.1
S626Y	-0.5	R739L	8.3
L630M	-1.9	W740R	-3.6
S632Y	-0.5	R743M	6.4
F638L	1.0	R743S	3.7
F640L	1.0	V744A	-2.4
M644I	2.6	E746K	-0.4
D646Y	2.2	E746G	3.1
F649L	1.0	W752R	-3.6
N652D	0.0	N753D	0.0
D654Y	2.2	T754P	-0.9
I660V	-0.3	N755D	0.0
L662M	-1.9	V756E	-7.7
L669I	0.7	V756A	-2.4
L673I	0.7	N765D	0.0
I679V	-0.3	N765S	2.7
L681I	0.7	C766R	-7.0
M682I	2.6	E767D	0.0
E684D	0.0	V769I	0.3
K688R	-0.6	V769D	-7.7
E692D	0.0	R771H	1.3
K694N	0.4	T772S	-0.1
Q700H	0.3	L773M	-1.9
T708A	2.5	L773Q	-7.3
S711G	0.4	L773P	-5.4
K714R	-0.6	F775S	-3.6
C715R	-7.0	S776Y	-0.5
M716K	-5.8	L777P	-5.4
M716T	-2.6	S783P	-0.8

M716I	2.6	G784W	-0.5
R717M	6.4	N786S	2.7
S722Y	-0.5	W787R	-3.6
G729W	-0.5	K788R	-0.6
F730Y	-4.1	N789S	2.7
F730L	1.0	F790L	1.0
T731A	2.5	L792M	-1.9
G734C	2.9	V793A	-2.4
K735N	0.4	R797M	6.4
D737Y	2.2	D798G	3.1
W740R	-3.6	D798V	7.7
R743M	6.4	A799V	2.4
R743S	3.7	R804S	3.7
V744A	-2.4	E811G	3.1
E746K	-0.4	V812F	-1.4
N748S	2.7	L814P	-5.4
W749L	4.7	K815E	0.4
W749C	3.4	H816Y	1.9
W752L	4.7	T818M	2.6
W752C	3.4	L821P	-5.4
N753S	2.7	E824G	3.1
N755D	0.0	D825G	3.1
I758T	-5.2	F829S	-3.6
D762Y	2.2	D831G	3.1
P763Q	-1.9	G836W	-0.5
N765D	0.0	G836V	4.6
E767V	7.7	E837G	3.1
E767D	0.0	K838N	0.4
L773M	-1.9		
F775S	-3.6		
S776Y	-0.5		
L777M	-1.9		
R781L	8.3		
S783P	-0.8		
G784W	-0.5		
G784V	4.6		
R785G	4.1		
R785I	9.0		
N786S	2.7		
K788R	-0.6		
K788N	0.4		
F790L	1.0		
L792M	-1.9		
L792P	-5.4		
V793A	-2.4		
L795I	0.7		

R797M	6.4		
R797S	3.7		
D798G	3.1		
D798V	7.7		
A799V	2.4		
R802L	8.3		
Q808K	-0.4		
E811G	3.1		
Q813K	-0.4		
T818M	2.6		
L821I	0.7		
E824G	3.1		
E824D	0.0		
E827V	7.7		
K830N	0.4		
D831G	3.1		
M833V	2.3		
M833I	2.6		
P835Q	-1.9		
G836W	-0.5		
G836V	4.6		

Appendix B

Table 2: List of temperature- and capsaicin-characterized 'less functional' mutations with their corresponding change in hydrophathy

Temperature-characterized mutations		Capsaicin-characterized mutations	
'Less functional clones'	Δ Hydrophathy (Hydrophathy _{mutant} - Hydrophathy _{WT})	'Less functional clones'	Δ Hydrophathy (Hydrophathy _{mutant} - Hydrophathy _{WT})
M1T	-2.6	M1I	2.6
A5V	2.4	Q3H	0.3
L7I	0.7	A5V	2.4
S9T	0.1	L7I	0.7
S9P	-0.8	D8Y	2.2
E10G	3.1	D8G	3.1
E10D	0.0	S9T	0.1
S12Y	-0.5	E10D	0.0
E13G	3.1	E11G	3.1
S14Y	-0.5	S12Y	-0.5
P16H	-1.6	S14Y	-0.5
S20Y	-0.5	S14T	0.1
P24T	0.9	P15T	0.9
P25Q	-1.9	P15Q	-1.9
D26Y	2.2	P16H	-1.6
R27I	9.0	Q17K	-0.4
P29T	0.9	E18G	3.1
C31Y	-3.8	E18D	0.0
P33Q	-1.9	S20Y	-0.5
P34H	-1.6	L22M	-1.9
P35Q	-1.9	L22Q	-7.3
P38H	-1.6	D23Y	2.2
I40N	-8.0	P24H	-1.6
I40V	-0.3	P24T	0.9
I40T	-5.2	P25T	0.9
R44W	3.6	D26G	3.1
R44S	3.7	D26Y	2.2
R46H	1.3	R27I	9.0
R48L	8.3	D28Y	2.2
G51V	4.6	P29T	0.9
G53C	2.9	N30I	8.0
D54V	7.7	K32M	5.8
E56D	0.0	P33Q	-1.9
S59Y	-0.5	P35Q	-1.9
P60H	-1.6	P38H	-1.6
D62Y	2.2	H39N	-0.3

C63Y	-3.8	H39R	-1.3
P64T	0.9	H39L	7.0
Y65N	-2.2	I40N	-8.0
E66D	0.0	I40T	-5.2
A71V	2.4	I40V	-0.3
A71T	-2.5	F41L	1.0
C73R	-7.0	T43I	5.2
P74T	0.9	R44W	3.6
I75T	-5.2	R44M	6.4
I76F	-1.7	R44S	3.7
I76T	-5.2	R46S	3.7
T77S	-0.1	R48L	8.3
S79N	-2.7	G51W	-0.5
S80P	-0.8	G51V	4.6
S80Y	-0.5	K52E	0.4
V81A	-2.4	K52R	-0.6
L82P	-5.4	K52N	0.4
Q85K	-0.4	G53C	2.9
R86W	3.6	D54Y	2.2
D89G	3.1	D54V	7.7
G90V	4.6	S55P	-0.8
P91H	-1.6	E56A	5.3
S93N	-2.7	E56V	7.7
P96Q	-1.9	P60T	0.9
S97T	0.1	P60H	-1.6
S97P	-0.8	P60L	5.4
S98T	0.1	D62Y	2.2
S98P	-0.8	P64T	0.9
Q99L	7.3	E66V	7.7
Q99H	0.3	E66D	0.0
D100Y	2.2	A71T	-2.5
S101T	0.1	C73R	-7.0
S101Y	-0.5	P74T	0.9
S103Y	-0.5	I75T	-5.2
P109T	0.9	I76N	-8.0
L111P	-5.4	V78D	-7.7
Y112H	-1.9	S79G	0.4
Y112C	3.8	S80Y	-0.5
D113E	0.0	S80P	-0.8
D113V	7.7	L82I	0.7
R114H	1.3	Q85K	-0.4
R115M	6.4	P87L	5.4
S116G	0.4	D89G	3.1
I117T	-5.2	G90V	4.6
I117V	-0.3	S93C	3.3
F118I	1.7	P96Q	-1.9

F118L	1.0	S98P	-0.8
D119Y	2.2	Q99H	0.3
V121E	-7.7	D100Y	2.2
V121M	-2.3	S101Y	-0.5
Q123K	-0.4	S103Y	-0.5
N125I	8.0	P109T	0.9
Q127H	0.3	R110G	4.1
E130D	0.0	Y112N	-2.2
S131G	0.4	D113E	0.0
S131C	3.3	D113V	7.7
Q137H	0.3	R115S	3.7
R138W	3.6	R115M	6.4
R138M	6.4	I117T	-5.2
K140M	5.8	I117V	-0.3
K140E	0.4	F118I	1.7
K140N	0.4	F118L	1.0
K141R	-0.6	D119Y	2.2
L143Q	-7.3	V121M	-2.3
D145G	3.1	V121E	-7.7
D145V	7.7	V121A	-2.4
S146C	3.3	Q123H	0.3
E147G	3.1	Q123K	-0.4
K149E	0.4	N125I	8.0
P151Q	-1.9	Q127L	7.3
E152G	3.1	Q127P	1.9
T153S	-0.1	L129Q	-7.3
T153I	5.2	E130G	3.1
G154V	4.6	E130D	0.0
K155R	-0.6	S131G	0.4
T156S	-0.1	L133P	-5.4
C157R	-7.0	Q137R	-1.0
L158Q	-7.3	Q137H	0.3
K160E	0.4	R138M	6.4
M162L	1.9	R138S	3.7
L163P	-5.4	K140R	-0.6
N164K	-0.4	K141E	0.4
N164S	2.7	K141R	-0.6
L165P	-5.4	L143Q	-7.3
H166L	7.0	L143P	-5.4
H166R	-1.3	D145Y	2.2
N167K	-0.4	F148L	1.0
N170K	-0.4	K149E	0.4
D171V	7.7	D150Y	2.2
T172S	-0.1	P151Q	-1.9
T172A	2.5	E152G	3.1
I173N	-8.0	E152D	0.0

L176P	-5.4	T153I	5.2
L177Q	-7.3	G154V	4.6
L177P	-5.4	K155N	0.4
D178V	7.7	K155T	3.2
D178Y	2.2	L158Q	-7.3
V179A	-2.4	M162T	-2.6
V179I	0.3	M162L	1.9
T183A	2.5	L163P	-5.4
S185G	0.4	N164S	2.7
L186P	-5.4	N164K	-0.4
K187R	-0.6	L165P	-5.4
F189L	1.0	N167D	0.0
V190D	-7.7	N167S	2.7
V190A	-2.4	G168V	4.6
N191D	0.0	Q169P	1.9
N191S	2.7	Q169H	0.3
Y194N	-2.2	D171Y	2.2
Y194H	-1.9	D171V	7.7
T195A	2.5	T172S	-0.1
Y198C	3.8	T172A	2.5
K200D	0.4	I173N	-8.0
K200C	6.4	L175M	-1.9
Q202L	7.3	L177Q	-7.3
L205Q	-7.3	L177P	-5.4
L205R	-8.3	D178Y	2.2
I207T	-5.2	D178V	7.7
I209N	-8.0	V179I	0.3
I209T	-5.2	V179A	-2.4
I209F	-1.7	K182R	-0.6
E210G	3.1	K182N	0.4
E210D	0.0	T183A	2.5
R211W	3.6	D184Y	2.2
R211L	8.3	D184G	3.1
T215S	-0.1	L186P	-5.4
L216Q	-7.3	K187R	-0.6
V217A	-2.4	F189I	1.7
V217M	-2.3	V190D	-7.7
V217E	-7.7	V190A	-2.4
T218S	-0.1	N191D	0.0
L219H	-7.0	N191S	2.7
L220F	-1.0	Y194N	-2.2
V221E	-7.7	Y194H	-1.9
E222D	0.0	T195A	2.5
N223D	0.0	D196Y	2.2
D226G	3.1	S197G	0.4
V227A	-2.4	Y198H	-1.9

Q228K	-0.4	Y198C	3.8
Q228L	7.3	G201D	-3.1
Q228H	0.3	G201C	2.9
A231T	-2.5	Q202L	7.3
N232I	8.0	Q202H	0.3
G233E	-3.1	L205Q	-7.3
F235S	-3.6	I207T	-5.2
F236L	1.0	I207F	-1.7
K237E	0.4	I209T	-5.2
K237N	0.4	I209F	-1.7
K240N	0.4	E210G	3.1
G241V	4.6	E210D	0.0
P243L	5.4	R211W	3.6
P243H	-1.6	R211L	8.3
G244C	2.9	R212L	8.3
F245S	-3.6	N213Y	2.2
F247S	-3.6	M214L	1.9
G248C	2.9	M214I	2.6
E249G	3.1	M214T	-2.6
E249V	7.7	L216Q	-7.3
P251H	-1.6	L216P	-5.4
L252Q	-7.3	V217E	-7.7
L252P	-5.4	V217A	-2.4
S253T	0.1	T218S	-0.1
S253Y	-0.5	L219I	0.7
A255T	-2.5	L219H	-7.0
C257R	-7.0	L220S	-4.6
T258A	2.5	L220F	-1.0
N259D	0.0	V221E	-7.7
N259Y	2.2	E222D	0.0
N259I	8.0	N223D	0.0
Q260R	-1.0	N223I	8.0
Q260L	7.3	G224V	4.6
L261Q	-7.3	D226G	3.1
V264E	-7.7	Q228R	-1.0
L267M	-1.9	Q228K	-0.4
L267P	-5.4	D234Y	2.2
N270S	2.7	F235S	-3.6
W272R	-3.6	F235V	1.4
W272L	4.7	F236L	1.0
D276Y	2.2	F236I	1.7
G284C	2.9	F236Y	-4.1
N285D	0.0	F236S	-3.6
N285I	8.0	K237E	0.4
V287E	-7.7	K237R	-0.6
L288P	-5.4	K237N	0.4

H289N	-0.3	T239S	-0.1
H289R	-1.3	G241V	4.6
L291P	-5.4	R242G	4.1
V292E	-7.7	R242M	6.4
V292G	-4.6	P243L	5.4
E293G	3.1	G244C	2.9
E293D	0.0	F245S	-3.6
V294E	-7.7	Y246H	-1.9
V294A	-2.4	F247S	-3.6
A295T	-2.5	G248C	2.9
D296E	0.0	E249G	3.1
D296V	7.7	E249V	7.7
N301D	0.0	L250P	-5.4
N301S	2.7	L252M	-1.9
N301I	8.0	L252Q	-7.3
T302A	2.5	L252P	-5.4
F304S	-3.6	S253T	0.1
V305A	-2.4	S253Y	-0.5
V305M	-2.3	L254M	-1.9
T306S	-0.1	C257R	-7.0
S307R	-3.7	T258A	2.5
S307G	0.4	Q260R	-1.0
M308T	-2.6	Q260L	7.3
Y309H	-1.9	L261P	-5.4
Y309C	3.8	I263T	-5.2
N310I	8.0	V264E	-7.7
E311G	3.1	F266L	1.0
I312N	-8.0	L267M	-1.9
I312T	-5.2	L267P	-5.4
L313S	-4.6	Q269R	-1.0
I314N	-8.0	Q269H	0.3
I314V	-0.3	N270S	2.7
G316W	-0.5	S271Y	-0.5
L319P	-5.4	W272R	-3.6
H320P	1.6	W272L	4.7
H320L	7.0	D276Y	2.2
T322M	2.6	D276V	7.7
L323P	-5.4	S278G	0.4
K324R	-0.6	D281Y	2.2
L325Q	-7.3	D281G	3.1
L325P	-5.4	G284C	2.9
I328T	-5.2	N285I	8.0
I328V	-0.3	V287E	-7.7
T329A	2.5	V287A	-2.4
N330Y	2.2	L288P	-5.4
N330I	8.0	H289N	-0.3

R331M	6.4	H289R	-1.3
R331S	3.7	L291M	-1.9
K332N	0.4	L291P	-5.4
G333W	-0.5	E293G	3.1
G333V	4.6	V294E	-7.7
T335P	-0.9	V294A	-2.4
T335A	2.5	A295V	2.4
T335M	2.6	A295T	-2.5
L337Q	-7.3	D296V	7.7
L337P	-5.4	N297I	8.0
L339Q	-7.3	T298A	2.5
L339P	-5.4	D300Y	2.2
S343R	-3.7	N301D	0.0
G344R	-4.1	N301I	8.0
G344V	4.6	T302A	2.5
K345R	-0.6	K303M	5.8
I346F	-1.7	V305E	-7.7
G347R	-4.1	T306S	-0.1
V348A	-2.4	S307G	0.4
L349S	-4.6	M308T	-2.6
L349F	-1.0	Y309C	3.8
I352V	-0.3	N310D	0.0
I352T	-5.2	N310I	8.0
L353P	-5.4	I312N	-8.0
L353I	0.7	I314N	-8.0
Q354R	-1.0	I314T	-5.2
Q354H	0.3	I314V	-0.3
R355S	3.7	G316W	-0.5
E356G	3.1	L319P	-5.4
H358R	-1.3	H320R	-1.3
H358L	7.0	P321H	-1.6
E359G	3.1	P321T	0.9
P360H	-1.6	L323P	-5.4
E361G	3.1	K324R	-0.6
H364R	-1.3	L325P	-5.4
L365I	0.7	E327G	3.1
R367M	6.4	I328N	-8.0
E371K	-0.4	T329A	2.5
W372L	4.7	N330I	8.0
W372R	-3.6	R331M	6.4
G375E	-3.1	R331S	3.7
P376S	0.8	K332N	0.4
P376L	5.4	G333W	-0.5
V377A	-2.4	G333V	4.6
H378R	-1.3	L334P	-5.4
S380Y	-0.5	T335P	-0.9

S380P	-0.8	L337Q	-7.3
Y382H	-1.9	A338V	2.4
L384M	-1.9	L339Q	-7.3
S385Y	-0.5	L339P	-5.4
C386Y	-3.8	A340T	-2.5
I387T	-5.2	S343R	-3.7
D388V	7.7	G344V	4.6
E391G	3.1	K345R	-0.6
K392E	0.4	I346F	-1.7
K392R	-0.6	G347R	-4.1
N393S	2.7	G347V	4.6
N393I	8.0	L349S	-4.6
S394P	-0.8	L349F	-1.0
V395A	-2.4	I352T	-5.2
L396Q	-7.3	L353P	-5.4
E397G	3.1	L353I	0.7
E397D	0.0	Q354R	-1.0
V398A	-2.4	Q354K	-0.4
I399N	-8.0	Q354H	0.3
S402G	0.4	R355W	3.6
S402C	3.3	R355S	3.7
S403G	0.4	E356G	3.1
S404G	0.4	P360H	-1.6
S404R	-3.7	E361V	7.7
E405V	7.7	R363L	8.3
E405D	0.0	H364R	-1.3
T406S	-0.1	R367M	6.4
N408S	2.7	F369L	1.0
N408I	8.0	F369S	-3.6
H410L	7.0	E371K	-0.4
D411N	0.0	W372L	4.7
D411V	7.7	G375W	-0.5
M412T	-2.6	G375E	-3.1
M412L	1.9	P376S	0.8
L413P	-5.4	P376L	5.4
L414I	0.7	V377A	-2.4
L414H	-7.0	V377E	-7.7
L414P	-5.4	S379Y	-0.5
L414F	-1.0	S379P	-0.8
V415E	-7.7	S380P	-0.8
V415A	-2.4	S380Y	-0.5
E416D	0.0	Y382C	3.8
P417H	-1.6	D383Y	2.2
P417S	0.8	D383G	3.1
N419Y	2.2	D383V	7.7
L421H	-7.0	L384M	-1.9

L422I	0.7	S385Y	-0.5
Q423R	-1.0	S385P	-0.8
Q423H	0.3	C386Y	-3.8
D424Y	2.2	C386R	-7.0
K425E	0.4	D388Y	2.2
D427V	7.7	D388V	7.7
D427G	3.1	E391G	3.1
D427Y	2.2	K392R	-0.6
K431E	0.4	K392N	0.4
I433I	0.0	N393I	8.0
I433L	-0.7	S394P	-0.8
Y435L	5.1	V395A	-2.4
F436D	-6.3	L396M	-1.9
N437S	2.7	L396Q	-7.3
N437I	8.0	E397D	0.0
N437L	7.3	V398A	-2.4
F439D	-6.3	I399N	-8.0
M445K	-5.8	I399T	-5.2
M445R	-6.4	S404G	0.4
I446L	-0.7	E405V	7.7
I446F	-1.7	E405D	0.0
I446N	-8.0	T406S	-0.1
F448L	1.0	N408I	8.0
Y453H	-1.9	H410N	-0.3
R455Q	1.0	D411Y	2.2
R455L	8.3	M412T	-2.6
V457A	-2.4	M412L	1.9
L460S	-4.6	L413P	-5.4
P461S	0.8	L414H	-7.0
P461L	5.4	L414P	-5.4
K464M	5.8	E416D	0.0
L465P	-5.4	P417H	-1.6
N467T	2.8	L418F	-1.0
T468A	2.5	N419Y	2.2
V469I	0.3	R420L	8.3
D471G	3.1	L421H	-7.0
D471Y	2.2	L422I	0.7
F473L	1.0	Q423R	-1.0
R474L	8.3	Q423H	0.3
V475D	-7.7	D424Y	2.2
V475A	-2.4	K425E	0.4
T476A	2.5	K425M	5.8
T476S	-0.1	W426R	-3.6
G477R	-4.1	W426C	3.4
G477E	-3.1	D427V	7.7
G477V	4.6	D427G	3.1

I479V	-0.3	D427Y	2.2
S481P	-0.8	K431E	0.4
S481F	3.6	I433T	-5.2
V482A	-2.4	F434L	1.0
S483T	0.1	F434I	1.7
S483P	-0.8	F436L	1.0
G484V	4.6	F438I	1.7
G485V	4.6	F438L	1.0
V486D	-7.7	F438S	-3.6
Y487C	3.8	V440D	-7.7
F488S	-3.6	V440A	-2.4
F489L	1.0	L443S	-4.6
F489S	-3.6	Y444H	-1.9
R491L	8.3	M445L	1.9
G492V	4.6	M445K	-5.8
I493V	-0.3	I446N	-8.0
F496S	-3.6	I446L	-0.7
F496L	1.0	I446F	-1.7
L497P	-5.4	I447F	-1.7
L497M	-1.9	F448L	1.0
R499G	4.1	Y454H	-1.9
S502P	-0.8	R455Q	1.0
S502Y	-0.5	V457A	-2.4
L503H	-7.0	P461H	-1.6
K504N	0.4	K464M	5.8
S505G	0.4	T468A	2.5
L506S	-4.6	G470W	-0.5
F507Y	-4.1	G470V	4.6
F507S	-3.6	D471Y	2.2
V508E	-7.7	F473L	1.0
V508A	-2.4	R474L	8.3
D509V	7.7	V475D	-7.7
D509G	3.1	T476A	2.5
Y511F	4.1	G477V	4.6
Y511H	-1.9	E478G	3.1
S512G	0.4	I479V	-0.3
E513G	3.1	S481P	-0.8
E513D	0.0	S481Y	-0.5
I514V	-0.3	S481F	3.6
I514M	-2.6	V482A	-2.4
L515P	-5.4	S483T	0.1
F516L	1.0	S483P	-0.8
F517I	1.7	G484V	4.6
F517L	1.0	G485V	4.6
Q519R	-1.0	V486D	-7.7
Q519L	7.3	Y487N	-2.2

L521P	-5.4	F488Y	-4.1
F522S	-3.6	F489L	1.0
M523T	-2.6	R491L	8.3
M523R	-6.4	G492W	-0.5
L524Q	-7.3	G492V	4.6
L524P	-5.4	I493V	-0.3
S526P	-0.8	Q494K	-0.4
V527A	-2.4	F496L	1.0
V527E	-7.7	L497P	-5.4
V528A	-2.4	L497M	-1.9
L529P	-5.4	R499G	4.1
L529Q	-7.3	R500L	8.3
Y530H	-1.9	P501Q	-1.9
Y530C	3.8	S502P	-0.8
S532G	0.4	S502Y	-0.5
Q533K	-0.4	L503H	-7.0
Q533R	-1.0	K504N	0.4
K535E	0.4	F507Y	-4.1
K535R	-0.6	F507S	-3.6
K535M	5.8	V508A	-2.4
K535N	0.4	V508E	-7.7
E536G	3.1	D509G	3.1
Y537F	4.1	D509Y	2.2
V538A	-2.4	S510G	0.4
M541K	-5.8	Y511H	-1.9
M541I	2.6	S512G	0.4
F543S	-3.6	S512R	-3.7
S544P	-0.8	E513G	3.1
L545Q	-7.3	I514V	-0.3
W549R	-3.6	L515P	-5.4
W549C	3.4	F516I	1.7
T550A	2.5	F516L	1.0
M552V	2.3	F517I	1.7
L553P	-5.4	F517L	1.0
Y554N	-2.2	Q519R	-1.0
Y554H	-1.9	Q519L	7.3
Y554C	3.8	S520P	-0.8
Y555H	-1.9	L521P	-5.4
Y555F	4.1	F522S	-3.6
Y555C	3.8	M523K	-5.8
T556A	2.5	M523R	-6.4
F559L	1.0	L524P	-5.4
Q560K	-0.4	V525A	-2.4
Q560R	-1.0	S526Y	-0.5
M562T	-2.6	S526P	-0.8
M562V	2.3	V527A	-2.4

M562L	1.9	V527E	-7.7
I564T	-5.2	V528A	-2.4
Y565H	-1.9	L529P	-5.4
Y565N	-2.2	L529Q	-7.3
Y565C	3.8	Q533H	0.3
V567A	-2.4	Q533K	-0.4
V567D	-7.7	Q533R	-1.0
M568V	2.3	Q533L	7.3
M568T	-2.6	K535E	0.4
M568I	2.6	K535R	-0.6
I569T	-5.2	Y537S	0.5
I569V	-0.3	Y537C	3.8
E570G	3.1	V538A	-2.4
K571E	0.4	V538E	-7.7
K571R	-0.6	F543L	1.0
M572T	-2.6	F543S	-3.6
M572V	2.3	S544Y	-0.5
M572L	1.9	S544P	-0.8
I573V	-0.3	S544T	0.1
L574H	-7.0	M547T	-2.6
L574P	-5.4	M547V	2.3
D576G	3.1	M547I	2.6
D576Y	2.2	W549R	-3.6
D576V	7.7	W549C	3.4
L577M	-1.9	T550A	2.5
L577P	-5.4	N551S	2.7
R579Q	1.0	L553P	-5.4
F580L	1.0	Y554N	-2.2
F580I	1.7	Y554H	-1.9
F580S	-3.6	G558E	-3.1
M581T	-2.6	F559L	1.0
M581V	2.3	Q560K	-0.4
M581K	-5.8	M562L	1.9
V583I	0.3	M562I	2.6
V583D	-7.7	M562T	-2.6
Y584C	3.8	M562V	2.3
Y584H	-1.9	I564N	-8.0
L585P	-5.4	Y565N	-2.2
F587Y	-4.1	Y565C	3.8
F587S	-3.6	V567D	-7.7
L588S	-4.6	V567A	-2.4
F589L	1.0	M568T	-2.6
F589S	-3.6	M568V	2.3
F591L	1.0	M568R	-6.4
F591S	-3.6	M568I	2.6
S592Y	-0.5	I569T	-5.2

S592P	-0.8	I569V	-0.3
T593S	-0.1	I569F	-1.7
V595A	-2.4	E570G	3.1
V595E	-7.7	M572L	1.9
V596M	-2.3	I573V	-0.3
V596A	-2.4	L574P	-5.4
T597S	-0.1	R575G	4.1
T597A	2.5	D576V	7.7
L598P	-5.4	D576G	3.1
I599T	-5.2	D576Y	2.2
I599F	-1.7	L577M	-1.9
E600G	3.1	L577P	-5.4
E600V	7.7	R579Q	1.0
E600D	0.0	F580L	1.0
D601G	3.1	F580S	-3.6
G602V	4.6	M581T	-2.6
K603N	0.4	M581K	-5.8
N604D	0.0	M581V	2.3
N604S	2.7	V583I	0.3
N604Y	2.2	V583D	-7.7
N605S	2.7	V583A	-2.4
L607P	-5.4	Y584H	-1.9
P608H	-1.6	Y584C	3.8
M609K	-5.8	L585P	-5.4
M609L	1.9	F587L	1.0
M609I	2.6	F587I	1.7
E610G	3.1	F587Y	-4.1
P613Q	-1.9	F587S	-3.6
H614R	-1.3	L588S	-4.6
C616R	-7.0	F589L	1.0
G618V	4.6	F589Y	-4.1
S619P	-0.8	F591L	1.0
S619Y	-0.5	F591S	-3.6
C621R	-7.0	S592Y	-0.5
K622R	-0.6	V595E	-7.7
K622E	0.4	V595A	-2.4
P623Q	-1.9	V596E	-7.7
G624C	2.9	V596M	-2.3
N625S	2.7	T597S	-0.1
S626P	-0.8	T597A	2.5
Y627H	-1.9	L598P	-5.4
Y627F	4.1	I599T	-5.2
N628D	0.0	I599F	-1.7
N628S	2.7	E600G	3.1
N628I	8.0	E600D	0.0
S629G	0.4	D601G	3.1

L630P	-5.4	D601E	0.0
L630Q	-7.3	G602V	4.6
Y631H	-1.9	K603R	-0.6
T633A	2.5	K603N	0.4
T633S	-0.1	N604D	0.0
C634R	-7.0	N605S	2.7
L635M	-1.9	S606Y	-0.5
L635P	-5.4	S606P	-0.8
E636G	3.1	L607M	-1.9
F638I	1.7	L607Q	-7.3
F638S	-3.6	P608H	-1.6
K639R	-0.6	M609I	2.6
F640I	1.7	M609L	1.9
F640Y	-4.1	E610V	7.7
F640S	-3.6	S611Y	-0.5
T641A	2.5	P613Q	-1.9
I642V	-0.3	H614R	-1.3
I642F	-1.7	K615E	0.4
G643S	-0.4	K615R	-0.6
G643C	2.9	C616R	-7.0
M644V	2.3	G618W	-0.5
M644T	-2.6	G618V	4.6
D646V	7.7	S619P	-0.8
L647M	-1.9	S619Y	-0.5
L647Q	-7.3	K622E	0.4
L647P	-5.4	P623Q	-1.9
E648G	3.1	G624C	2.9
F649Y	-4.1	N625I	8.0
T650A	2.5	S626Y	-0.5
E651G	3.1	S626P	-0.8
E651V	7.7	S626T	0.1
E651D	0.0	N628D	0.0
N652Y	2.2	N628S	2.7
N652I	8.0	L630Q	-7.3
Y653F	4.1	L630P	-5.4
D654G	3.1	Y631H	-1.9
D654V	7.7	Y631C	3.8
F655L	1.0	S632Y	-0.5
K656E	0.4	S632P	-0.8
K656R	-0.6	T633S	-0.1
K656M	5.8	C634R	-7.0
V658A	-2.4	L635M	-1.9
V658D	-7.7	L635Q	-7.3
F659L	1.0	L635P	-5.4
I661T	-5.2	E636G	3.1
L662Q	-7.3	L637R	-8.3

L663S	-4.6	F638L	1.0
L664P	-5.4	F638Y	-4.1
Y666C	3.8	F638S	-3.6
V667A	-2.4	K639E	0.4
I668T	-5.2	K639R	-0.6
I668F	-1.7	F640L	1.0
L669H	-7.0	F640Y	-4.1
L669P	-5.4	F640S	-3.6
T670A	2.5	T641A	2.5
Y671H	-1.9	T641I	5.2
I672V	-0.3	I642V	-0.3
I672T	-5.2	I642N	-8.0
L673P	-5.4	I642T	-5.2
L675F	-1.0	I642F	-1.7
L675H	-7.0	G643S	-0.4
L675P	-5.4	G643C	2.9
N676S	2.7	M644K	-5.8
N676D	0.0	M644T	-2.6
M677T	-2.6	M644I	2.6
M677V	2.3	M644V	2.3
M677L	1.9	D646Y	2.2
L678P	-5.4	D646V	7.7
L678H	-7.0	L647M	-1.9
I679T	-5.2	L647Q	-7.3
L681P	-5.4	L647P	-5.4
L681H	-7.0	L647R	-8.3
M682V	2.3	E648G	3.1
M682T	-2.6	F649Y	-4.1
M682L	1.9	F649L	1.0
G683S	-0.4	F649S	-3.6
G683C	2.9	T650A	2.5
E684G	3.1	E651G	3.1
T685A	2.5	E651D	0.0
N687D	0.0	N652S	2.7
N687S	2.7	N652Y	2.2
N687I	8.0	N652I	8.0
I689T	-5.2	Y653H	-1.9
I689V	-0.3	Y653F	4.1
A690T	-2.5	D654G	3.1
Q691R	-1.0	D654Y	2.2
E692G	3.1	F655L	1.0
S693C	3.3	F655V	1.4
S693G	0.4	K656R	-0.6
K694R	-0.6	K656M	5.8
N695D	0.0	V658A	-2.4
N695I	8.0	V658D	-7.7

N695H	0.3	F659L	1.0
N695S	2.7	F659S	-3.6
N695Y	2.2	I660T	-5.2
I696T	-5.2	I660V	-0.3
I696V	-0.3	I661T	-5.2
W697R	-3.6	I661N	-8.0
K698R	-0.6	L662M	-1.9
K698M	5.8	L662P	-5.4
L699P	-5.4	L662Q	-7.3
Q700R	-1.0	L662R	-8.3
Q700L	7.3	L663S	-4.6
R701G	4.1	L664P	-5.4
R701I	9.0	Y666H	-1.9
I703N	-8.0	Y666C	3.8
I703T	-5.2	V667A	-2.4
I703F	-1.7	I668F	-1.7
T704A	2.5	I668T	-5.2
I705V	-0.3	I668V	-0.3
I705T	-5.2	L669I	0.7
L706P	-5.4	L669H	-7.0
L706M	-1.9	L669P	-5.4
D707Y	2.2	T670A	2.5
E709G	3.1	T670I	5.2
E709V	7.7	Y671H	-1.9
E709D	0.0	I672V	-0.3
K710R	-0.6	I672T	-5.2
K710E	0.4	L673I	0.7
K710M	5.8	L673P	-5.4
K710N	0.4	L674P	-5.4
F712L	1.0	L675P	-5.4
L713P	-5.4	N676D	0.0
L713Q	-7.3	N676S	2.7
K714E	0.4	M677V	2.3
M716R	-6.4	M677K	-5.8
M716V	2.3	M677T	-2.6
R717G	4.1	M677L	1.9
R717S	3.7	L678H	-7.0
K718E	0.4	L678P	-5.4
K718N	0.4	I679T	-5.2
A719T	-2.5	I679L	-0.7
F720S	-3.6	L681I	0.7
F720L	1.0	L681H	-7.0
R721H	1.3	L681P	-5.4
R721S	3.7	M682T	-2.6
G723D	-3.1	M682V	2.3
G723C	2.9	M682L	1.9

K724E	0.4	G683C	2.9
L725P	-5.4	E684G	3.1
L726P	-5.4	E684D	0.0
Q727R	-1.0	T685A	2.5
Q727H	0.3	N687D	0.0
V728E	-7.7	N687S	2.7
V728A	-2.4	N687I	8.0
G729V	4.6	I689V	-0.3
F730S	-3.6	Q691R	-1.0
P732T	0.9	E692D	0.0
P732H	-1.6	E692G	3.1
D733G	3.1	S693C	3.3
D733V	7.7	S693G	0.4
D733Y	2.2	K694N	0.4
G734D	-3.1	K694R	-0.6
D736Y	2.2	N695Y	2.2
D737G	3.1	N695H	0.3
D737V	7.7	N695D	0.0
R739L	8.3	N695S	2.7
W740L	4.7	N695I	8.0
C741S	-3.3	I696V	-0.3
C741R	-7.0	I696N	-8.0
F742L	1.0	I696T	-5.2
D745G	3.1	W697R	-3.6
D745Y	2.2	W697L	4.7
E746G	3.1	K698R	-0.6
E746D	0.0	K698E	0.4
N748I	8.0	L699P	-5.4
W749R	-3.6	Q700L	7.3
T750A	2.5	Q700H	0.3
W752R	-3.6	R701G	4.1
T754A	2.5	R701I	9.0
N755K	-0.4	A702V	2.4
V756A	-2.4	I703N	-8.0
V756E	-7.7	I703T	-5.2
G757C	2.9	I703F	-1.7
I758N	-8.0	I705T	-5.2
I759N	-8.0	I705F	-1.7
I759T	-5.2	L706M	-1.9
I759F	-1.7	L706P	-5.4
I759V	-0.3	D707G	3.1
N760D	0.0	D707Y	2.2
N760I	8.0	E709V	7.7
N760S	2.7	E709D	0.0
E761V	7.7	K710M	5.8
E761D	0.0	K710N	0.4

D762G	3.1	F712L	1.0
C766R	-7.0	F712S	-3.6
C766Y	-3.8	L713P	-5.4
G768C	2.9	C715Y	-3.8
K770E	0.4	M716I	2.6
R771H	1.3	M716V	2.3
L773Q	-7.3	R717S	3.7
L773P	-5.4	K718N	0.4
S776P	-0.8	R721S	3.7
R778M	6.4	S722Y	-0.5
S779T	0.1	S722P	-0.8
G780D	-3.1	G723D	-3.1
V782D	-7.7	G723C	2.9
V782A	-2.4	K724M	5.8
G784R	-4.1	L726P	-5.4
R785S	3.7	Q727H	0.3
N786D	0.0	V728E	-7.7
W787R	-3.6	G729V	4.6
W787L	4.7	F730I	1.7
N789D	0.0	F730S	-3.6
P794T	0.9	P732T	0.9
L795P	-5.4	P732H	-1.6
R797G	4.1	D733Y	2.2
D798Y	2.2	D733V	7.7
T801A	2.5	G734D	-3.1
D803G	3.1	G734C	2.9
R804I	9.0	G734S	-0.4
H805R	-1.3	K735N	0.4
A806T	-2.5	D736G	3.1
T807S	-0.1	D736Y	2.2
Q808R	-1.0	D737Y	2.2
Q809R	-1.0	D737G	3.1
Q809H	0.3	D737V	7.7
L814P	-5.4	Y738C	3.8
K815R	-0.6	W740L	4.7
Y817C	3.8	F742S	-3.6
T818A	2.5	F742L	1.0
S820P	-0.8	D745G	3.1
K822R	-0.6	D745Y	2.2
D825G	3.1	E746D	0.0
D825V	7.7	N748S	2.7
E827D	0.0	N748D	0.0
F829L	1.0	W749L	4.7
K830R	-0.6	W749R	-3.6
D831Y	2.2	W749C	3.4
S832Y	-0.5	T750A	2.5

M833T	-2.6	W752L	4.7
V834D	-7.7	W752C	3.4
P835T	0.9	N753S	2.7
E837G	3.1	T754A	2.5
E837D	0.0	N755Y	2.2
		G757C	2.9
		I758N	-8.0
		I759T	-5.2
		I759V	-0.3
		N760D	0.0
		N760S	2.7
		E761V	7.7
		E761D	0.0
		D762Y	2.2
		P763Q	-1.9
		P763T	0.9
		C766Y	-3.8
		E767G	3.1
		E767V	7.7
		G768C	2.9
		T772A	2.5
		L777M	-1.9
		R778M	6.4
		S779T	0.1
		S779L	4.6
		G780D	-3.1
		R781L	8.3
		R781Q	1.0
		V782D	-7.7
		V782A	-2.4
		G784V	4.6
		R785G	4.1
		R785I	9.0
		R785S	3.7
		N786D	0.0
		W787L	4.7
		W787C	3.4
		K788N	0.4
		N789D	0.0
		F790I	1.7
		L792P	-5.4
		P794T	0.9
		L795I	0.7
		L795P	-5.4
		R797S	3.7
		T801A	2.5

		R802L	8.3
		D803G	3.1
		R804I	9.0
		A806T	-2.5
		T807A	2.5
		T807S	-0.1
		Q808K	-0.4
		Q808R	-1.0
		Q809R	-1.0
		Q809H	0.3
		V812A	-2.4
		Q813K	-0.4
		Q813R	-1.0
		Y817C	3.8
		T818A	2.5
		S820P	-0.8
		L821I	0.7
		K822R	-0.6
		E824D	0.0
		E827G	3.1
		E827D	0.0
		F829L	1.0
		K830R	-0.6
		K830N	0.4
		D831Y	2.2
		S832Y	-0.5
		M833V	2.3
		M833I	2.6
		V834D	-7.7
		V834A	-2.4
		P835Q	-1.9
		P835T	0.9
		E837D	0.0

References

- Adkar, B. V, Tripathi, A., Sahoo, A., Bajaj, K., Goswami, D., Chakrabarti, P., Swarnkar, M.K., Gokhale, R.S., and Varadarajan, R. (2012). Protein model discrimination using mutational sensitivity derived from deep sequencing. *Structure* 20, 371–381.
- Aggarwal, S.K., and MacKinnon, R. (1996). Contribution of the S4 segment to gating charge in the Shaker K⁺ channel. *Neuron* 16, 1169–1177.
- Alberts, B., Johnson, A., Lewis, J., Raff, M., Roberts, K., and Walter, P. (2008). *Molecular biology of the cell* (New York: Garland Science; Taylor & Francis Group, LLC).
- Baldwin, R.L. (1986). Temperature Dependence of the Hydrophobic Interaction in Protein Folding. *Proc. Natl. Acad. Sci.* 83, 8069–8072.
- Bandell, M., Dubin, A.E., Petrus, M.J., Orth, A., Mathur, J., Hwang, S.W., and Patapoutian, A. (2006). High-throughput random mutagenesis screen reveals TRPM8 residues specifically required for activation by menthol. *Nat. Neurosci.* 9, 493–500.
- Bautista, D.M., Siemens, J., Glazer, J.M., Tsuruda, P.R., Basbaum, A.I., Stucky, C.L., Jordt, S.-E., and Julius, D. (2007). The menthol receptor TRPM8 is the principal detector of environmental cold. *Nature* 448, 204–208.
- Bautista, D.M., Pellegrino, M., and Tsunozaki, M. (2013). TRPA1: A gatekeeper for inflammation. *Annu. Rev. Physiol.* 75, 181–200.
- Bichet, D., Haass, F. a, and Jan, L.Y. (2003). Merging functional studies with structures of inward-rectifier K(+) channels. *Nat. Rev. Neurosci.* 4, 957–967.
- Bill, A., Rosethorne, E.M., Kent, T.C., Fawcett, L., Burchell, L., Van Diepen, M.T., Marelli, A., Batalov, S., Miraglia, L., Orth, A.P., et al. (2014). High throughput mutagenesis for identification of residues regulating human prostacyclin (hIP) receptor. *PLoS One* 9, 1–11.
- Bischof, J.C., and He, X. (2005). Thermal stability of proteins. *Ann. N. Y. Acad. Sci.* 1066, 12–33.
- Brauchi, S., Orio, P., and Latorre, R. (2004). Clues to understanding cold sensation : Thermodynamics and electrophysiological analysis of the cold receptor TRPM8. *Proc. Natl. Acad. Sci. U. S. A.* 101, 15494–15499.
- Brown, D.J.A., Brugger, H., Boyd, J., and Paal, P. (2012). Accidental Hypothermia. *N. Engl. J. Med.* 367, 1930–1938.
- Cao, E., Liao, M., Cheng, Y., and Julius, D. (2013a). TRPV1 structures in distinct conformations reveal activation mechanisms. *Nature* 504, 113–118.
- Cao, E., Cordero-Morales, J.F., Liu, B., Qin, F., and Julius, D. (2013b). TRPV1 channels are intrinsically heat sensitive and negatively regulated by phosphoinositide lipids. *Neuron* 77, 667–679.

- Cao, X., Ma, L., Yang, F., Wang, K., and Zheng, J. (2014). Divalent cations potentiate TRPV1 channel by lowering the heat activation threshold. *J. Gen. Physiol.* 143, 75–90.
- Caspani, O., and Heppenstall, P. a (2009). TRPA1 and cold transduction: an unresolved issue? *J. Gen. Physiol.* 133, 245–249.
- Caterina, M.J., Schumacher, M.A., Tominaga, M., Rosen, T.A., Levine, J.D., and Julius, D. (1997). The capsaicin receptor : a heat-activated ion channel in the pain pathway. *Nature* 389, 816–824.
- Caterina, M.J., Leffler, A., Malmberg, a B., Martin, W.J., Trafton, J., Petersen-Zeitz, K.R., Koltzenburg, M., Basbaum, a I., and Julius, D. (2000). Impaired nociception and pain sensation in mice lacking the capsaicin receptor. *Science* (80-.). 288, 306–313.
- Chatzigeorgiou, M., Yoo, S., Watson, J.D., Lee, W.H., Spencer, W.C., K., K.S., Hwang, S.W., Miller, D.M., 3rd, Treinin, M., Driscoll, M., and S., and W.R. (2010). Specific roles for DEG/ENaC and TRP channels in touch and thermosensation in *C. elegans* nociceptors. *Nat. Neurosci.* 13, 861–868.
- Chen, J., Kang, D., Xu, J., Lake, M., Hogan, J.O., Sun, C., Walter, K., Yao, B., and Kim, D. (2013). Species differences and molecular determinant of TRPA1 cold sensitivity. *Nat. Commun.* 4, 2501.
- Chen, Z., Alcayaga, C., Suarez-Isla, B. a, O'Rourke, B., Tomaselli, G., and Marban, E. (2002). A “minimal” sodium channel construct consisting of ligated S5-P-S6 segments forms a toxin-activatable ionophore. *J. Biol. Chem.* 277, 24653–24658.
- Cho, H., Yang, Y.D., Lee, J., Lee, B., Kim, T., Jang, Y., Back, S.K., Na, H.S., Harfe, B.D., Wang, F., et al. (2012). The calcium-activated chloride channel anoctamin 1 acts as a heat sensor in nociceptive neurons. *Nat. Neurosci.* 15, 1015–1021.
- Chowdhury, S., Jarecki, B.W., and Chanda, B. (2014). A molecular framework for temperature-dependent gating of ion channels. *Cell* 158, 1148–1158.
- Clapham, D.E., and Miller, C. (2011). A thermodynamic framework for understanding temperature sensing by transient receptor potential (TRP) channels. *Proc. Natl. Acad. Sci. U. S. A.* 108, 19492–19497.
- Colburn, R.W., Lubin, M. Lou, Stone, D.J., Wang, Y., Lawrence, D., D'Andrea, M.R., Brandt, M.R., Liu, Y., Flores, C.M., and Qin, N. (2007). Attenuated Cold Sensitivity in TRPM8 Null Mice. *Neuron* 54, 379–386.
- Cordero-Morales, J.F., Gracheva, E.O., and Julius, D. (2011). Cytoplasmic ankyrin repeats of transient receptor potential A1 (TRPA1) dictate sensitivity to thermal and chemical stimuli. *Proc. Natl. Acad. Sci. U. S. A.* 108, E1184-91.
- Dhaka, A., Murray, A.N., Mathur, J., Earley, T.J., Petrus, M.J., and Patapoutian, A. (2007). TRPM8 is required for cold sensation in mice. *Neuron* 54, 371–378.
- Doyle, D.A., Cabral, J.M., Pfuetzner, R.A., Kuo, A., Gulbis, M., Cohen, S.L., Chait, B.T., Mackinnon, R., Cabral, J.M., and Gulbis, J.M. (2013). The Structure of the

- Potassium Channel: Molecular Basis of K⁺ Conduction and Selectivity. *Science* (80-.). 280, 69–77.
- Dubin, A.E., and Patapoutian, A. (2010). Nociceptors: The sensors of the pain pathway. *J. Clin. Invest.* 120, 3760–3772.
- Fowler, D.M., Araya, C.L., Fleishman, S.J., Kellogg, E.H., Stephany, J.J., Baker, D., and Fields, S. (2010). High-resolution mapping of protein sequence-function relationships. *Nat. Methods* 7, 741–746.
- Fujita, F., Uchida, K., Takaishi, M., Sokabe, T., and Tominaga, M. (2013). Ambient temperature affects the temperature threshold for TRPM8 activation through interaction of phosphatidylinositol 4,5-bisphosphate. *J. Neurosci.* 33, 6154–6159.
- Gao, Y., Cao, E., Julius, D., and Cheng, Y. (2016). TRPV1 structures in nanodiscs reveal mechanisms of ligand and lipid action. *Nature* 534, 347–351.
- Garcia-Elias, A., Berna-Erro, A., Rubio-Moscardo, F., Pardo-Pastor, C., Mrkonjić, S., Sepúlveda, R. V., Vicente, R., González-Nilo, F., and Valverde, M.A. (2015). Interaction between the Linker, Pre-S1, and TRP Domains Determines Folding, Assembly, and Trafficking of TRPV Channels. *Structure* 23, 1404–1413.
- Goujon, M., McWilliam, H., Li, W., Valentin, F., Squizzato, S., Paern, J., and Lopez, R. (2010). A new bioinformatics analysis tools framework at EMBL-EBI. *Nucleic Acids Res.* 38, 695–699.
- Goulding, E.H., Tibbs, G.R., and Siegelbaum, S.A. (1994). Molecular mechanism of cyclic-nucleotide-gated channel activation. *Nature* 372, 369–374.
- Gracheva, E.O., Ingolia, N.T., Kelly, Y.M., Cordero-Morales, J.F., Hollopeter, G., Chesler, A.T., Sánchez, E.E., Perez, J.C., Weissman, J.S., and Julius, D. (2010). Molecular basis of infrared detection by snakes. *Nature* 464, 1006–1011.
- Grandl, J., Hu, H., Bandell, M., Bursulaya, B., Schmidt, M., Petrus, M., and Patapoutian, A. (2008). Pore region of TRPV3 ion channel is specifically required for heat activation. *Nat. Neurosci.* 11, 1007–1013.
- Grandl, J., Kim, S.E., Uzzell, V., Bursulaya, B., Petrus, M., Bandell, M., and Patapoutian, A. (2010). Temperature-induced opening of TRPV1 ion channel is stabilized by the pore domain. *Nat. Neurosci.* 13, 708–714.
- Haltia, T., and Freire, E. (1995). Forces and factors that contribute to the structural stability of membrane proteins. *Biochim. Biophys. Acta* 1228, 1–27.
- Hibino, H., Inanobe, A., Furutani, K., Murakami, S., Findlay, I., and Kurachi, Y. (2010). Inwardly rectifying potassium channels: their structure, function, and physiological roles. *Physiol. Rev.* 90, 291–366.
- Holmqvist, E., Reimegård, J., and Wagner, E.G.H. (2013). Massive functional mapping of a 5'-UTR by saturation mutagenesis, phenotypic sorting and deep sequencing. *Nucleic Acids Res.* 41, e122.

- Horrigan, F.T., and Aldrich, R.W. (2002). Coupling between voltage sensor activation, Ca²⁺ binding and channel opening in large conductance (BK) potassium channels. *J. Gen. Physiol.* 120, 267–305.
- Hu, H., Grandl, J., Bandell, M., Petrus, M., and Patapoutian, A. (2009). Two amino acid residues determine 2-APB sensitivity of the ion channels TRPV3 and TRPV4. *Proc. Natl. Acad. Sci. U. S. A.* 106, 1626–1631.
- Huynh, K.W., Cohen, M.R., Jiang, J., Samanta, A., Lodowski, D.T., Zhou, Z.H., and Moiseenkova-Bell, V.Y. (2016). Structure of the full-length TRPV2 channel by cryo-EM. *Nat. Commun.* 7, 11130.
- Jabba, S., Goyal, R., Sosa-Pagán, J.O., Moldenhauer, H., Wu, J., Kalmeta, B., Bandell, M., Latorre, R., Patapoutian, A., and Grandl, J. (2014). Directionality of temperature activation in mouse TRPA1 ion channel can be inverted by single-point mutations in ankyrin repeat six. *Neuron* 82, 1017–1031.
- Jara-Oseguera, A., Bae, C., and Swartz, K.J. (2016). An external sodium ion binding site controls allosteric gating in TRPV1 channels. *Elife* 5, 1–33.
- Jordt, S., Julius, D., and Francisco, S. (2002). Molecular Basis for Species-Specific Sensitivity to “ Hot ” Chili Peppers. *Cell* 108, 421–430.
- Jordt, S.-E., Tominaga, M., and Julius, D. (2000). Acid potentiation of the capsaicin receptor determined by a key extracellular site. *Proc. Natl. Acad. Sci. U. S. A.* 97, 8134–8139.
- Julius, D. (2013). TRP channels and pain. *Annu Rev Cell Dev Biol* 29, 355–384.
- Kang, K., Panzano, V.C., Chang, E.C., Ni, L., Dainis, A.M., Jenkins, A.M., Regna, K., Muskavitch, M. a T., and Garrity, P. a (2012). Modulation of TRPA1 thermal sensitivity enables sensory discrimination in *Drosophila*. *Nature* 481, 76–80.
- Karashima, Y., Talavera, K., Everaerts, W., Janssens, A., Kelvin, Y., Vennekens, R., Nilius, B., Voets, T., Birnbaumer, L., Karashima, Y., et al. (2017). Linked references are available on JSTOR for this article : TRPA1 acts as a cold sensor in vitro and in vivo. *Proc. Natl. Acad. Sci. U. S. A.* 106, 1273–1278.
- Kautzman, W. (1959). Some factors in the interpretation of protein denaturation. *Adv. Prot. Chem* 14, 1–63.
- Kim, S.E., Patapoutian, A., and Grandl, J. (2013). Single residues in the outer pore of TRPV1 and TRPV3 have temperature-dependent conformations. *PLoS One* 8, e59593.
- Knowlton, W.M., Bifolck-Fisher, A., Bautista, D.M., and McKemy, D.D. (2010). TRPM8, but not TRPA1, is required for neural and behavioral responses to acute noxious cold temperatures and cold-mimetics in vivo. *Pain* 150, 340–350.
- Kubo, Y., and Murata, Y. (2001). Control of rectification and permeation by two distinct sites after the second transmembrane region in Kir2.1 K⁺ channel. *J. Physiol.* 531, 645–660.

- Kurganov, E., Zhou, Y., Saito, S., and Tominaga, M. (2014). Heat and AITC activate green anole TRPA1 in a membrane-delimited manner. *Pflgers Arch. Eur. J. Physiol.* 466, 1873–1884.
- Kyte, J., and Doolittle, R.F. (1982). A Simple Method for Displaying the Hydrophobic Character of a Protein. *J. Mol. Biol.* 157, 105–132.
- Latorre, R., Brauchi, S., Orta, G., Zaelzer, C., and Vargas, G. (2007). ThermoTRP channels as modular proteins with allosteric gating. *Cell Calcium* 42, 427–438.
- Leon, L.R., and Bouchama, A. (2015). Heat stroke. *Compr. Physiol.* 5, 611–647.
- Letunic, I., Doerks, T., and Bork, P. (2015). SMART: Recent updates, new developments and status in 2015. *Nucleic Acids Res.* 43, D257–D260.
- Li, H., and Durbin, R. (2009). Fast and accurate short read alignment with Burrows-Wheeler transform. *Bioinformatics* 25, 1754–1760.
- Li, M., Jan, Y.N., and Jan, L.Y. (1992). Specification of subunit assembly by the hydrophilic amino-terminal domain of the Shaker potassium channel. *Science* (80-.). 257, 1225–1230.
- Liao, M., Cao, E., Julius, D., and Cheng, Y. (2013). Structure of the TRPV1 ion channel determined by electron cryo-microscopy. *Nature* 504, 107–112.
- Lishko, P. V., Procko, E., Jin, X., Phelps, C.B., and Gaudet, R. (2007). The Ankyrin Repeats of TRPV1 Bind Multiple Ligands and Modulate Channel Sensitivity. *Neuron* 54, 905–918.
- Liu, B., Hui, K., and Qin, F. (2003). Thermodynamics of heat activation of single capsaicin ion channels VR1. *Biophys. J.* 85, 2988–3006.
- Long, S.B., Campbell, E.B., and Mackinnon, R. (2005). Crystal Structure of a Mammalian Voltage-Dependent Shaker Family K⁺ Channel. *Science* (80-.). 309, 897–903.
- van Lunteren, E., Elmslie, K., and Jones, S. (1993). Effects of temperature on calcium current of bullfrog sympathetic neurons. *J. Physiol.* 466, 81–93.
- Macpherson, L.J., Dubin, A.E., Evans, M.J., Marr, F., Schultz, P.G., Cravatt, B.F., and Patapoutian, A. (2007). Noxious compounds activate TRPA1 ion channels through covalent modification of cysteines. *Nature* 445, 541–545.
- Martin, M. (2011). Cutadapt removes adapter sequences from high-throughput sequencing reads. *Eur. Mol. Biol. Netw.* 17, 10–12.
- Matta, J. a, and Ahern, G.P. (2007). Voltage is a partial activator of rat thermosensitive TRP channels. *J. Physiol.* 585, 469–482.
- McKemy, D., Neuhauser, W., and Julius, D. (2002). Identification of a cold receptor reveals a general role for TRP channels in thermosensation. *Nature* 416, 52–58.
- Montell, C. (1998). TRP trapped in fly signaling web. *Curr. Opin. Neurobiol.* 8, 389–397.
- Montell, C., and Rubin, G.M. (1989). Molecular characterization of the drosophila trp locus: A putative integral membrane protein required for phototransduction. *Neuron* 2, 1313–1323.

- Moparthy, L., Survery, S., Kreir, M., Simonsen, C., Kjellbom, P., Högestätt, E.D., Johanson, U., and Zygmunt, P.M. (2014). Human TRPA1 is intrinsically cold- and chemosensitive with and without its N-terminal ankyrin repeat domain. *Proc. Natl. Acad. Sci. U. S. A.* 111, 16901–16906.
- Moqrich, A., Hwang, S.W., Earley, T.J., Petrus, M.J., Murray, A.N., Spencer, K.S.R., Andahazy, M., Story, G.M., and Patapoutian, A. (2005). Impaired thermosensation in mice lacking TRPV3, a heat and camphor sensor in the skin. *Science* 307, 1468–1472.
- Mosavi, L., Cammett, T., and Desrosiers, D. (2004). The ankyrin repeat as molecular architecture for protein recognition. *Protein Sci.* 13, 1435–1448.
- Mosavi, L.K., Minor, D.L., and Peng, Z.-Y. (2002). Consensus-derived structural determinants of the ankyrin repeat motif. *Proc. Natl. Acad. Sci. U. S. A.* 99, 16029–16034.
- Paulsen, C.E., Armache, J.-P., Gao, Y., Cheng, Y., and Julius, D. (2015). Structure of the TRPA1 ion channel suggests regulatory mechanisms. *Nature* 520, 511–517.
- Peier, A.M., Moqrich, A., Hergarden, A.C., Reeve, A.J., Andersson, D.A., Story, G.M., Earley, T.J., Dragoni, I., McIntyre, P., Bevan, S., et al. (2002a). A TRP channel that senses cold stimuli and menthol. *Cell* 108, 705–715.
- Peier, A.M., Reeve, A.J., Andersson, D.A., Moqrich, A., Earley, T.J., Hergarden, A.C., Story, G.M., Colley, S., Hogenesch, J.B., McIntyre, P., et al. (2002b). A Heat-Sensitive TRP Channel Expressed in Keratinocytes. *Science* (80-.). 296, 2046–2049.
- Pettersen, E.F., Goddard, T.D., Huang, C.C., Couch, G.S., Greenblatt, D.M., Meng, E.C., and Ferrin, T.E. (2004). UCSF Chimera - A visualization system for exploratory research and analysis. *J. Comput. Chem.* 25, 1605–1612.
- Prabhu, N. V., and Sharp, K.A. (2005). Heat Capacity in Proteins. *Annu. Rev. Phys. Chem.* 56, 521–548.
- Prescott, E.D., and Julius, D. (2003). A Modular PIP2 Binding Site as a Determinant of Capsaicin Receptor Sensitivity. *Science* (80-.). 300, 1284–1288.
- Privalov, P.L. (1989). THERMODYNAMIC PROBLEMS OF PROTEIN STRUCTURE. *Annu. Rev. Biophys. Biophys. Chem.* 18, 47–69.
- Romero-Romero, S., Gomez-Lagunas, F., and Balleza, D. (2017). Side chain flexibility and coupling between the S4-S5 linker and the TRP domain in thermo-sensitive TRP channels: Insights from protein modeling. *Proteins Struct. Funct. Bioinforma.* 1–51.
- Saito, S., Nakatsuka, K., Takahashi, K., Fukuta, N., Imagawa, T., Ohta, T., and Tominaga, M. (2012). Analysis of transient receptor potential ankyrin 1 (TRPA1) in frogs and lizards illuminates both nociceptive heat and chemical sensitivities and coexpression with TRP vanilloid 1 (TRPV1) in ancestral vertebrates. *J. Biol. Chem.* 287, 30743–30754.

- Salazar, H., Jara-Oseguera, A., Hernández-García, E., Llorente, I., Arias-Olguín, I.I., Soriano-García, M., Islas, L.D., and Rosenbaum, T. (2009). Structural determinants of gating in the TRPV1 channel. *Nat. Struct. Mol. Biol.* 16, 704–710.
- Schoppa, N.E., McCormack, K., Tanouye, M.A., and Sigworth, F.J. (1992). The size of gating charge in wild-type and mutant Shaker potassium channels. *Science* (80-.). 255, 1712–1715.
- Schulteis, C.T., Nagaya, N., and Papazian, D.M. (1996). Intersubunit interaction between amino- and carboxyl-terminal cysteine residues in tetrameric Shaker K⁺ channels. *Biochemistry* 35, 12133–12140.
- Schultz, J., Milpetz, F., Bork, P., and Ponting, C.P. (1998). SMART, a simple modular architecture research tool: identification of signaling domains. *Proc. Natl. Acad. Sci. U. S. A.* 95, 5857–5864.
- Sedgwick, S.G., and Smerdon, S.J. (1999). The ankyrin repeat: A diversity of interactions on a common structural framework. *Trends Biochem. Sci.* 24, 311–316.
- Seoh, S., Sigg, D., Papazian, D.M., and Bezanilla, F. (1996). Voltage-Sensing Residues in the S2 and S4 Segments of the Shaker K⁺ Channel. *Neuron* 16, 1159–1167.
- Sievers, F., Wilm, A., Dineen, D., Gibson, T.J., Karplus, K., Li, W., Lopez, R., McWilliam, H., Remmert, M., Söding, J., et al. (2011). Fast, scalable generation of high-quality protein multiple sequence alignments using Clustal Omega. *Mol. Syst. Biol.* 7, 1–6.
- Smith, G.D., Gunthorpe, M.J., Kelsell, R.E., Hayes, P.D., Reilly, P., Facer, P., Wright, J.E., Jerman, J.C., Walhin, J.-P., Ooi, L., et al. (2002). TRPV3 is a temperature-sensitive vanilloid receptor-like protein. *Nature* 418, 186–190.
- Song, K., Wang, H., Kamm, G.B., Pohle, J., Reis, F.C., Heppenstall, P., Wende, H., and Siemens, J. (2016). The TRPM2 channel is a hypothalamic heat sensor that limits fever and can drive hypothermia. *Science* (80-.). 353, 1393–1398.
- Starita, L.M., Pruneda, J.N., Lo, R.S., Fowler, D.M., Kim, H.J., Hiatt, J.B., Shendure, J., Brzovic, P.S., Fields, S., and Klevit, R.E. (2013). Activity-enhancing mutations in an E3 ubiquitin ligase identified by high-throughput mutagenesis. *Proc. Natl. Acad. Sci. U. S. A.* 110, E1263-72.
- Story, G.M., Peier, A.M., Reeve, A.J., Eid, S.R., Mosbacher, J., Hricik, T.R., Earley, T.J., Hergarden, A.C., Andersson, D. a, Hwang, S.W., et al. (2003). ANKTM1, a TRP-like channel expressed in nociceptive neurons, is activated by cold temperatures. *Cell* 112, 819–829.
- Tao, X., Avalos, J.L., Chen, J.Y., and MacKinnon, R. (2009). Crystal Structure of the Eukaryotic Strong Inward-Rectifier K(+) Channel Kir2.2 at 3.1 angstrom Resolution. *Science* (80-.). 326, 1668–1674.
- Tattersall, G.J., Sinclair, B.J., Withers, P.C., Fields, P.A., Seebacher, F., Cooper, C.E., and Maloney, S.K. (2012). Coping with thermal challenges: Physiological adaptations to environmental temperatures. *Compr. Physiol.* 2, 2151–2202.

- Tibbs, G.R., Goulding, E.H., and Siegelbaum, S.A. (1997). Allosteric activation and tuning of ligand efficacy in cyclic-nucleotide-gated channels. *Nature* 386, 612–615.
- Tiwari, J., and Sikdar, S. (1999). Temperature-dependent conformational changes in a voltage-gated potassium channel. *Eur. Biophys. J.* 28, 338–345.
- Tominaga, M., Caterina, M.J., Malmberg, A.B., Rosen, T.A., Gilbert, H., Skinner, K., Raumann, B.E., Basbaum, A.I., and Julius, D. (1998). The cloned capsaicin receptor integrates multiple pain-producing stimuli. *Neuron* 21, 531–543.
- Traxlmayr, M.W., Hasenhindl, C., Hackl, M., Stadlmayr, G., Rybka, J.D., Borth, N., Grillari, J., Rüker, F., and Obinger, C. (2012). Construction of a stability landscape of the CH3 domain of human IgG1 by combining directed evolution with high throughput sequencing. *J. Mol. Biol.* 423, 397–412.
- Vivienne Shen, N., Chen, X., Boyer, M.M., and Pfaffinger, P.J. (1993). Deletion analysis of K⁺ channel assembly. *Neuron* 11, 67–76.
- Voets, T. (2012). Quantifying and Modeling the Temperature-Dependent Gating of TRP Channels. *Rev. Physiol. Biochem. Pharmacol.*
- Voets, T., Droogmans, G., Wissenbach, U., Janssens, A., Flockerzi, V., and Nilius, B. (2004). The principle of temperature-dependent gating in cold- and heat-sensitive TRP channels. *Nature* 430, 748–754.
- Voets, T., Owsianik, G., Janssens, A., Talavera, K., and Nilius, B. (2007). TRPM8 voltage sensor mutants reveal a mechanism for integrating thermal and chemical stimuli. *Nat. Chem. Biol.* 3, 174–182.
- Vriens, J., Nilius, B., and Voets, T. (2014). Peripheral thermosensation in mammals. *Nat. Rev. Neurosci.* 15, 573–589.
- Wei, Z., Wang, W., Hu, P., Lyon, G.J., and Hakonarson, H. (2011). SNVer: a statistical tool for variant calling in analysis of pooled or individual next-generation sequencing data. *Nucleic Acids Res.* 39, e132.
- Wetsel, W.C. (2011). Sensing hot and cold with TRP channels. *Int. J. Hyperthermia* 27, 388–398.
- White, S.H., and Wimley, W.C. (1999). Membrane protein folding and stability: Physical principles. *Ann. Rev. Biophys. Biomol. Struct.* 28, 319–365.
- Winter, Z., Buhala, A., Ötvös, F., Jósavay, K., Vizler, C., Dombi, G., Szakonyi, G., and Oláh, Z. (2013). Functionally important amino acid residues in the transient receptor potential vanilloid 1 (TRPV1) ion channel—an overview of the current mutational data. *Mol. Pain* 9, 1–30.
- Xu, H., Ramsey, I., Kotecha, S., Moran, M., Chong, J., Lawson, D., Ge, P., Lilly, J., Silos-Santiago, I., Xie, Y., et al. (2002). TRPV3 is a calcium-permeable temperature-sensitive cation channel. *Nature* 418, 181–186.

- Xu, H., Blair, B., and Clapham, D. (2005). Camphor Activates and Strongly Desensitizes the Transient Receptor Potential Vanilloid Subtype 1 Channel in a Vanilloid-Independent Mechanism. *J. Neurosci.* 25, 8924–8937.
- Yang, F., Cui, Y., Wang, K., and Zheng, J. (2010). Thermosensitive TRP channel pore turret is part of the temperature activation pathway. *Proc. Natl. Acad. Sci. U. S. A.* 107, 7083–7088.
- Yang, J., Jan, Y.N., and Jan, L.Y. (1995). Control of rectification and permeation by residues in two distinct domains in an inward rectifier K⁺ channel. *Neuron* 14, 1047–1054.
- Yang, S., Yang, F., Wei, N., Hong, J., Li, B., Luo, L., Rong, M., Yarov-Yarovoy, V., Zheng, J., Wang, K., et al. (2015). A pain-inducing centipede toxin targets the heat activation machinery of nociceptor TRPV1. *Nat. Commun.* 6, 1–11.
- Yao, J., Liu, B., and Qin, F. (2010a). Kinetic and energetic analysis of thermally activated TRPV1 channels. *Biophys. J.* 99, 1743–1753.
- Yao, J., Liu, B., and Qin, F. (2010b). Pore turret of thermal TRP channels is not essential for temperature sensing. *Proc. Natl. Acad. Sci. U. S. A.* 107, E125; author reply E126-7.
- Yao, J., Liu, B., and Qin, F. (2011). Modular thermal sensors in temperature-gated transient receptor potential (TRP) channels. *Proc. Natl. Acad. Sci. U. S. A.* 108, 11109–11114.
- Zakharian, E., Cao, C., and Rohacs, T. (2010). Gating of transient receptor potential melastatin 8 (TRPM8) channels activated by cold and chemical agonists in planar lipid bilayers. *J. Neurosci.* 30, 12526–12534.
- Zhong, L., Bellemer, A., Yan, H., Honjo, K., and Robertson, J. (2012). Thermosensory and non-thermosensory isoforms of *Drosophila melanogaster* TRPA1 reveal heat sensor domains of a thermoTRP channel. *Cell Rep.* 1, 43–55.
- Zubcevic, L., Herzik, M. a, Chung, B.C., Liu, Z., Lander, G.C., and Lee, S.-Y. (2016). Cryo-electron microscopy structure of the TRPV2 ion channel. *Nat. Struct. Mol. Biol.* 23, 180–186.

Biography

Jason O. Sosa Pagán was born in Aguadilla, Puerto Rico in March 15, 1987. He received a Bachelor of Science with Honors in Chemistry from the University of Puerto Rico at Río Piedras. As an undergraduate he was also the recipient of the Isidoro Alberto Colón Award that is granted to a Chemistry major student for his outstanding contribution to Chemistry studies. He then moved to North Carolina and joined the Postbaccalaureate Research Education Program (PREP) at the University of North Carolina at Chapel Hill where he worked as a research assistant in the laboratory of Benjamin Philpot. After a year as a PREP scholar he was accepted to the Cell and Molecular Biology (CMB) program to pursue his PhD degree. He then joined the laboratory of Jörg Grandl to complete his dissertation work and affiliated with the Department of Neurobiology. Articles published by Jason include:

Sosa-Pagán, J.O., Iversen, E.S., and Grandl, J. (2017). TRPV1 temperature activation is specifically sensitive to strong decreases in amino acid hydrophobicity. *Sci. Rep.* 7:549. doi: 10.1038/s41598-017-00636-4.

Jabba, S., Goyal, R., Sosa-Pagán, J.O., Moldenhauer, H., Wu, J., Kalmeta, B., Bandell, M., Latorre, R., Patapoutian, A., and Grandl, J. (2014). Directionality of temperature activation in mouse TRPA1 ion channel can be inverted by single-point mutations in ankyrin repeat six. *Neuron* 82, 1017–1031.

Judson, M.C., Sosa-Pagan, J.O., Delcid, W. a, Han, J.E., and Philpot, B.D. (2014). Allelic specificity of Ube3a expression in the mouse brain during postnatal development. *J. Comp. Neurol.* 522, 1874–1896.

Voinov, M.A., Sosa Pagán, J.O., Morrison, E., Smirnova, T.I., and Smirnov, A.I. (2011). Surface-mediated production of hydroxyl radicals as a mechanism of iron oxide nanoparticle biotoxicity. *J. Am. Chem. Soc.* 133, 35–41.